



OROGENIC ARCHITECTURE AND CRUSTAL GROWTH FROM ACCRETION TO COLLISION



МОНГОЛ УЛСЫН ШИНЖЛЭХ УХААН
ТЕХНОЛОГИЙН ИХ СУРГУУЛЬ
MONGOLIAN UNIVERSITY OF SCIENCE AND TECHNOLOGY



FACULTY OF SCIENCE
Charles University



IGCP - 662 PROJECT Field Guide



Gobi-Altai Accretionary Orogeny

Compiled by P. Hanžl, O. Lexa and K. Schulmann



July 5–9, 2019

Chandman soum, Gobi-Altai Aimag

IGCP – 662 Project

OROGENIC ARCHITECTURE AND
CRUSTAL GROWTH FROM
ACCRETION TO COLLISION

Field Guide

Gobi-Altai Accretionary Orogeny

July 5–9, 2019

Chandman soum, Gobi-Altai Aimag

Compiled by P. Hanžl, O. Lexa and K. Schulmann

with contribution of

C. Aguilar Gil, A. Broussolle, P. Budil, D. Buriánek,
A. Chimedtseren, O. Gerel, V. Janoušek, O. Javkhlan, Y. Jiang,
J. Lehmann, Ts. Narantsetseg, D. Otgonbaatar, V. Peřestý,
D. Sanchir, I. Soejono, P. Štípská, S. Turbold

Czech Geological Survey
Charles University Prague
Mongolian University of Science & Technology
Institute of Paleontology & Geology, MAS

Sponsored by:
UNESCO-IUGS-IGCP
Ministry of Mining and Heavy Industry
Zhenyuang Company
BMNS Co. Ltd.
Tsairt Minerals Co. Ltd.
Zaamar Gold Co. Ltd.

Orogenic architecture and crustal growth from accretion to collision
IGCP 662 project, 2nd workshop
Ulaanbaatar, 4-10 July, 2019

FIELD GUIDE
Gobi-Altai Accretionary Orogeny
Edited by P. Hanžl, O. Lexa and K. Schulmann

Published by Institute of Petrology and Structural Geology, Charles University
Typeset in L^AT_EX by Ondrej Lexa
Printed by Mongolian University of Science and Technology
First edition, 81 pages, 100 copies

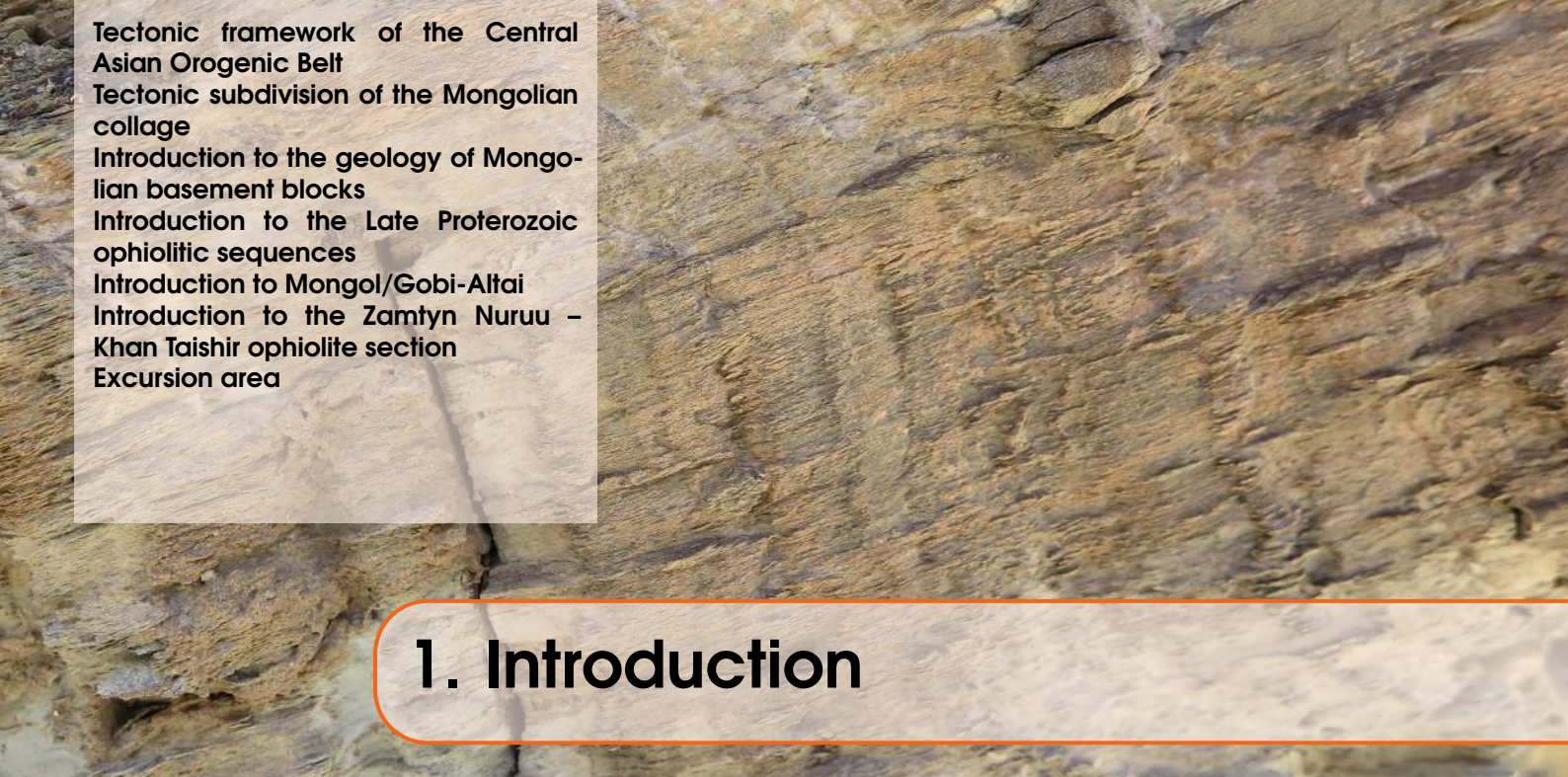
Cover photo: Zamtyn Nurru Range in Gobi Altai with cliff of Cambrian limestone

ISBN 978-99978-57-85-9

Contents

1	Introduction	3
1.1	Tectonic framework of the Central Asian Orogenic Belt	3
1.2	Tectonic subdivision of the Mongolian collage	4
1.3	Introduction to the geology of Mongolian basement blocks	5
1.4	Introduction to the Late Proterozoic ophiolitic sequences	7
1.5	Introduction to Mongol/Gobi-Altai	8
1.6	Introduction to the Zamtyн Nuruu – Khan Taishir ophiolite section	10
1.7	Excursion area	11
2	Day I.	15
2.1	Metamorphism of Taatsyngol Complex (1)	15
3	Day II.	19
3.1	Ophiolite sequence of the Erdene Uul, Lake Zone (2)	19
3.2	Cambrian molase, Boomyn Khudag (3)	24
4	Day III.	27
4.1	Borogol Suite, Lake Zone, the Bayan Aarag locality (4)	27
4.2	Devonian Gichigene Suite, the Tsakhir Khaalgyn Nuruu locality (5)	29
4.3	The Tugrug Formation and Tsogt metamorphic dome	32
4.4	Variegated lithology and folding of the Tugrug Suite (6A)	42

4.5	Contact of Tugrug Suite and Tsogt metamorphic core (6B)	44
4.6	High-grade rocks of Tsogt metamorphic core (6C)	44
4.7	Migmatite of the Tsogt metamorphic core (6D)	45
5	Day IV.	47
5.1	Introduction to the Chandman Massif	47
5.2	Chandman Massif magmatism (7A)	48
5.3	Quartzitic phyllite in wall rocks of the Chandman Massif (7B)	51
5.4	Cambrian gabbros of Ikh Mongol Arc, Khaya Khudag (8)	53
5.5	HP-micaschist between Zamtyn Nuruu and Alag Khadny (9)	56
5.6	Tonian orthogneiss of the Zamtyn Nuruu, Ekhen Khudug (10)	58
5.7	Cambrian HP tectonic melange in Alag Khad Mt. area (11A–B)	61
5.8	Cambrian limestone (12)	65
5.9	Turbidite sediments of the Naran Formation (13)	67
5.10	Khan Taishir Formation (14A–B)	68



Tectonic framework of the Central Asian Orogenic Belt
Tectonic subdivision of the Mongolian collage
Introduction to the geology of Mongolian basement blocks
Introduction to the Late Proterozoic ophiolitic sequences
Introduction to Mongol/Gobi-Altai
Introduction to the Zamtyn Nuruu – Khan Taishir ophiolite section
Excursion area

1. Introduction

1.1 Tectonic framework of the Central Asian Orogenic Belt

The general structure of the Central Asian Orogenic Belt (CAOB) form a supercollage that can be divided into three large collages (Xiao et al. 2015): From east to west it is the Kazakhstan oroclinal collage separated from the eastern Mongolian collage by giant Erquis fault zone. Much of these two domains are dominated by accreted oceanic fragments represented by accretionary wedges, island arcs and related back arcs (e.g. Sengör et al. 1993; Windley et al. 2007). The abundance of ophiolites of Late Proterozoic to Early Palaeozoic age led Zonenshain (1973) to define the Paleo-Asian Ocean as a precursor of the CAOB. These rocks show primitive Nd isotopic signatures, as do Carboniferous and Permian granitoids, interpreted to result from continuous crustal growth during the whole Palaeozoic (Jahn 2004). For these reasons, Windley et al. (2007) proposed that this part of the CAOB represents the site of the most important Phanerozoic crustal growth resulting from long-lived frontal accretion. Alternative geodynamic interpretation was proposed by Sengör et al. (1993) and Yakubchuk (2008) based on the general structure of this domain characterized by two giant oroclines interpreted as having resulted from buckling and strike-slip duplication of a giant long-lived intra-oceanic arc system. In contrast, the younger southern collage of the CAOB in Chinese and Kyrgyzstan Tianshan shows a different evolution being marked by amalgamation of multiple E–W striking linear components such as Devonian–Carboniferous magmatic arcs and Proterozoic ribbon microcontinents along short-lived subduction zones, UHP metamorphism and active margin magmatism with a strong continental crustal component typical of “interior” collisional orogens (Xiao et al. 2004, 2015). Large variety of geodynamic models arises from ambiguity of the Paleo-Asian ocean and its location in “interior” (Scotese 2004; Zonenshain et al. 1985) or “peripheral” position (Cocks et al. 2007). Another source of uncertainty is the magmatic evolution of the CAOB, marked by the migration of calc-alkaline and alkaline magmatic provinces in space and time across the whole CAOB. This led to contrasting geodynamic models as Pacific-type accretion (Jahn 2004), ridge-subduction (M. Sun et al. 2009) or synorogenic hot-spot activity (Yarmolyuk et al. 2000, 2014).

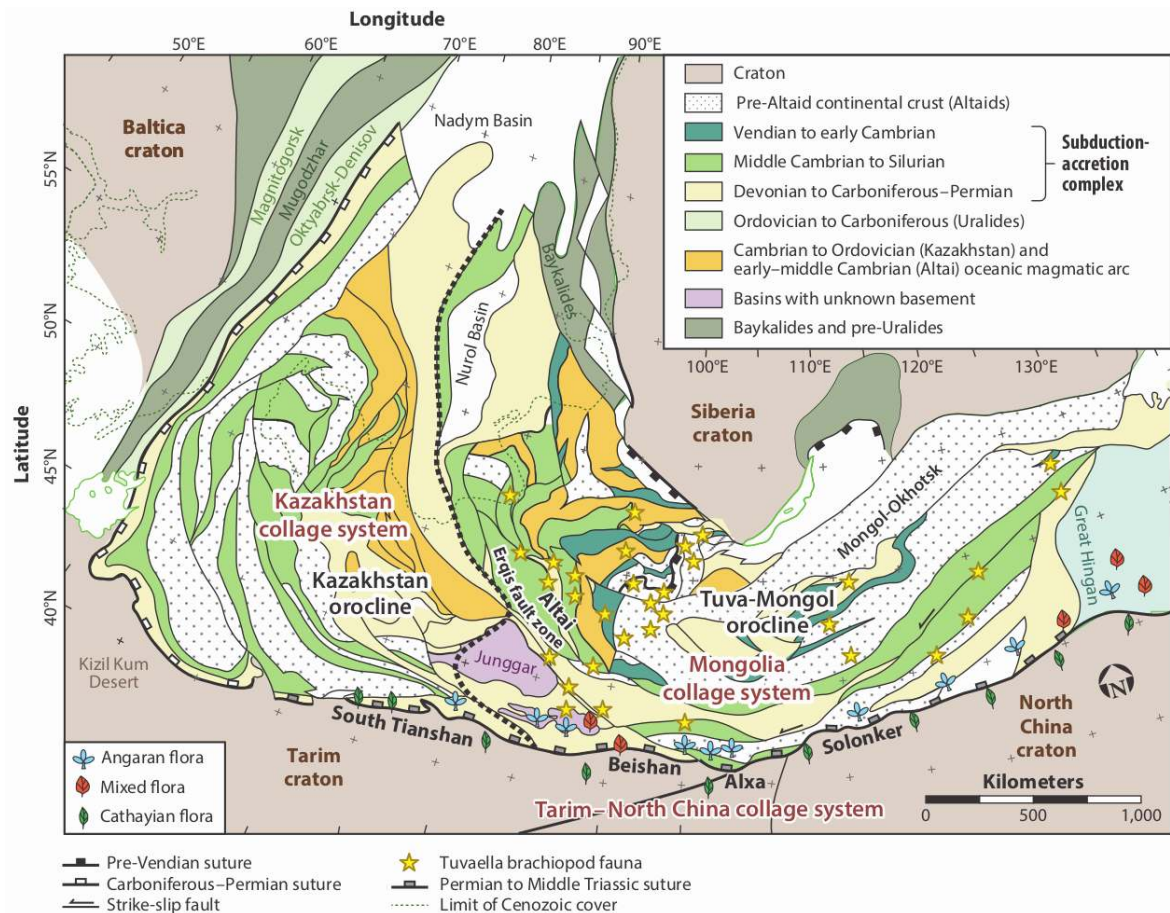


Figure 1.1: Tectonic map of the main components of the Central Asian Orogenic Belt, showing the Kazakhstan, Mongolia, and Tarim–North China collage systems, separated by a thick black dotted line, and the South Tianshan–Solonker suture (after Xiao et al. (2015)).

1.2 Tectonic subdivision of the Mongolian collage

The Mongolian collage occurs mainly in Mongolia and adjacent parts of China and Russia (Fig. 1.1). It is formed by a string of Precambrian continental and Island arc fragments (Barguzin, Tuva, Dzavkhan, Baydrag and Erguna blocks) that form an arcuate fold like structure known as Tuva-Mongolian orocline (Sengör et al. 1993; Yakubchuk 2008). The core of this fold-like structure is formed by imbricated Devonian-Carboniferous sedimentary strata, volcanic series and Carboniferous ophiolites coinciding with Mongol-Okhotsk oceanic suture zone (Parfenov et al. 2001; Ruzhentsev and Nekrasov 2009; Tomurtogoo et al. 2005). To the north the continental blocks are attached to the Siberian continent by the Baikalian Late Proterozoic to Cambrian orogenic belt (Donskaya et al. 2000; Gladkochub et al. 2008). To the W and SW the Precambrian continental blocks are rimmed by allochthonous Late Proterozoic ophiolitic suites (Buriánek et al. 2017; Jian et al. 2014; Khain et al. 2003; Kovach et al. 2011) forming so called Lake Zone. The whole tectonic domain was called Caledonian according to Cambro-Ordovician age of deformation and metamorphism (Mossakovsky et al. 1993). The Lake Zone is rimmed by early Palaeozoic volcano-sedimentary complex forming bulk of Mongolian and Chinese Altai called Mongol-Altai Zone. This giant domain is affected by Devonian to Carboniferous metamorphism and magmatism thereby reflecting Hercynian orogenic event in Russian literature. The Mongol-Altai Zone is bounded to the south by late Ordovician

to Devonian-Carboniferous volcanics and volcanosedimentary units called Trans-Altai zone in Mongolia and Junggar zone in China. These, often shallow marine volcanosedimentary sequences are imbricated with Devonian to Ordovician ophiolitic sheets (Helo et al. 2006; Jian et al. 2014, 2008; Xiao et al. 2009b; Zonenshain 1973) supposedly during Carboniferous “Hercynian” orogeny. This 2000 km long zone is limited to the south and south-east by Precambrian blocks forming south Gobi, Xing’an and Songliao basement outliers in the far east China (Wilde et al. 2005).

Like in other orogens, this tectonic sub-division of the CAOBS was based mainly on structural and metamorphic overprints which led to definition of Proterozoic Baikalian, and Palaeozoic, Caledonian and Hercynian orogens. However, this classical strategy does not allow defining the geodynamic and chronological significance of principal units. Accordingly, the classical tectonic zones forming the Mongolian collage can be re-defined on the basis of mutual affinities of lithological sequences and igneous assemblages: 1) Precambrian continents and continental margins sequences, 2) oceanic Late Proterozoic ophiolitic units corresponding to the Lake Zone, 3) Early Palaeozoic sedimentary accretionary wedge corresponding to the Mongol-Altai, 4) Early to Late Paleozoic oceanic systems covering the Trans-Altai Zone.

1.3 Introduction to the geology of Mongolian basement blocks

Precambrian continents and continental margin sequences

Continental basement units of the Mongolian collage are unconformably covered by Neoproterozoic to Early Cambrian autochthonous continental margin sequences that developed on Rodinia supercontinent. The Proterozoic and Lower Palaeozoic sequences vary in Precambrian continental blocks thereby allowing subdivision into Siberian continental assemblage and Mongolian (Tarim type) continental assemblage (Rojas-Agramonte et al. 2011; Wilhem et al. 2012).

The oldest igneous rocks of Mongolian blocks are of Neo-archean to Paleoproterozoic age with two peak activity around 2.5 and 1.9 Ga (Kuzmichev et al. 2001; Rojas-Agramonte et al. 2011, for summary). The most characteristic is a large group of Grenville age magmatic rocks ranging from 1 to 0.8 Ga (e.g. Demoux et al. 2009b; Kuzmichev et al. 2005; Yarmolyuk et al. 2005). The westernmost Tuva-Mongol block is a composite terrane which originated thanks to 800 Ma amalgamation of Grenville age Dunzhugur magmatic arc with Paleoproterozoic Gargan microcontinent (Kuzmichev et al. 2001). Easterly Zavkhan and Baydrag Palaeoproterozoic basement is characterized by important Grenville age event represented by major magmatic activity of Japan type “Dund or Zamtyn Nuruu” arcs (Bold et al. 2016; Buriánek et al. 2017). The composite basement rocks of all Mongolian blocks are affected by second period of arc magmatism represented by intrusions of gabbros, tonalities and granodiorites at period between 520–480 Ma (Bold et al. 2016; Buriánek et al. 2017; Salnikova et al. 2001). This magmatic suite intruded eastern and southern margins of Mongolian blocks and forms a giant Japan type structure called Ikh Mongol arc (Janoušek et al. 2018).

Tuva Mongol and Zavkhan blocks show quite similar sedimentary record starting with Tonian volcanoclastic series deposited on Palaeoproterozoic basement and/or 800 Ma ophiolites in Tuva-Mongol block. These sediments are interpreted to represent an accretionary wedge related to accretion of the 800 Ma Shishkhid ophiolite in the Tuva-Mongolian block (Kuzmichev et al. 2007) or marginal basin above the Dund arc in the Zavkhan block (Bold et al. 2016). The Tonian clastic sequences are unconformably covered by Late Proterozoic –

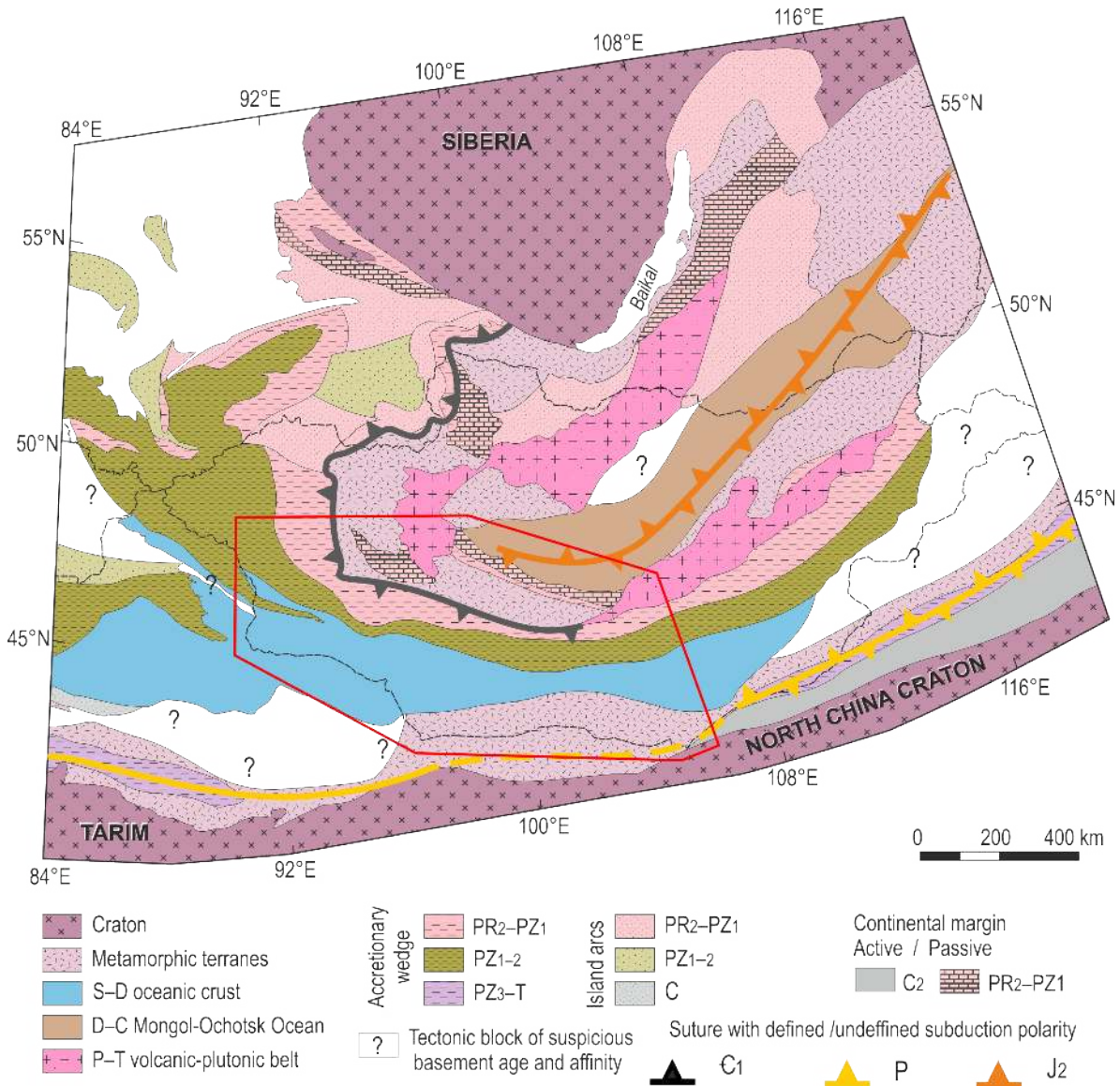


Figure 1.2: Position of Mongolian tract of the Central Asian Orogenic Belt, simplified from Wilhem et al. (2012) (for the frame see Fig. 1.5).

Early Cambrian limestones (Badarch et al. 2002; Khain et al. 1995; Kuzmichev et al. 2005) interpreted as passive margin sequences. The Baydrag continental block shows well developed Late Proterozoic – Early Cambrian carbonate platform sediments deposited on early Proterozoic basement still in passive margin setting (Buriánek et al. 2017). The easternmost Erguna massif shows presence of well-developed paleontologically unconstrained clastic sequence of Tonian age (Zhang et al. 2014).

Late Proterozoic HP-LT and MP-MT orogenic event (570–530 Ma)

The Late Vendian – Early Cambrian orogenic cycle is well recorded by HP accretionary wedges spatially related to emplacement of Late Proterozoic ophiolites thrust over Precambrian Mongolian blocks (e.g., 16 kbar at 600°C Khain et al. 2003; Štípská et al. 2010). The thrusting of ophiolites is associated with Barrovian (Ky-St-Gr_t) schists at footwall Neoproterozoic metasedimentary sequences such as footwall of Bayankhongor ophiolite (570–620°C, 8–10

Kbar), Moren complex of Tuva Mongol block (500–600°C, 5–8 kbar) and the retrograde eclogites (600–700°C, 7.7–8.5 kbar) of the Kan greenstone belt in Sayan Mts. (Kozakov et al. 2012a; Nozhkin et al. 2001). The timing of HP-LT and MP-MT metamorphism was estimated to 570–530 Ma based on U-Pb zircon geochronology of syn and post-tectonic intrusions and Ar-Ar cooling ages of micas and amphiboles (Kozakov et al. 2012b; Nozhkin et al. 2011; Štípská et al. 2010). All these data reflect metamorphic gradient varying between 17°C/km to 24°C/km typical for oceanic subduction to continental collision and crustal thickening. This event had to be related to the building of topography as manifested by development of giant late Vendian foreland basin covering southern margin of Siberian stable continent.

Late Cambrian – Early Ordovician HT-LP event (510–490 Ma)

This HT-LP (510–490 Ma) event is developed along southern and SW margin of Baydrag, Zavkhan and Tuva Mongol blocks (Kozakov et al. 2012b). Tuva-Mongol, Zavkhan and Baydrag continental sequences are overprinted by LP-HT metamorphism (Sill, Crd, And, locally reaching granulite facies, 6 kbar at 850°C). In all regions the LP granulite facies metamorphism is associated with intrusions of arc type gabbros, tonalites and other granitoids and widespread anatexis of surrounding rocks (Buriánek et al. 2017; Gladkochub et al. 2008; Kozakov et al. 2012b). The 510–490 Ma metamorphic event is characterized by metamorphic field gradient ranging from 30 to 40°C/km typical for extreme heat input and lithospheric thinning of previously accreted and thickened crust.

1.4 Introduction to the Late Proterozoic ophiolitic sequences

There are two types of Late Proterozoic oceanic units thrust over the Baydrag and Zavkhan blocks: 1) the Bayankhongor ophiolite suite rimming the northern margin of the Baydrag block, and 2) the ophiolitic units collectively grouped in the Lake Zone fringing Mongolian continental blocks from the south and west.

Bayankhongor ophiolite

The Bayankhongor ophiolite mélangé is bordering the northern margin of the Baydrag block and the southern margin of Khantay basin of Mongol-Okhotsk assemblage. This 300 km long and 20 km wide flower structure is tectonically wedged against accretionary complexes to the south and to the north (Buchan et al. 2002). The 655–635 Ma U-Pb zircon ages of gabbros, diorites, rodingites and plagiogranites are interpreted to date the formation of oceanic crust during sea floor spreading (Jian et al. 2008) while the intrusion of 523 Ma postkinematic syenite porphyrite is interpreted to date the end of accretion of ophiolite crust. The ophiolite is in the north juxtaposed to late Ordovician psammitic weakly metamorphosed Dzag unit composed of interbedded sandstones and argilites with strong volcanic detrital component. Detrital zircons show age spectra typical for other sedimentary complexes of southern Mongolia, such as strong 500 Ma, 800–900 Ma and Paleoproterozoic peaks suggesting source from southerly late Cambrian and Grenville-age arc domains reworking the Paleoproterozoic crust of the Baydrag continent (Kröner et al. 2011).

Lake Zone ophiolite sequences

The Lake Zone is a giant island-arc system (e.g. Kozakov et al. 2002) forming the substantial part of the “Caledonian” tectonic province in Mongolia. In the east, it consists of the almost

complete (Dariv, Khan Taishir and Zamtyn Nuruu) ophiolitic sequences represented by serpentinized peridotites, gabbros, pillow lavas and bedded cherts all dated at ca. 570 Ma using U-Pb zircon method or by overlying sediments (Khain et al. 2003; Rauzer et al. 1987). Further west occurs the Lake Zone s.s. which consists of island arc volcanic units, siliceous-terrigenous complexes and arc related magmatic rocks (Kovach et al. 2011). Basalt–andesite-dacite island arc volcanic sequences formed at the Ediacaran–Cambrian boundary at ca. 545 Ma (Kovalenko et al. 2004). The whole volcanic and sedimentary sequence (Fig. 1.3) is intruded by arc-related layered gabbros and quartz diorite-tonalite-trondhjemite-granodiorite plutons dated between 530–480 Ma (Buriánek et al. 2017; Janoušek et al. 2018; Rudnev et al. 2009; Soejono et al. 2017; Yarmolyuk et al. 2011). These granitoids form a giant magmatic structure rimming the whole southern and eastern margin of Mongolian continental block and were recently interpreted as a principal Early Palaeozoic magmatic arc structure (Janoušek et al. 2018). The ophiolite sequences together with arc magmatites are in many places unconformably overlaid by turbiditic, usually tuffaceous sediments of the Naran formation with supposedly Late Cambrian depositional age (Rauzer et al. 1987). However, clastic zircons dated by Kröner et al. (2010) indicate that these deposits can be at least locally younger than 406 Ma.

1.5 Introduction to Mongol/Gobi-Altai

The Early Palaeozoic turbiditic volcano-sedimentary sequence (Fig. 1.3) extends from Mongolia to China, Kazakhstan and Russia (Fig. 1.1) for two thousands kilometers and was recently interpreted as a giant accretionary sedimentary wedge (Jiang et al. 2017; Xiao et al. 2009b). This unit is dominated by late Cambrian and Ordovician metamorphosed schists, volcano-sedimentary succession, sandstones, siltstones and intermediate to mafic volcanic rocks (e.g. Badarch et al. 2002; Safonova et al. 2009). The low grade part of the sequence is characterized by dominant terrigenous components mixed with variable amounts of volcanogenic material called Tugrug Formation in Mongolia and the Habahe Group in northern China (Long et al. 2008). It is chemically immature, compositionally analogous to greywacke and marked by significant input of felsic to intermediate arc components, pointing to an active continental margin depositional setting. The low-grade rocks are juxtaposed to a high-grade metamorphic rocks that are well exposed along the southern slopes of the Altai Range. The dominant metamorphic rocks include high-grade paragneiss, granitic gneiss, schist with subordinate intercalations of amphibolite, gabbro bodies. Based on comparable chemistry and zircon age patterns, the high-grade gneissic rocks were recently interpreted to be high-grade metamorphic equivalents of the Ordovician sedimentary sequence (i.e., Tugrug and Habahe formations) (Jiang et al. 2016, 2012). Importantly, no Precambrian basement rocks were described in both the Chinese and Mongol-Altai suggesting a possibility that the whole sequence was deposited on oceanic crust. Indeed, Xiao et al. (2009a) describes numerous ophiolitic fragments scattered over the Chinese Altai and in particular along its southern margin in so-called Erquis accretionary zone, where numerous fragments of gabbros, serpentinite and Ordovician–Silurian radiolarian cherts occur. Abundant granitoids dated as Silurian–Devonian, intruded the Ordovician gneisses and low grade rocks (e.g. Yuan et al. 2007), coevally with the migmatization of the deeper part of the sequence. These arc-type granitoids were recently interpreted to have originated from the anatexis of greywacke dominated detritus (e.g. Jiang et al. 2016). Chinese and Mongol/Gobi-Altai is also characterized by numerous gabbroic intrusions, as well as high Mg adakitic rocks of Devonian age (He et al. 2015) suggesting melting of subducting slab and

emplacement of immature arc magmas. The whole complex is irregularly covered by Silurian basalt, tuff and siliciclastic sediments, locally interlayered with thick carbonates, followed by thick early Devonian siliciclastic sediments, fossiliferous limestones and interbedded felsic volcanic rocks dated at ca. 390 Ma (Demoux et al. 2009a; Hanžl et al. 2016; Jiang et al. 2015). Local accumulations of Early Carboniferous siliciclastic sediments were interpreted as intra-mountain basins (Markova 1975).

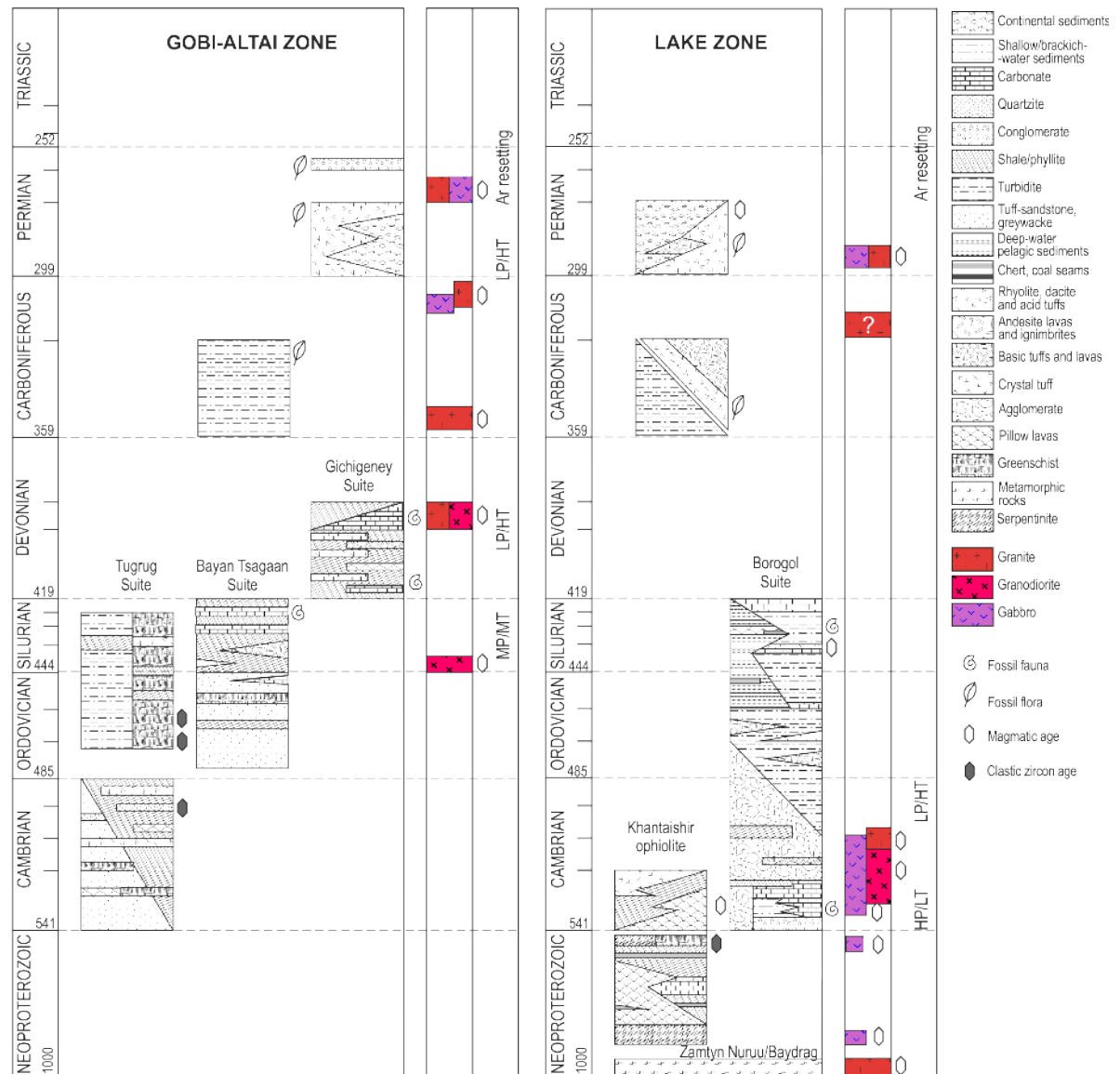


Figure 1.3: Lithostratigraphic scheme of the Gobi-Altai and Lake Zone on the map sheet L-47-V. Modified from (Hanžl et al. 2019).

Devonian–Carboniferous MP-HT metamorphism (390–360 Ma)

An Early Paleozoic Barrovian-type metamorphism (Ky-Sill-St-Gt, peak 9 kbar, 600°C) is developed in the late Cambrian and Ordovician flysch sediments of peri-continental sequences in Chinese and Mongol/Gobi-Altai (e.g. Burenjargal et al. 2014; Jiang et al. 2015; Wei et al. 2007) indicating maximum burial to depth of >30km for metamorphic gradient of 20°C/km (Fig. 5.21). Deeply buried metasediments subsequently experienced high-temperature reequili-

bration dated at 390–370 Ma and associated with important anatexis of fertile metasediments at the stability of Sill, Kfs, Crd corresponding to P-T conditions of 6–7 kbar and 700–800°C (e.g. Broussolle et al. 2015; Burenjargal et al. 2014; Jiang et al. 2015). HT re-equilibration locally reached granulite facies conditions (Kozakov et al. 2002) under high geothermal gradient of (~30–40°C/km). The partially molten rocks were subsequently vertically extruded in form of elongated large migmatite-magmatite domes alternating with weakly metamorphosed metasedimentary synforms during late Devonian – Early Carboniferous shortening (Lehmann et al. 2010). The HT metamorphism is connected with melting of fertile sediments and production of large quantities of arc-like Devonian granitoids that emplaced in middle and upper crustal levels (Jiang et al. 2016).

1.6 Introduction to the Zamtyn Nuruu – Khan Taishir ophiolite section

Recent studies of the southern Baydrag continental margin in Mongolia allowed to propose a new Early Palaeozoic geodynamic model for the Mongolian collage (Buriánek et al. 2017; Janoušek et al. 2018; Soejono et al. 2016). So far best sequence was described in the Zamtyn Nuruu region, where the complete architecture of the Baydrag basement, Early Cambrian accretionary wedge and Late Proterozoic ophiolites could have been defined (Buriánek et al. 2017; Štípská et al. 2010). Here, the structurally deepest Zamtyn Nuruu Complex is composed of highly deformed orthogneisses and amphibolites intruded by syntectonic diorites and gabbros. Geochemical affinity of the amphibolites varies from continental arc to within-plate tholeiites, while the Grenvillian (948 ± 6 and 941 ± 11 Ma) orthogneisses show typical magmatic arc-type setting. The synmetamorphic gabbros and diorites intruded coevally with regional anatexis at around 540 Ma (Buriánek et al. 2017; Lehmann et al. 2010). Zircon-in Hf isotopes and geochemistry data indicate a primitive source of mafic rocks formed in Early Cambrian arc developed on Grenvillian basement. The basement is overlain by Alag Kladny subduction mélange involving eclogites and amphibolites of MORB affinity including orthogneiss fragments (ca. 953 Ma) characterized by late-collisional geochemical signature. The subduction event was dated by zircon at ca 538 Ma which is also an age of cooling of the whole wedge as documented by Ar-Ar cooling ages at around 530 Ma (Štípská et al. 2010). The matrix of mélange is formed by HP metapelites and marbles most likely derived from Late Proterozoic – Early Cambrian carbonate platform that was scraped off from subducting plate by during Cambrian accretion. The hanging wall of the wedge is formed by Khan Taishir - Erdene Uul ophiolite nappe that is composed of serpentinites, gabbros, Neoproterozoic pillow lavas and cherts. The gabbro from Erdene Uul was dated at ca. 973 Ma (Buriánek et al. 2017) which indicates involvement of mid-Proterozoic oceanic lithosphere into Late Proterozoic ophiolitic system. The whole structure of the HP wedge and ophiolitic system represent large scale Late Proterozoic to Early Cambrian suprasubduction system. Based on these findings it was proposed that Grenvillian age magmatism represents a vestige a Mirovoi Ocean subduction system beneath Rodinia followed by typical passive margin sequences characteristic for Rodinia fragmentation. These events were followed by formation of active margin setting represented by growth of Cambrian magmatic arc, development of accretionary wedge and obduction of suprasubduction ophiolites reflecting an initiation of Early Pacific subduction (Buriánek et al. 2017).

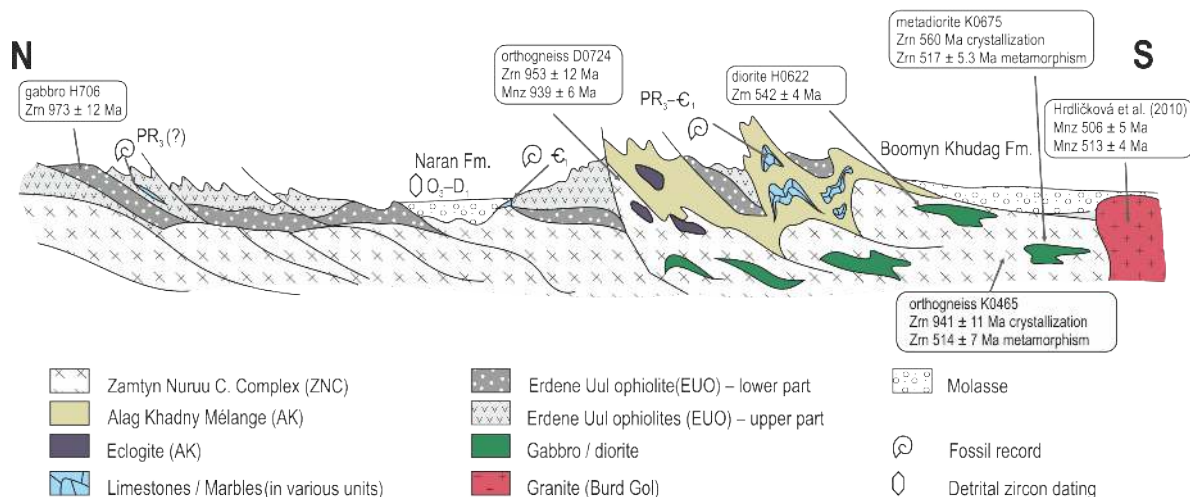


Figure 1.4: Section of the Zamtyn Nuruu (from Buriánek et al. (2017)).

1.7 Excursion area

Excursion area cover two geological transects from Lake to Gobi-Altai zones (Figs. 1.5, 1.6 and 1.7) in area of Chandman, Biger and Tsog soums in Gobi-Altai aymag. Presented localites were selected based on data collected in the framework of the geological survey (project Zamtyn Nuruu-50) funded by the International Development Cooperation of the Czech Republic and in the framework of the scientific research financed by Grant Agency of the Czech Republic and the Ministry of Education, Youth and Sports of the Czech Republic.

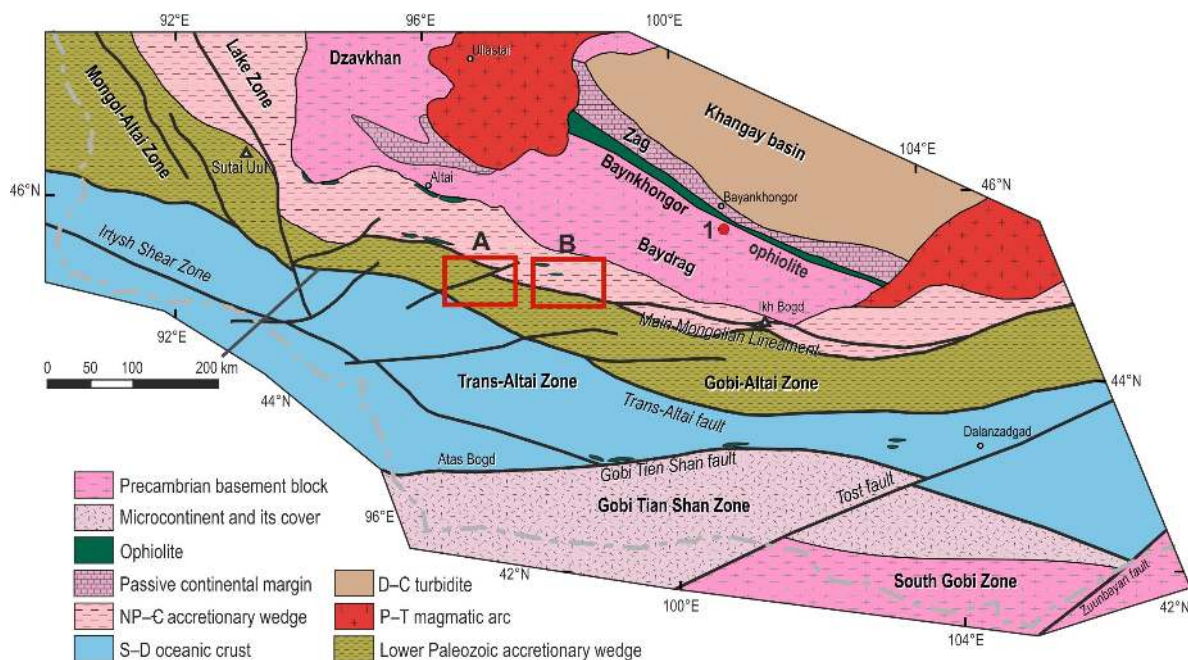


Figure 1.5: Overview of tectonic zonation of SW Mongolia with position of maps from Tsogt (A), Chandman area (B) and Bayankhongor locality (1). Modified from Buriánek et al. (2017).

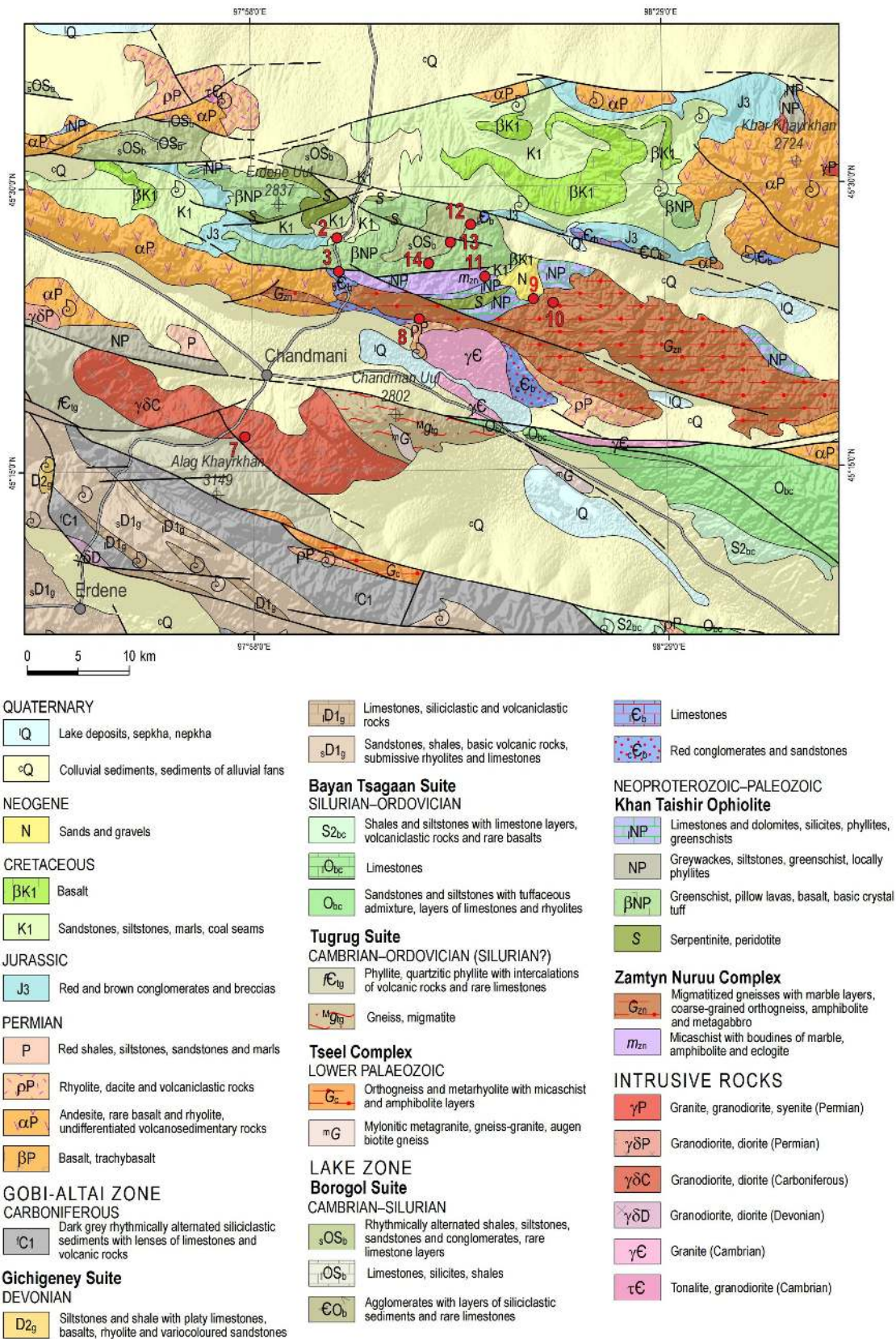


Figure 1.6: Position of excursion points on a geological map 1:500,000 of Chandmani area. Modified from (Hanžl et al. 2019).

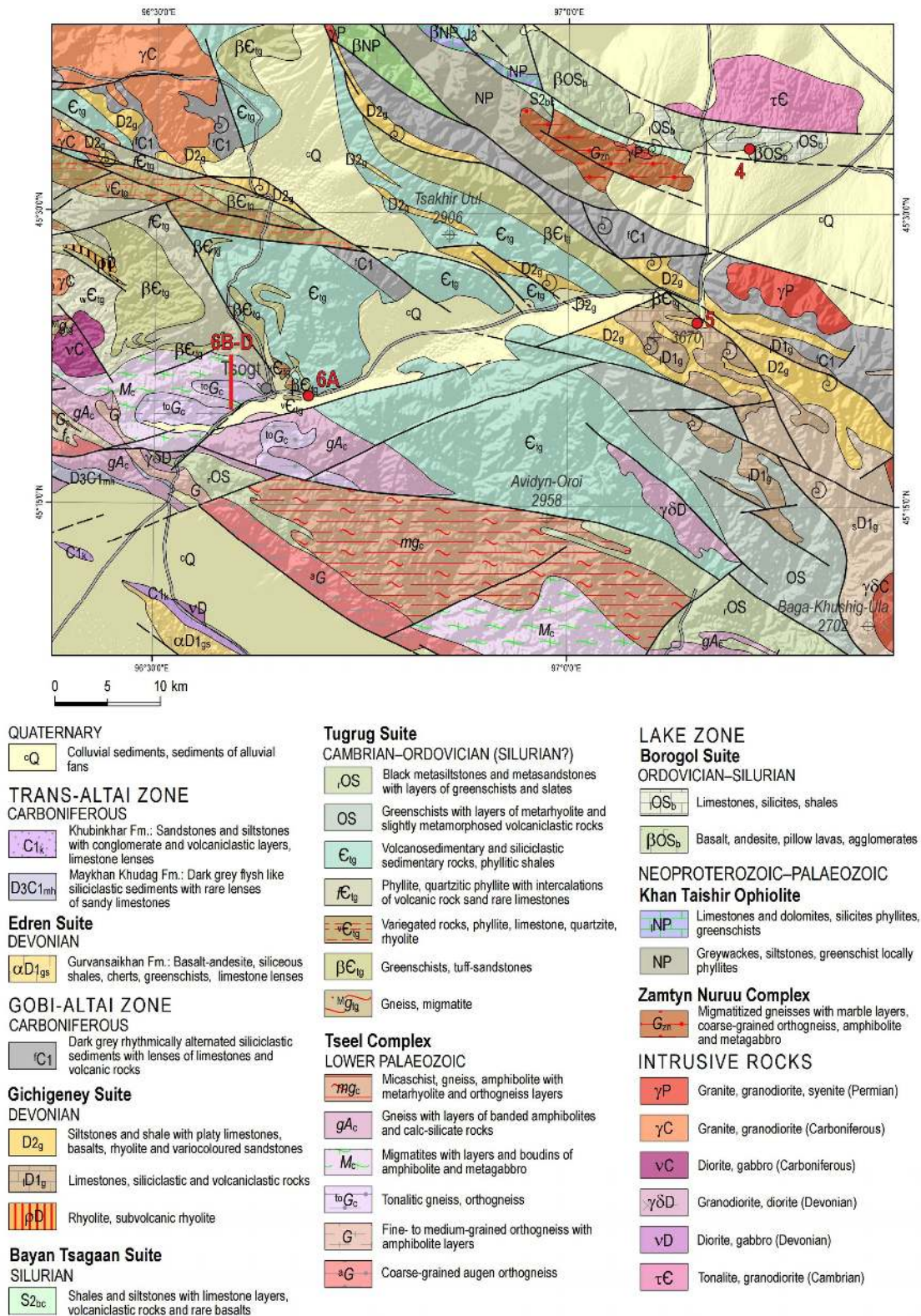


Figure 1.7: Position of excursion points on a geological map 1:500,000 of Tsogt area. Modified from (Hanžl et al. 2019).

2. Day I.

2.1 Metamorphism of Taatsyngol Complex (1)

A: N45°55' 22", E100°53' 21" E, B: N45°50' 51", E100°49' 47" E, C: N45°49' 19", E100°48' 6" E, south of Bayankhongor

The Taatsyngol section (Fig. 2.1) represents an excellent transect from the rocks of Dzag Formation and Bayankhongor ophiolite in the north to the metamorphic series to the south (Fig. 2.2 and 2.3). The low-grade rocks in the north are attributed to Bayankhongor ophiolite and are tectonically juxtaposed to a very low grade Early Palaeozoic Dzag Formation. However, the nature of depositional and tectonic contact of these two units is presently unclear. The southern margin of the low grade „ophiolitic unit“ is formed by an igneous complex consisting of gabbros and granitoids of Neoproterozoic–Cambrian age. This unit is covered unconformably by clastic sequences of probably Late Devonian to Carboniferous age. Further to the south occurs a high-grade complex of migmatites, granitoids and paragneisses, which was dated by Kozakov et al. (2007, 2012a) as Late Proterozoic to Early Cambrian. This unit shows polyphase tectono-metamorphic history that is revealing early MP-MT event followed by HT re-equilibration (Kozakov et al. 2012a). This author describes assemblage kyanite–staurolite–garnet–biotite–plagioclase–quartz and garnet–kyanite–muscovite–biotite–plagioclase–quartz schists that can be traced from the northwest to the southeast from the Ulziit Gol river to the Tuiin Gol river (Fig. 2.3). Kozakov et al. (2012a) reported PT conditions of 570–620°C and 8–10 kbar for kyanite bearing rocks. This author also reported a zircon age of the kyanite bearing granite and syenite estimated at 562 ± 2 and 564 ± 5 Ma (Kozakov et al. 2007) which supposedly characterizes the oldest amphibolite facies metamorphism of the Barrovian type. These previous studies also reported second metamorphic andalusite–sillimanite association typical for Buchan metamorphic series. An attempt was made to date second event by dating granitoids that show distinct crosscutting contacts with the main structural elements of the Taatsyngol Complex which yielded the zircon age at Vendian–Early Cambrian boundary (542 ± 2 Ma).

In the field, three generations of fabrics can be observed, from which the two early deformations may be related to the two events mentioned above. Going to the south, the degree of anatexis decreases continuously so that one passes progressively from staurolite bearing

gneisses (Figs. 2.4a, 2.5a–c) and garnet amphibolites (Fig. 2.4b) to garnet bearing schists (Fig. 2.5d) and finally to biotite phyllites. This spectacular Barrovian sequence is exposed in the valley of river Tuin Gol.

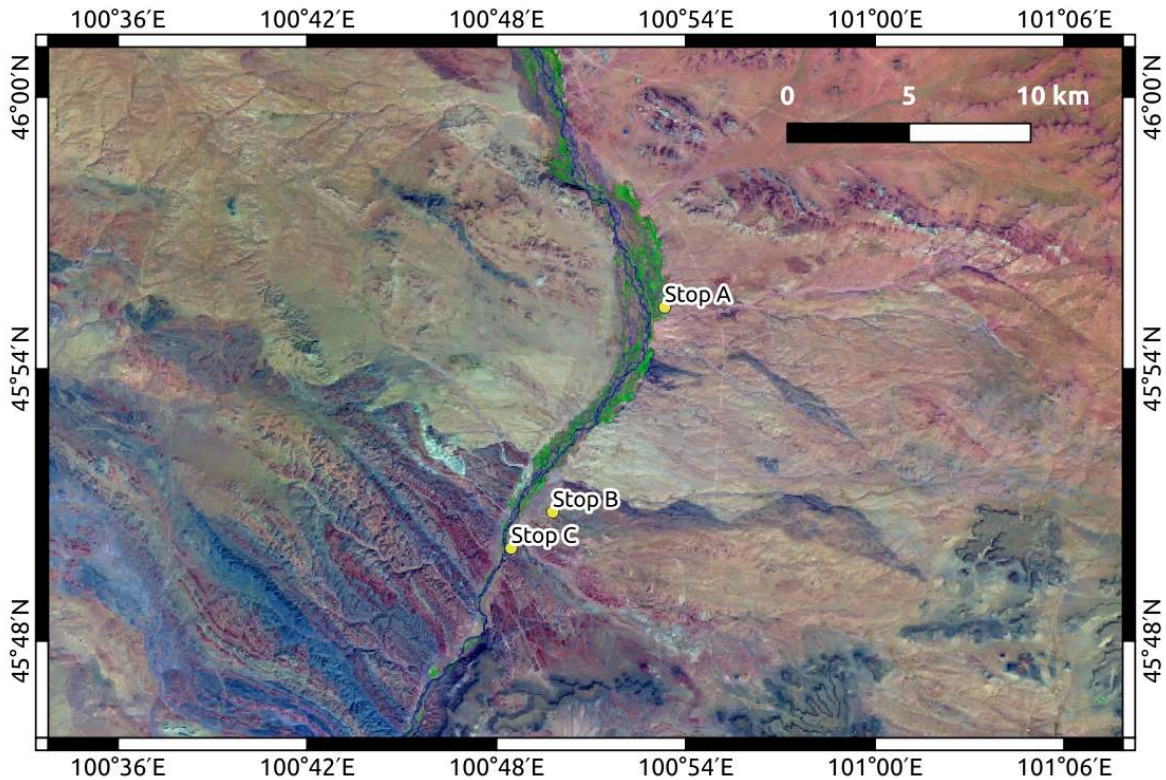


Figure 2.1: Position of excursion localities in Baydrag block south of Bayankhogor on Landsat 8 imagery.

The structures in all units show polyphase evolution characterized by early schistosity S1 reworking sedimentary bedding. This schistosity is reworked by secondary deformation, that is associated with upright folding and formation of regional cleavage S2 (Figs. 2.3, 2.4a), the metamorphic grade of which is increasing to the north. The last deformation is upright post-metamorphic folding F3 which is best documented by verticalization of the Devonian–Carboniferous sediments. This event modified pre-existing so far poorly understood architecture by intense steepening of the system, but without significant metamorphic overprint. Altogether, the relationships between metamorphism, magmatism, and deformation clearly point to an active margin setting and not to the old basement – an observation made already by Kozakov et al. (2007).

The first stop (Stop 1A) is located within the high-grade unit. Major lithologies are migmatitic biotite-garnet paragneisses, with garnet and sometimes with sillimanite. Amphibolites and metagabbros are also present. The whole migmatitic complex is crosscut by numerous granitic to pegmatitic dykes which show syn- to post-tectonic relationships with respect to the main NNW–SSE steep foliation S2. At several places relics of isoclinal folds can be observed with fold axis typically plunging steeply to the ENE.

The locality (Stop 1B) is a nice example of transposition of bedding-parallel gently west dipping foliation S1 into steeply ENE dipping cleavage S2 (Fig. 2.4a, 2.5a–b). The rock is a micaschist which contain porphyroblasts of garnet (around 5 mm large) and staurolite (up to 3 cm large). In the thin section, garnet is sometimes enclosed in staurolite and both

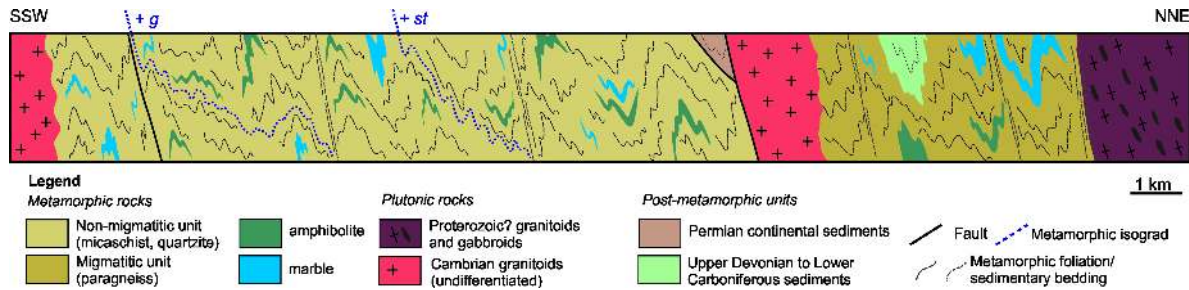


Figure 2.2: Schematic cross section along the line shown in Fig. 2.3

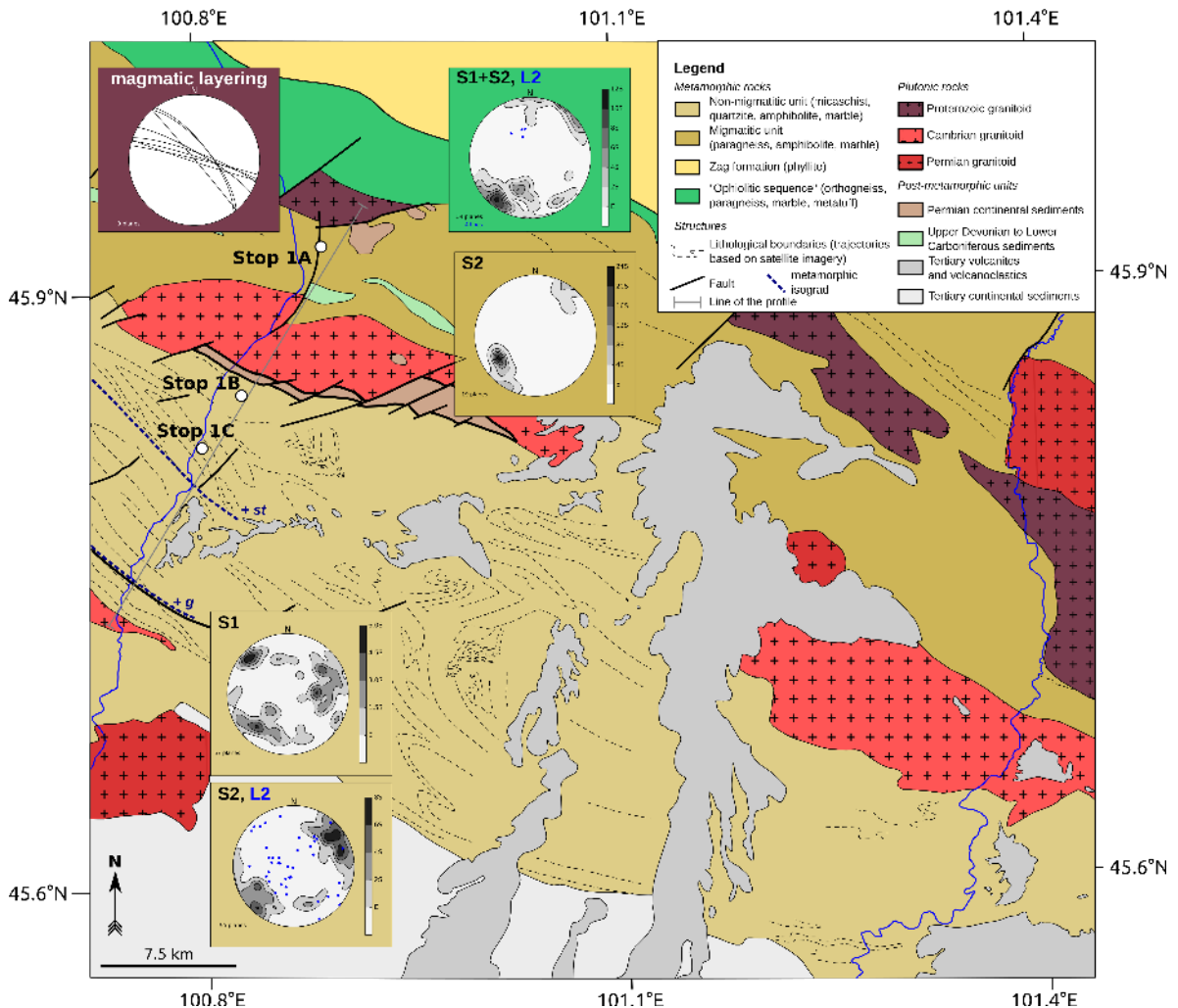


Figure 2.3: Simplified geological map of the Bayankhongor cross-section. Based on Soviet geological map at a scale 1:200,000 and satellite imagery.

minerals have straight and parallel inclusion trails, which imply sequential growth in the same deformation regime.

Garnet bearing amphibolites are typical rock-type at Stop 1C. The foliation is subvertical and WNW–ESE trending. The lower-grade metasediments will not be visited. However, rocks from garnet zone are dominantly fine-grained micaschists to muscovite quartzites with garnet porphyroblasts, which are intercalated by less abundant marbles, amphibolites and locally by



(a) Stop 1B - folding of S01 into main metamorphic fabric S2.



(b) Stop 1C - garnet-bearing amphibolites within a metasedimentary sequence.

Figure 2.4: Field photographs

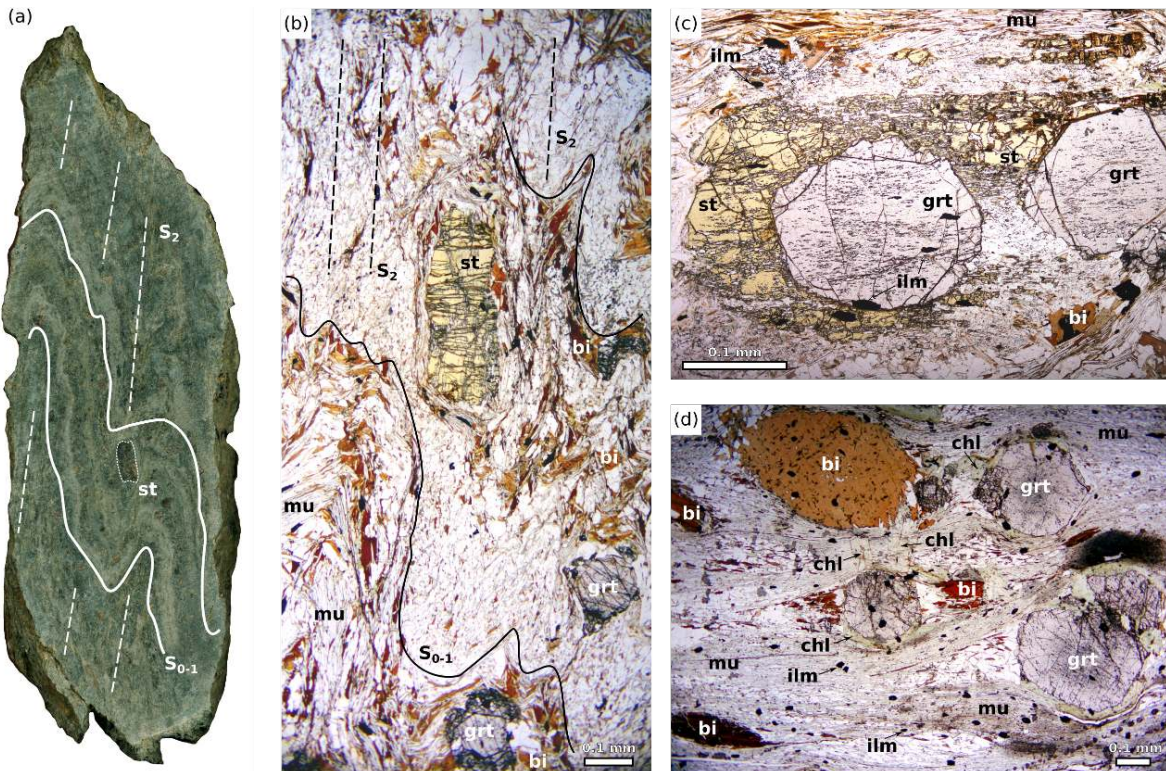


Figure 2.5: Hand specimen in (a) is 4 cm wide, and microphotographs (b), (c) from the staurolite zone (Stop 1B). Note folded bedding parallel foliation S0-1 and axial planar cleavage S2 (a-b). Staurolite porphyroblasts have oblique inclusion trails to the matrix foliation, but have parallel to inclusion trails in the garnets (c). (d) Thin section from the garnet zone in the south. Fine-grained micaschist containing garnet and biotite porphyroblasts affected by static chloritization. Parallel polars.

amphibole bearing gneisses. In the thin section (Fig. 2.5d), micaschists have fine-grained muscovite dominated matrix and garnet porphyroblasts. The main foliation is overgrown by randomly oriented porphyroblasts of biotite up to 1cm large.

Ophiolite sequence of the Erdene Uul,
Lake Zone (2)
Cambrian molase, Boomyn Khudag
(3)

3. Day II.

3.1 Ophiolite sequence of the Erdene Uul, Lake Zone (2)

N45°27' 7", E98°4' 23", viewpoint on the main road 16 km NNE from Chandman soum
A panoramic view (Fig 3.1) to southern slopes of the Erdene Uul (2837 m a.s.l.) opens from the band of the main road Chandman – Gobi-Altai. Red Upper Jurassic conglomerates and varicoloured Lower Cretaceous deltaic sediments expose in valley in foreland of the mountain. The Erdene Uul was traditionally classified as a part of the Khan Taishir formation which was defined and assigned to Neoproterozoic (Vendian) by Markova (1975) in the Khan Taishir ridge south of Altai town. The ophiolite association inside the Khan Taishir massif was described by Zonenshain and Kuzmin (1978).

The Erdene Uul ophiolite further west represents a relic of nearly complete ophiolite sequence (Hanžl et al. 2007; Perfiliev and Kheraskov 1980) characterized by pillow lavas with red cherts and associated ultramafic rocks, complemented by gabbros and ophicarbonates (Fig. 3.2). Various types of metabasalts including pillow lavas, greenschists and agglomerate tuffs with lenses of limestones are predominant rocks in the formation (Fig 3.4). The lithological character of the sequence points to the oceanic environment of sedimentation accompanied by huge volcanic activity. Ultramafic rocks are exposed as large boudins in the bottom of the sequence. All rocks of the suite were metamorphosed under the greenschist facies conditions and are usually deformed. Rocks form layers and lenses, which follow E–W trending, south dipping metamorphic foliation which rotates in the N to NW–SE trend.

Epidotized greenschists, metabasalts and mafic tuffs are the most common rocks of the Khan Taishir Fm. The boundaries between the rocks are transitional. All these rocks are strongly chloritized and epidotized, the deformation is inhomogeneous and is marked by foliation development and transition to greenschists. The oval, up to 50 cm large volcanic bombs and fragments are up to 2 cm long, prismatic crystals of black amphibole are a characteristic feature of the agglomerate tuffs. Metabasalts are massive, fine- to medium-grained and they consist of chlorite, plagioclase, epidote, actinolite and minor titanite, magnetite and carbonates. Pillow lava structures are well preserved on the S slope of the Erdene Uul accompanied by **red cherts and silicite** (Figs. 3.4a and 3.4b).

Recrystallized limestones and ophicarbonate are exposed in the form of lenticular



Figure 3.1: Erdene Uul Mt. on Google Earth imagery. View to N.

bodies and layers on the N slope of the Erdene Uul, the thickness of the largest body is about 35 meters (Fig. 3.4c). They are fine-grained, strongly foliated, grey. Consist of recrystallized calcite but primary textures can also be recognized in some cases (sparite, micrite, fossils). Isolated quartz grains or small quartz veins are common. Zhuravleva in (Rauzer et al. 1987) described the oncolites *Ambigolamellatus horrida* Z. Zhur and *Osagia nimia* Z. Zhur to be of Vendian age here. Locally limestones contain fragments of deformed basalts and ultramafic rocks (Fig. 3.4d).

Serpentinized peridotite, serpentinite (Fig. 3.3a) form numerous tectonic boudins with the largest body intruded by gabbros to tonalites in the SE foot of the Erdene Uul. Metamorphic mineral assemblage in serpentinites from the Erdene Uul (Atg + Di) indicates PT conditions $\sim 450\text{--}550^\circ\text{C}$ (Spear 1993). Primary enstatite ($\text{Fe}/(\text{Fe}+\text{Mg}) = 0.11$) is partially replaced by diopside ($\text{Fe}/(\text{Fe}+\text{Mg}) = 0.00\text{--}0.09$).

Altered and usually deformed **gabbro, anorthosite and gabbro-amphibolite** form irregular body intruded between serpentinite and metabasalts and thin tectonic slices in metabasalts. Gabbros with lenses of anorthosites and tonalite like rocks are strongly altered. The rocks generally correspond to gabbro (with exception of two strongly altered samples) in chemical classification TAS as well as P-Q. They are medium- to coarse-grained. Laths of plagioclase and pyroxene grains are the main constituents of these rocks, the mineral composition further comprises actinolite, carbonate and chlorite (Fig. 3.3b). Rare quartz grains are secondary. Pyroxenes are often replaced by actinolite and chlorite. Opaque minerals and biotite partially replaced by chlorite are accessory. Cumulate layers composed by plagioclase or amphibole (\pm pyroxene) are common in these rocks.

Metabasalts and greenschists correspond to basalt and basaltic-andesite, the crystal and agglomerate tuffs have a composition of basalt to andesite in the TAS classification. Studied

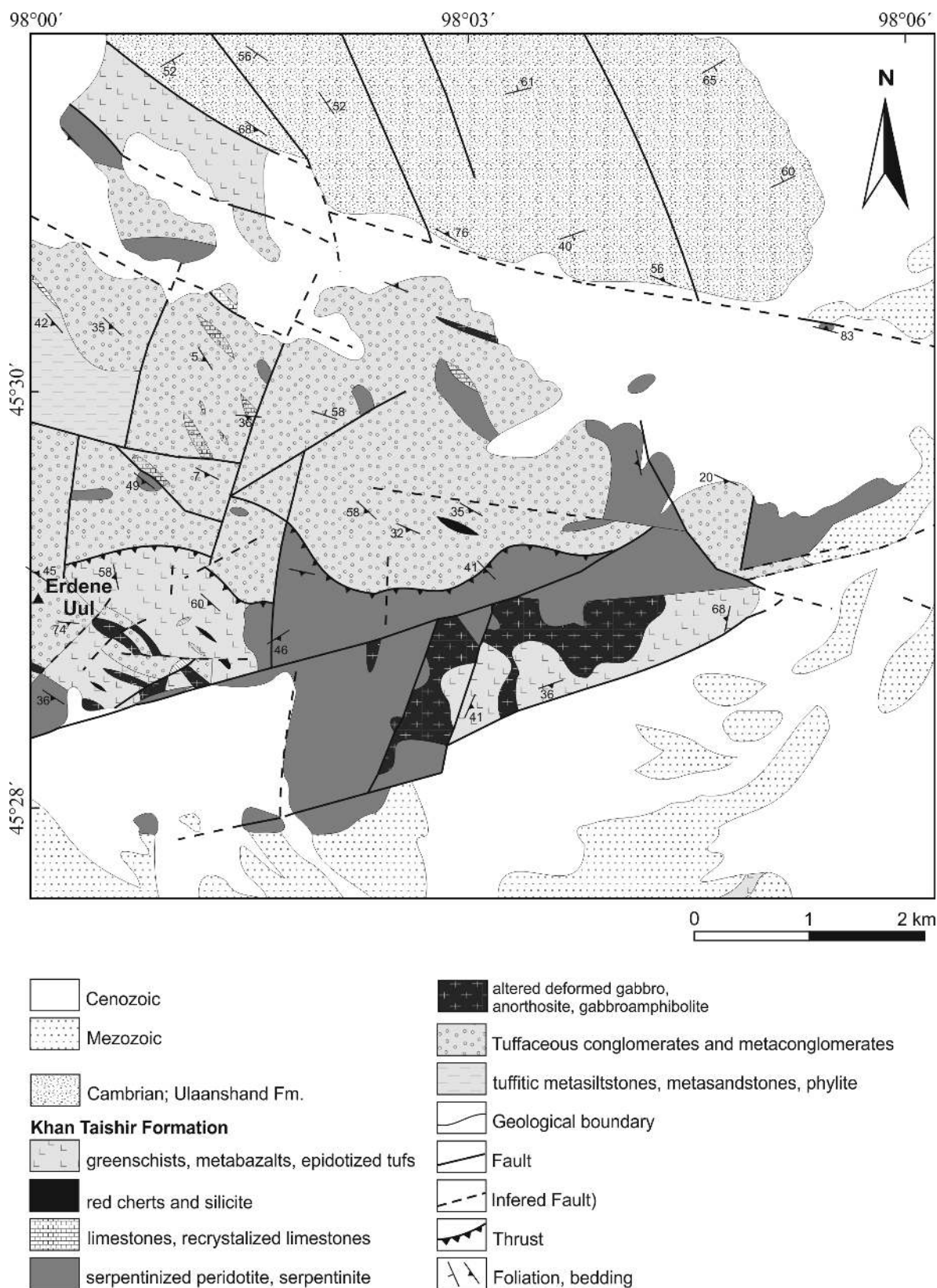
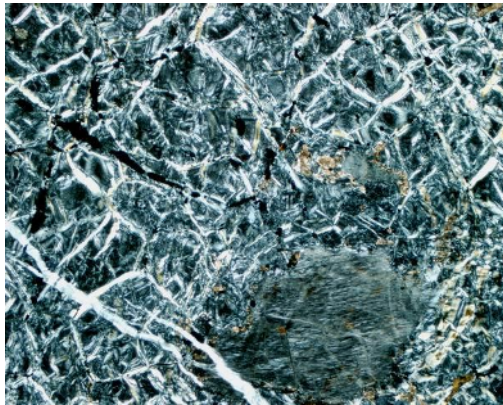


Figure 3.2: Geological map of the eastern part of the Erdene Uul.



(a) Relics of pyroxene in serpentinite.



(b) Ophitic texture in gabbro.

Figure 3.3: Microphotographs



(a) Pillow lavas.



(b) Red Cherts.



(c) Limestone layer in metabasalts.



(d) Sheared ophicarbonates.

Figure 3.4: Field photographs.

igneous rocks show dominantly the trace-element signature indicating an oceanic island-arc geotectonic environment; some even tend to a boninitic affinity. The newly obtained highly radiogenic whole-rock Nd isotopic compositions ($\epsilon_{940}^{Nd} > +6.5$) together with primitive Sr isotopic signature ($^{87}\text{Sr}/^{86}\text{Sr}_{940} < 0.703$) indicate a direct derivation from Depleted Mantle-like reservoir. Gabbros of the ophiolites from southern slopes of the Erdene Uul show tholeiitic character and in various geotectonic plots fit to island-arc fields. The U–Pb ages obtained

from these rocks are 1493 ± 33 and 973 ± 12 Ma. The former, upper intercept age seems to represent the inheritance of zircon grains while the latter, lower intercept one reflects probably the crystallization. These ages are distinctly older than the published U–Pb zircon ages from classic outcrops of Khan Taishir ophiolite south of Altai city (180 km NW of Erdene Uul) of 568 ± 4 (Gibsher et al. 2001) and 566–573 Ma (Jian et al. 2014). Younger ages provided also other ophiolites N of the Main Mongolian Lineament, e.g. plagiogranites from Dariv ophiolites (571 ± 4 Ma: Kozakov et al. 2002), Sm–Nd isochron data for amphibole gabbro from Bayankhongor ophiolite (569 ± 21 Ma: Kepezhinskias et al. 1991) and U–Pb zircon ages for anorthosite, gabbro and plagiogranite (636–655 Ma: Jian et al. 2010; Kovach et al. 2005). In conclusion, gabbro from the Erdene Uul represents the oldest oceanic rock of the CAOB, probably corresponding to a Mirovoi oceanic fragment (Buriánek et al. 2017).

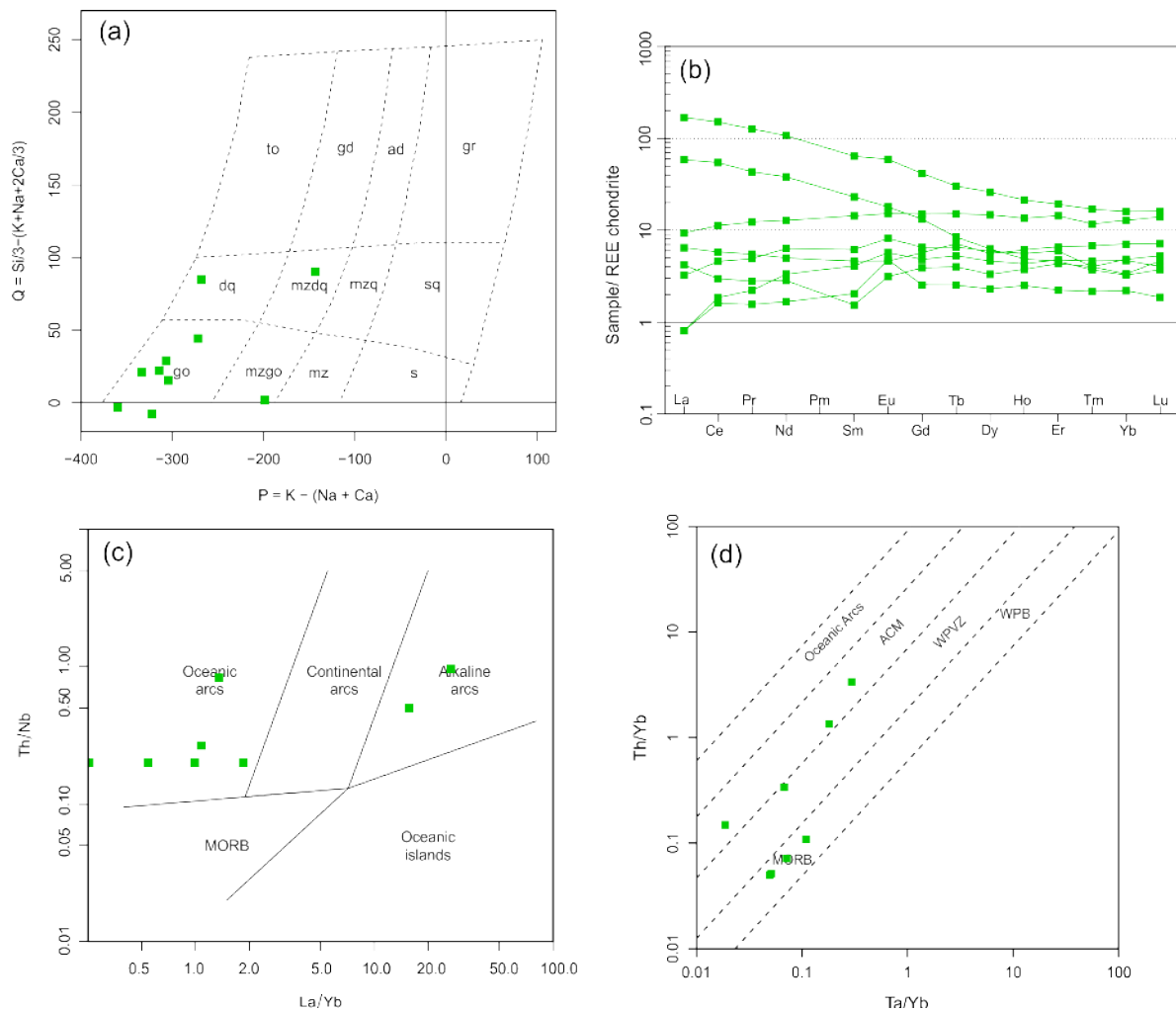


Figure 3.5: Geochemical characteristic of ultramafic and gabbroic rocks from the Erdene Uul. (a) P-Q classification of Debon and Le Fort (1983); (b) REE patterns (Boydton 1984); (c) geotectonic diagrams of Hollocher et al. (2012) and (d) Schandl and Gorton (2002).

3.2 Cambrian molase, Boomyn Khudag (3)

N45°23' 55", E98°4' 58", rock along the road 15 km NE from Chandman

The Boomyn Khudag Formation defined by Hanžl et al. (2007) corresponds to a part of sedimentary rock sequence described by Rauzer et al. (1987) as an undifferentiated Lower–Middle Devonian formation. It is exposed in a narrow NW–SE oriented belt between Boomyn Khudag and Khooroiin Khudag (Fig. 3.6) at western tips of the Zamtyn Nuruu and Unegt Uul mountain ranges. These sediments do not contain any palaeontological record that would enable to determine their age. They unconformably overlie the Neoproterozoic metamorphic rocks of the Zamtyn Nuruu and form the footwall of the Permian volcanic rocks. These sediments were intruded by the Late Cambrian Burd Gol Massif, which encloses thermally metamorphosed septa of sandstones in its northern part.

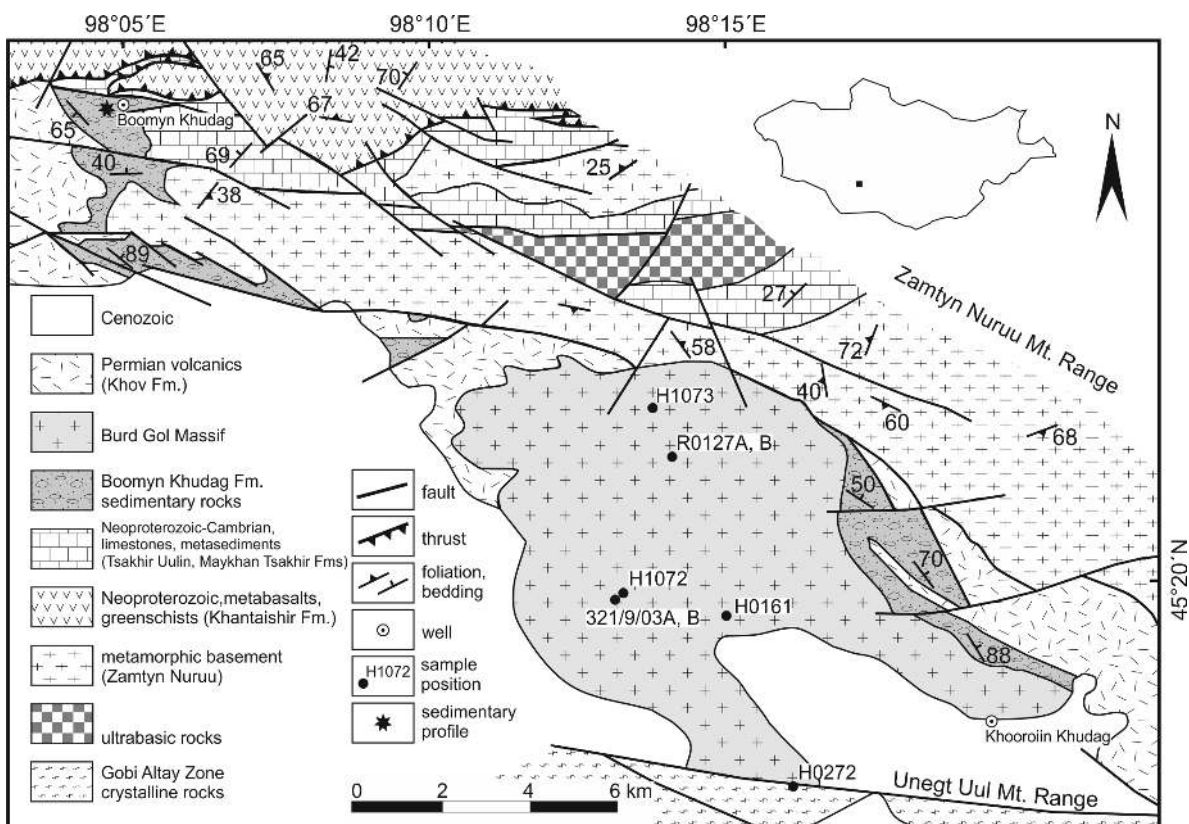


Figure 3.6: Map of the Boomyn Khudag Fm. exposures (Hrdličková et al. 2010). Position of profile on Fig. 3.8 shown by asterix.

The Boomyn Khudag Formation is formed mainly by conglomerates. They are characterized as red to light brown, massive, matrix-supported, poorly sorted, ungraded cobble conglomerates. The conglomerates locally alternate with small lenses and layers of medium-grained, massive sandstones. The cobbles of average diameter of ca. 8 cm (A-axis) and maximum size of c.1 m are well rounded, consisting of gneisses, basalts, undifferentiated volcanic rocks, cherts and quartz in particular. Matrix is composed of grains of quartz, K-feldspars, plagioclases and rock fragments. Biotite and carbonates are also present. The massive cobble conglomerates correspond to lithofacies Gm and massive sandstones to lithofacies Sh (Bridge 1993; Miall 1978).

Red to purple-red, very coarse- to fine-grained arkosic sandstones and arkoses with layers of mudstones and siltstones occur in the hanging wall of the conglomerates (Fig. 3.7). They are poorly sorted, being composed mainly of subrounded to subangular grains of quartz, K-feldspar and plagioclase. Quartz grains predominate; K-feldspars and plagioclases are present in variable amounts. Micas and ultra-stable minerals (zircon, tourmaline, rutile), ore minerals, zoisite, epidote and monazite are the common accessories. Sharp fragments of vitrite and volcanic rocks are rarely present. Basal matrix is composed of clay minerals (locally sericitized), chlorite and carbonate.



Figure 3.7: (a) Well sorted matured conglomerates are most pronounced lithology of formation, locally they are cleaved, (b) Rhythmic alternation of red siltstones and sandstone.

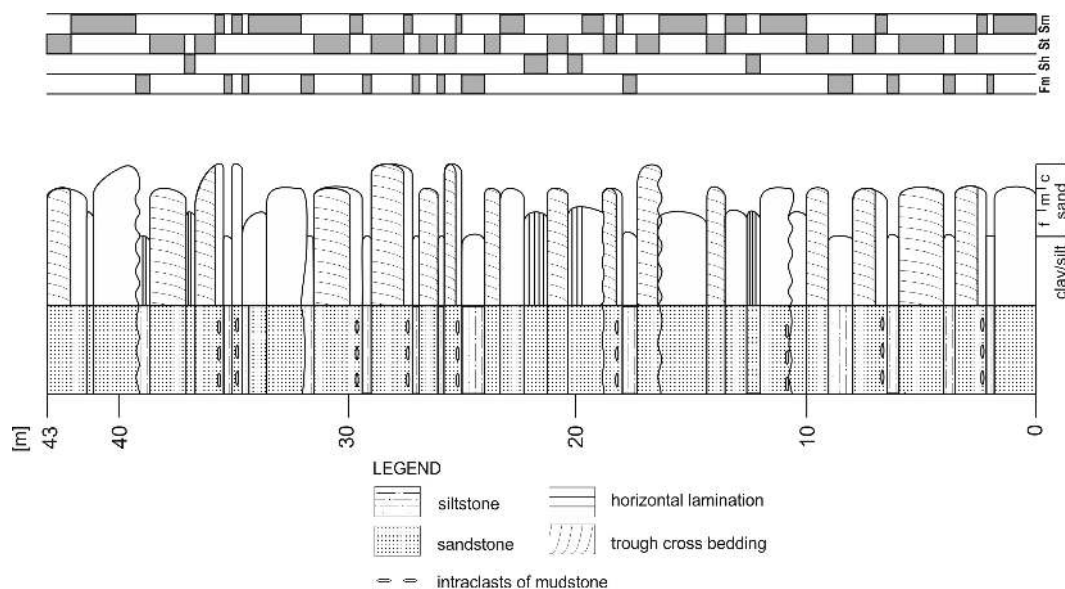
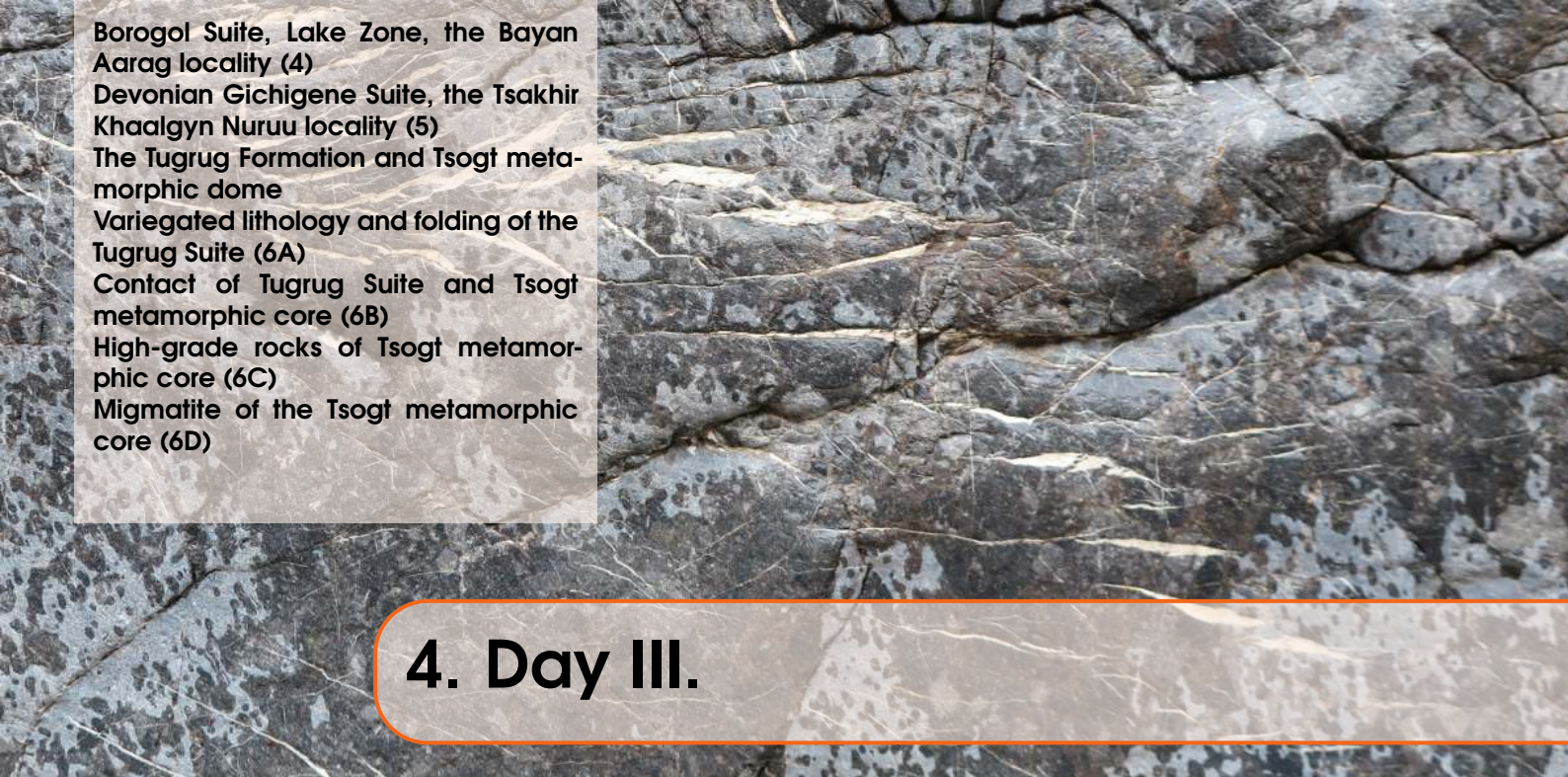


Figure 3.8: Profile of the fine-grained sequence of Boomyn Khudag Formation in hanging wall of conglomerates.

A section, 43 m long, of arkosic sandstones and arkoses with layers of mudstones and siltstones has been studied in detail (Fig. 3.8). Four lithofacies (Fm, Sh, St and Sm according to Miall 1978 and Bridge 1993) have been recognized within the logged profile on the basis of sedimentary textures and structures.

Conglomerates, sandstones, mudstones and siltstones of the Boomyn Khudag Formation are terrestrial sediments deposited in arid and semiarid conditions. The lithofacial transitions Gm–Sm were mostly caused by catastrophic sheet floods. The facial association could be the most likely interpreted as sediments of debris-flows deposited in alluvial fans eventually or as cores of levees of a braided river.

The rocks are represented by medium-grained red arkoses to arkosic sandstones with intercalations and layers of siltstones and mudstones. Sedimentary bedding is preserved; locally, small-scale structures such as cross bedding can be observable. The mineral composition corresponds to original quartzo-feldspathic arkoses with no preserved matrix and with the relics of the rock fragments, stable minerals as zircon and rutile are relatively common accessories. The newly formed muscovite porphyroblasts, quartz recrystallization and extensive silicification bear evidence of thermal and fluid affection during the emplacement of Late Cambrian Burd Gol granite massif. The sediments of the Boomyn Khudag Formation onlapping the metamorphic rocks of the Zamtyn Nuruu are indirectly dated as Cambrian, because they are affected by thermal metamorphism caused by the Burd Gol granite intrusion (Hrdličková et al. 2010). Conglomerates, sandstones and siltstones of the Boomyn Khudag Formation are of terrestrial origin, deposited under arid or semiarid conditions in alluvial fans environment. Sedimentary character and transgressive position on the metamorphic rock of Zamtyn Nuruu indicate molasse-like character of the sediments.



Borogol Suite, Lake Zone, the Bayan Aarag locality (4)
Devonian Gichigene Suite, the Tsakhir Khaalgyn Nuruu locality (5)
The Tugrug Formation and Tsogt metamorphic dome
Variegated lithology and folding of the Tugrug Suite (6A)
Contact of Tugrug Suite and Tsogt metamorphic core (6B)
High-grade rocks of Tsogt metamorphic core (6C)
Migmatite of the Tsogt metamorphic core (6D)

4. Day III.

4.1 Borogol Suite, Lake Zone, the Bayan Aarag locality (4)

N45°33' 40", E97°14' 1", valley 19 km SSE from Biger soum

Rocks on the left bank of wadi represent deep water sequence of the Ulaanshand Formation together with Naran Formation which are part of the Borogol Suite (Markova 1975) in the Lake Zone (Fig. 1.3). The studied locality is situated north of E–W trending branch of Ikh Bogd fault. The Ulaanshand Formation defined by Markova (1975) of assumed Cambrian age consists of deep marine sediments and coeval bimodal volcanic and volcanoclastic rocks. These facies, as well as whole rock chemical composition volcanic rocks, provides evidence for an island arc setting (Dergunov 2001).

Recrystallized silicified dolomitic limestones with intercalations of dark, horizontally laminated, shales and reddish to brownish cherts (up to 50 cm thick layers) are dominating rocks on the presented profile. Intraformational limestone breccia (up to 1 m thick layers) and slump textures (Fig. 4.1a). These textures indicate submarine slope environment probably related to coeval volcanic activity. Deformed and low-grade metamorphosed volcanic and volcanoclastic rocks of the formation are exposed to the NW from the main road Biger–Tsogt. Basaltic hyaloclastite, tuff and bedded volcanoclastic rocks dominate there. Pillow lavas with individual pillows sized between 30 to over 50 cm are locally preserved (Fig. 4.1b). Lava flow covered by red chert and crosscut by up to 5 m thick sills of dolerite basalts are more common. Basalts are fine- to medium-grained, porphyritic with sub-ophitic texture. Fine-grained laminated rhyolite tuffs form up to several m thick layers. Rhyolite and dacite dykes cutting the sedimentary and pyroclastic deposits. Acid lava consists of K-feldspar, quartz, plagioclase. Muscovite is embedded in a fine-grained groundmass.

Sample of massive lava from E part of ridge yields age of 425 Ma, zircon data from tuff conglomerate are scattered showing “clastic” ages of 550 to 480 Ma (unpublished data of CGS). These ages indicate younger, even Ordovician age of sequence than assumed middle Cambrian age (Kröner et al. 2010). Volcanic rocks have a bimodal composition and were classified as basaltic andesite and rhyolite in the TAS diagram. Low K₂O contents correspond to tholeiitic series of Peccerillo and Taylor (1976). Geotectonic discriminations diagrams point to island arc paleoenvironment (Fig. 4.2). Trace element spider patterns (Fig. 4.3a) are

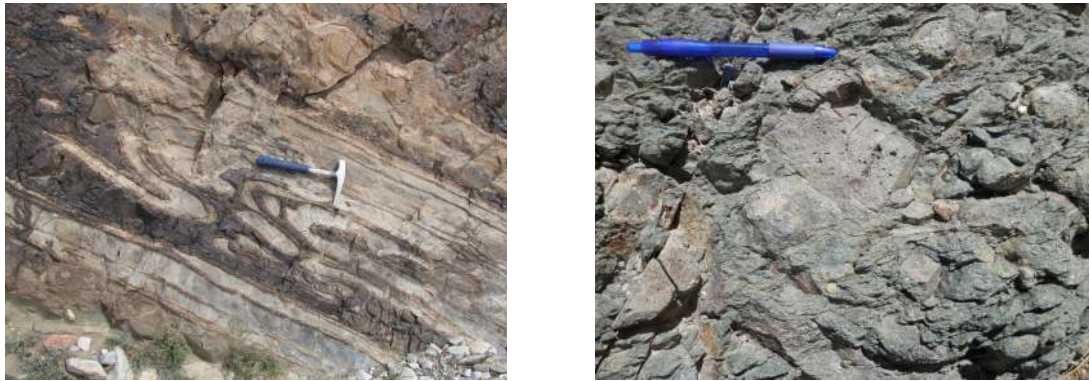


Figure 4.1: (a) Intraformational slump folds in limestones with cherts layers, (b) amygdaloidal basaltic lava with poorly preserved pillows.

characteristic by strong depletion in Nb, Ta and Ti. Chondrite-normalized REE patterns (Fig. 4.3b) are flat with depletion in LREE for basalts similar to NMORB trends. REE contents in rhyolites are very low, trends are flat only with negligible negative Eu anomaly.

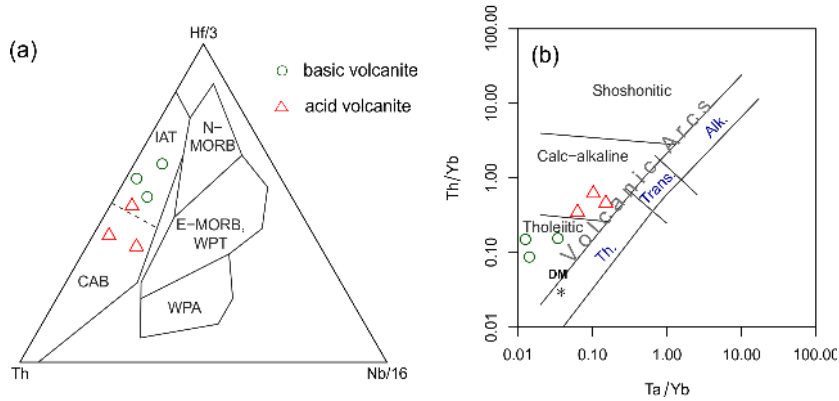


Figure 4.2: Volcanic rocks of the Ulaanshand Formation close to Biger in geotectonic diagram of (a) Wood (1980) and (b) Pearce (1982).

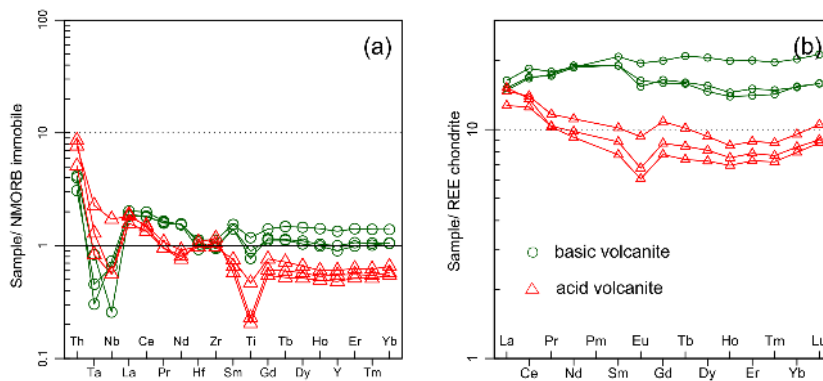


Figure 4.3: Trace elements patterns in (a) NMORB (S. S. Sun and McDonough 1989) and (b) chondrite normalized diagrams (Boynton 1984).

4.2 Devonian Gichigene Suite, the Tsakhir Khaalgyn Nuruu locality (5)

N45°24' 44", E97°9' 32", 34 km S from Biger soum

Representative outcrops of the Palaeozoic sequences of the Gichigene Suite (Hanžl et al. 2018) composed of Takhilt, Duchiindavaa and Gichigene formations (Hanžl et al. 2007; Rauzer et al. 1987) are exposed in the canyon just S of the remarkable turning of the road Biger–Tsogt (Fig. 4.4). The profile starts in weathered Carboniferous siltstones while the tectonic slice of the Middle Devonian claystones is overburden by the Quaternary debris. Following outcrop of quartzitic chlorite-sericite phyllite could be correlated with the Cambrian–Ordovician Tugrug Suite. These low-grade metasediments with quartz layers are intensively folded by small irregular folds. The contact of the overlying Lower Devonian sequence with the Tugrug Formation is discordant, steeply dipping to the S (Fig. 4.5). The Lower Devonian quartz sandstones passing to conglomerates are exposed at the bottom whereas in the hanging wall limestones and locally lenses of black siltstones dominate. In the canyon, white, massive recrystallized limestones dominate and towards the S contain tectonic lenses of black siltstones belonging to the flysch sequence of the Tsokhoriin Nuruu Formation.



Figure 4.4: Lower Devonian limestones in the NW termination of the Gichigene Nuruu range, view from the N.

The Lower Devonian limestone and terrigenous and/or volcanic sequences form NW–SE trending belt in the eastern Mongolian Altay which was termed as the Gichigene Nuruu Fm. by Tsukernikov in Rauzer et al. (1987). Lower Devonian rocks were firstly described in the area of Gichigene–Erdene Sum by Zonenshain (1970). The overlying Middle Devonian Takhilt Fm. was firstly described by Markova and Sharkova (1977) in the mountain range of Tsakhir Khalgain.

The Gichigene Suite can be generally characterized as a volcano-sedimentary complex including both basic and acid volcanics, pyroclastics and a wide spectrum of sediments, usually with substantial volcanic admixture. The sandstones and mudstones associated with conglomerates dominated in the lower part of the Gichigene Suite. Sandstones (greywackes) represent a mixture of detritus derived from slightly metamorphosed sediments (sericitic schist) and volcanic rocks of magmatic arc. The average thickness of a body of massive conglomerates in the bottom of the sequence is 5 m. An average diameter of the pebbles varies between 2–5 cm (maximum diameter is around 15 cm). Volcano-sedimentary lithofacies dominate in the hanging wall and consist of volcanic and volcanoclastic rocks, locally with several m thick layers of clastic sediments. Basic to intermediate volcanic rocks form lenticular bodies up to several meters thick usually consist of pillow flows and minor lobate flows accompanied

with hyaloclastites. Felsic rocks and their tuffs are common mainly in the upper part of the sequences. The chemical composition of basic volcanic rocks of the Gichigene Suite range from basalt to basaltic andesite (rare also trachyandesite) according to TAS diagram classification (Le Bas 2000). Felsic rocks can be classified as rhyolite to dacite according to SiO_2 content (66.5 and 81.4 wt.%). In geotectonic diagrams of Meschede (1986) and Wood (1980), the samples occupy the fields Volcanic-Arc Basalts with calc-alkaline signatures. Mudstones and biostromal limestone are dominant member uppermost part of both formations.

The Lower Devonian (Upper Lochkovian to Emsian) age has been determined at least for part of the Gichigene Fm. in the light grey, white and pink-grey biosparitic limestones, often forming tectonically confined cliffs. These, often lens-like limestone bodies, contain locally very rich association of crinoid-coral-brachiopod.

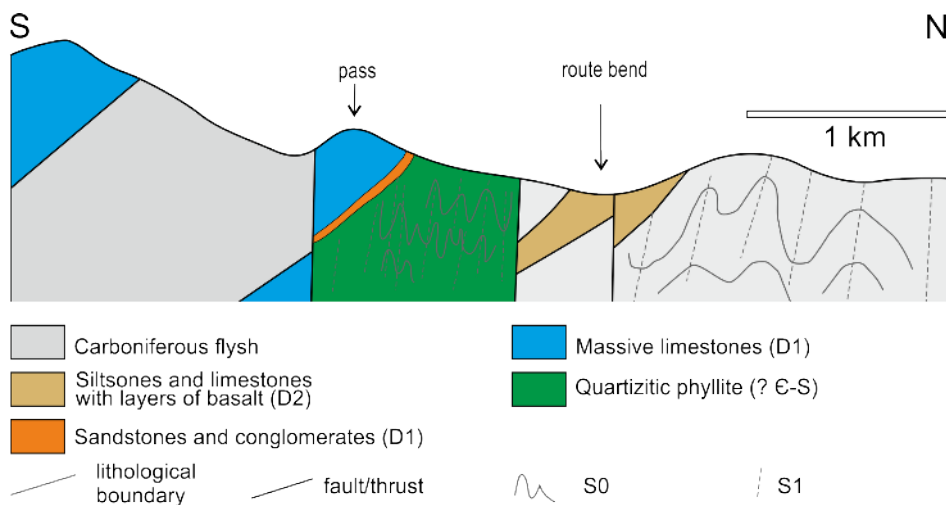


Figure 4.5: Idealized cross section through the contact of the Devonian and Carboniferous rocks on the N slope of Tsakhir Khaalgyn Nuruu.

Although the fossil remains mostly suffered from recrystallization, the columnals and pluricolumnals of massive crinoids *Trybliocrinus* sp. (col.), *Mediocrinus* sp. (col.), *Salaiocrinus* sp. (col.), articulate brachiopods (*Atrypa* sp., *Leptaenopyxis* sp., *Athyridae* indet., *Rhynchonellidae* indet.), were found at together with common, but indeterminable tabulate corals, algal structures, remains of the ?cephalopods, indeterminable trepostomate bryozoans a. o. An extremely rich faunal association in well-preserved reef structure containing frequent corals *Cladopora* sp., *Favosites* div sp. and *Thamnopora* were found. The findings of branching tabulate coral cf. *Lecomptia* sp. indicates the Pragian age. The remains (Fig. 4.6a) of massive crinoids *Cyclocaudex* sp. (col.), brachiopods *Sieberella* sp. and rare remains of gastropods *Praenatica?* sp. support this age determination. The associations collected in the SE Gichigene range (Hanžl et al. 2007) indicate rather Pragian (late Lochkovian to Emsian) age and their composition is very similar to the association from some localities of the Takhilt Fm. These locally very rich faunal associations indicate the shallow-water marine environment in the photic zone, with developed biostromes and bioherms buildups, inhabiting the upper portions of the seafloor elevations. These observations correspond well with the older concept (Rauzer et al. 1987) mostly shallow-water Takhilt Fm. (Pragian age) and rather deeper-water (but with isolated shallow-water carbonate reefs) of the Gichigene Fm. s. l. (Pragian–Emsian age).

The rock belt of the Gichigene Suite generally displays NW–SE course; the bedding is generally subparallel with the belt trend. Bedding planes dip under medium angles both to the SW and NE. Along the fault contacts, the bedding is rearranged to the sub-vertical position. The character of bedding orientation proved the presence of large folds in the unit. The cleavage of NNE–SSW trending and steeply dipping to the S cleavage is commonly developed in the rocks (Fig. 4.6b).



Figure 4.6: (a) Block of the fossiliferous limestone in bottom of valley, (b) pencil like disintegration of fine-grained sandstone along intersection of bedding and cleavage.

Black siltstones exposed in tectonic slices are part of the Tsokhoriin Nuruu Formation of Lower Carboniferous Age. The unit was firstly described by Rauzer et al. (1987) in Mongolian Altai as 2–8 km wide, NW–SE trending belt of deep-water marine sediments. They described transgressive discordant contact with the Middle Devonian Togotyn Fm. The age was based on rare finds of brachiopods, crinoids and lepidophytes (Rauzer et al. 1987). New finds of rare crinoid (*Cyclocaudiculus* sp. col.) and brachiopod remnants range from middle Devonian to Carboniferous age (up to Viséan). There were occasional findings of ichnofossils (*Planolites* isp. and *Dictyodora liebeana*) (Fig. 4.7). The Early Carboniferous age is most likely. In detrital zircons from two samples from the belt of flysch NW of site, population of about 500 Ma dominates and minor clusters ranging from 500 to 1000 Ma (unpublished data of CGS).

The Tsokhoriin Nuruu Fm. is formed of rhythmic alternation of grey to dark grey siltstones, greywackes and conglomerates. Calcareous sandstones and undifferentiated tuffs and tuffaceous sediments are less abundant. The formation is intruded by dykes and sills of basalts and rhyolites with a thickness of up to the first tens of meters. Sediments have a flysch character, with deep-water turbidite origin. Ripple and current marks and bioturbations are sporadically preserved on the bedding planes. The psammites probably represent a mixture of detritus derived from craton and slightly metamorphosed sediments, which were randomly supplied with detritus from the core of a magmatic arc. Based on the whole rock analyses, siliciclastics of the Tsokhoriin Nuruu Fm. were derived from chemically fresh detritus mostly of acid volcanic rocks and granitoids. The rocks of the Tsokhoriin Nuruu Fm. are folded into open, steep folds of an order of X00 m large. The axial planes are generally subparallel to the cleavage and dip steeply to the SSW. The general vergence of folds is to the NNE, but vertical axial planes are quite common. The fold axes are gently dipping both to E and W.



Figure 4.7: Examples of sedimentary structures of the Tsokhoriin Nuruu Fm.

4.3 The Tugrug Formation and Tsogt metamorphic dome

The Tugrug Formation was defined by Markova (1975) on the southern slopes of the Mongolian Altai. In the northern part of the Tsogt region, the Tugrug Formation is formed by slates to sericite-chlorite phyllites with carbonaceous admixture and layers of tuffitic sandstones. Towards the south prevail epidote-chlorite greenschists alternating with layers of tuffitic sandstones (greywackes) and locally preserved flattened pillow lavas (Hanžl et al. 2017). Volcanic rocks of the Tugrug Formation are represented by subalkaline series forming a basalt – basaltic andesite – dacite – rhyolite compositional trend.

The Silurian stratigraphic age of the Tugrug Formation was assumed by analogy to similar sequences in the Shine-Jinst district to the east (Markova 1975). However, Cambro-Ordovician age was proposed for this slightly metamorphosed volcanosedimentary sequence in the geological maps of Borzakovskii (1985) and Rauzer et al. (1987). As there are no palaeontological data from the study area we assume Cambrian to Ordovician age for the Tugrug Formation based on detrital zircon age spectra from the paragneisses of the Mongolian Altai further west (Jiang et al. 2012) and recent data from the Tsogt area (Jiang et al. 2017). These authors also suggested that the Tugrug Formation is equivalent to Habahe Group in Chinese Altai. The Tugrug Formation was affected by post-deposition deformation and metamorphism, resulting in the formation of superposed structures, fold interference pattern and polymetamorphic fabrics. The rocks of this formation show a penetrative flat greenschist-facies fabric (Hanžl et al. 2016), whereas its high-grade metamorphic equivalents were affected by upper amphibolite- to granulite-facies metamorphism (Jiang et al. 2017).

The regional metamorphic grade of the Tugrug Formation increases to the S where meta-greywackes gradually pass into garnet-biotite schists and the underlying high-grade metamorphic core i.e. Tsogt metamorphic dome.

The Tsogt metamorphic dome (Fig. 4.8) is formed by garnet-bearing amphibolites, garnet-sillimanite paragneisses, stromatitic migmatites, high-grade orthogneisses and granitoids. Similarly to overlaying Tugrug Formation, the high-grade rocks show also polyphase structural evolution. In the deepest part of the metamorphic core, the relics of S1 fabrics are reworked by ubiquitous metamorphic fabric S2, that is generally gently dipping either to the south or to the north. These two fabrics (Fig. 4.9) are refolded by two orthogonal systems of upright folds. In the south, the whole region is truncated by large-scale NW–SE trending shear zone, which makes the main boundary with southerly Trans-Altai zone.

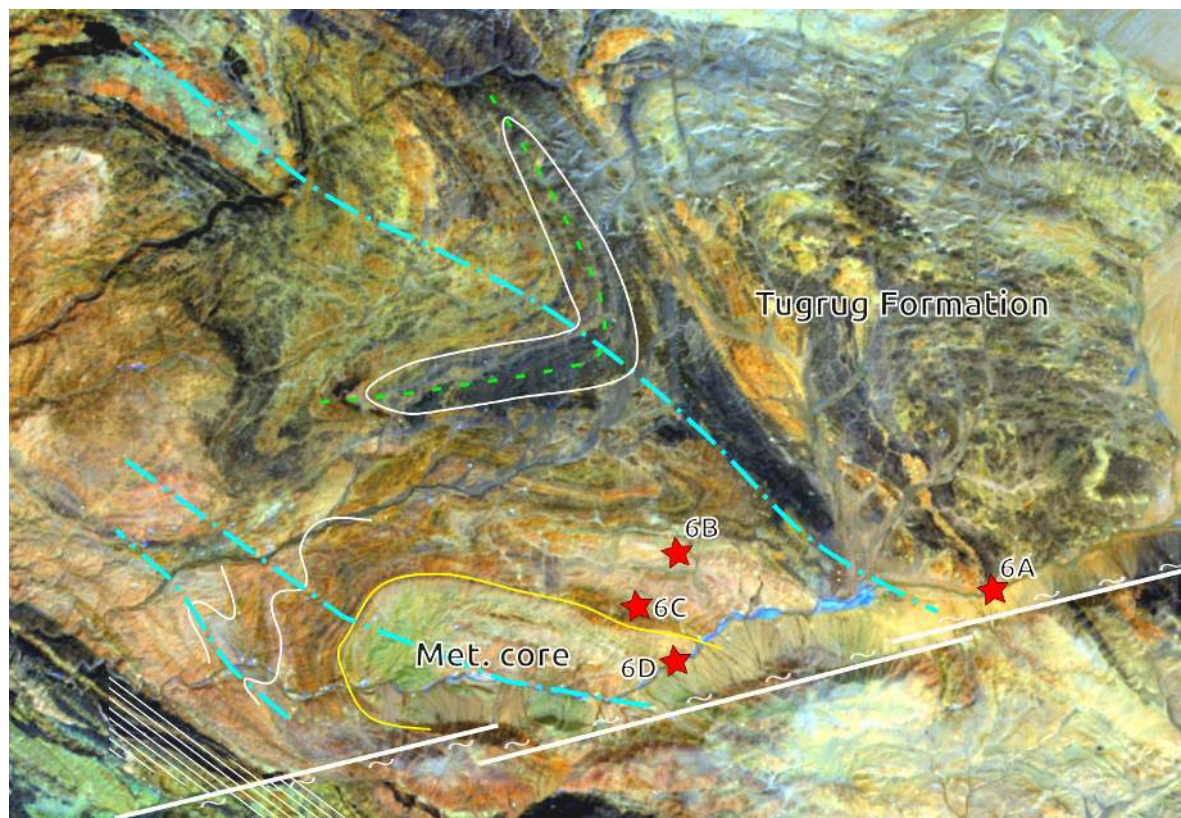


Figure 4.8: Principal structures and position of Tsogt metamorphic dome on Landsat image. The excursion localities are shown by red stars.

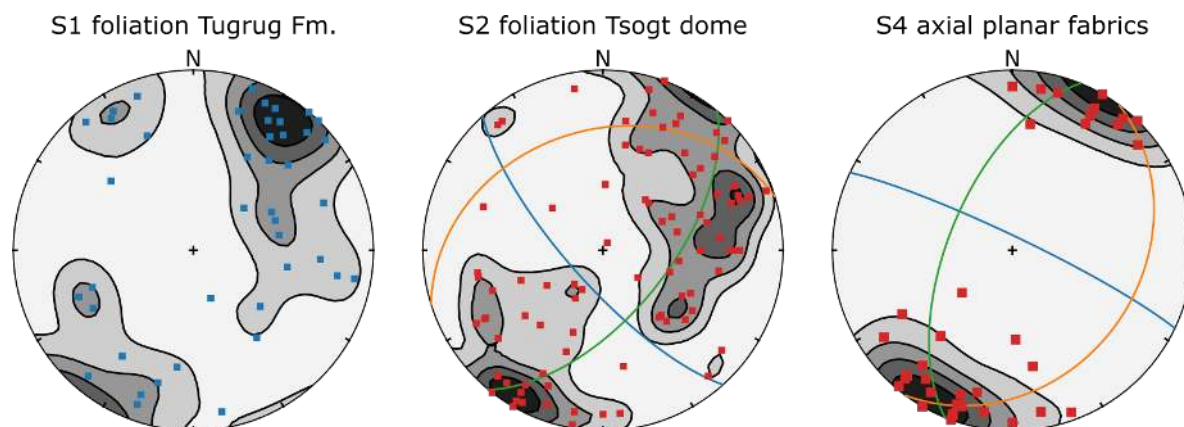


Figure 4.9: Structural data from Tsogt metamorphic dome and surrounding Tugrug Formation.

Geochemistry of Tugrug Formation

The analysed metavolcanic rocks belong to a bimodal metarhyolite–metabasalt association, accompanied by greenschists and metatuffs (Fig. 4.10a). The metarhyolites–metabasalts are all subalkaline, with the mafic types showing tholeiitic, and the felsic ones high-K calc-alkaline character (Fig. 4.10b–c). The strong peraluminosity some of the metarhyolites shows a marked mobility of alkalis due to metamorphism (Fig. 4.10d).

The NMORB-normalized spiderplots (S. S. Sun and McDonough 1989) for the supposedly little mobile elements (Pearce 2014) in the metabasalts show smooth trends, enriched in more

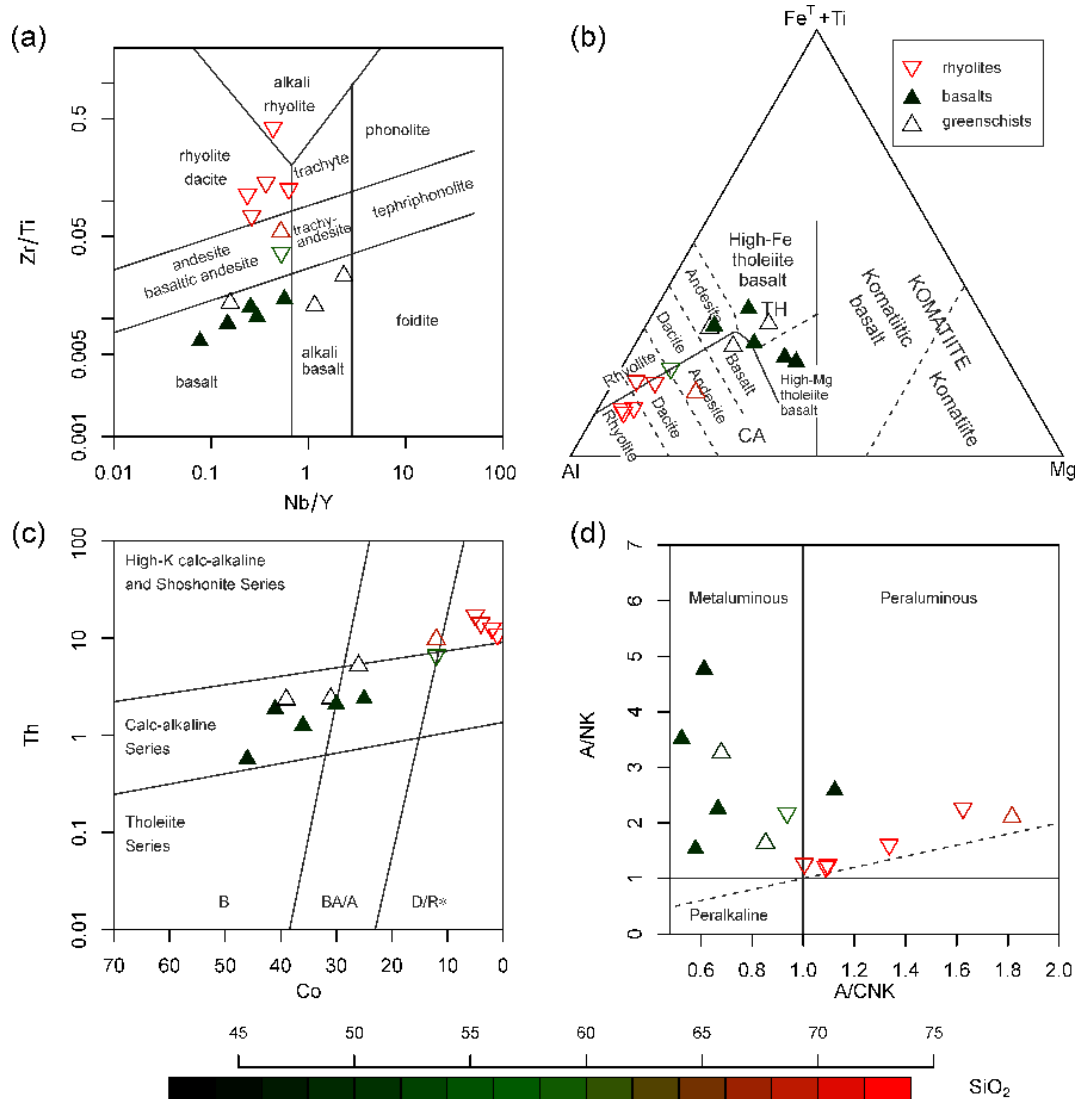


Figure 4.10: Classification diagrams for Tugrug Formation. (a) Nb/Y vs. Zr/Ti diagram of Winchester and Floyd (1977) modified by Pearce (1996a). (b) Cation plot Al-(Fe^T + Ti)-Mg of Jensen (1976): TH = tholeiitic, CA = calc-alkaline. (c) Co-Th binary plot of Hastie et al. (2007), a proxy for the SiO₂ vs. K₂O plot of Peccerillo and Taylor (1976) using relatively immobile trace elements. B = basalt, BA/A = basaltic andesite and andesite, D/R* = dacite and rhyolite. (d) Binary plot of molar A/CNK = Al₂O₃/(CaO + Na₂O + K₂O) vs. A/NK = Al₂O₃/(Na₂O + K₂O) (Shand 1943).

incompatible elements, with significant negative anomalies for Ta-Nb and Hf-Zr (Fig. 4.11a). Even more enriched are the metarhyolites (Fig. 4.11b), but a characteristic feature here is the presence of the so-called ‘TNT’ (negative Ta-Nb-Ti) anomalies. For all samples, normalized HREE concentrations are close to unity. Such patterns are typically interpreted as reflecting fluid/melt enrichment in subduction setting (Pearce and Peate 1995; Tatsumi and Eggins 1995).

In the chondrite-normalized (Boynnton 1984) spiderplot, the REE patterns of the metabasalts are fairly LREE-enriched and lacking Eu anomalies (Fig. 4.12a). Metarhyolite patterns are strongly fractionated, convex down, with deep negative Eu anomalies.

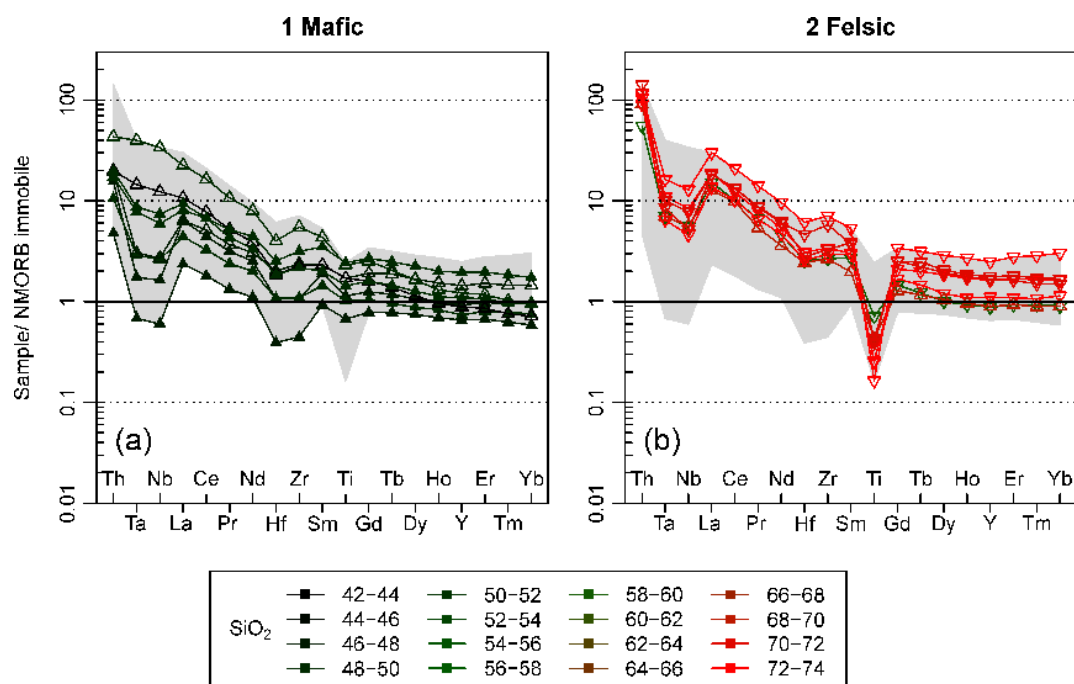


Figure 4.11: NMORB-normalized (S. S. Sun and McDonough 1989) spiderplot for presumably immobile elements (Pearce 2014). The diagrams are colour-coded by silica, the grey field shows the overall variability in the whole dataset.

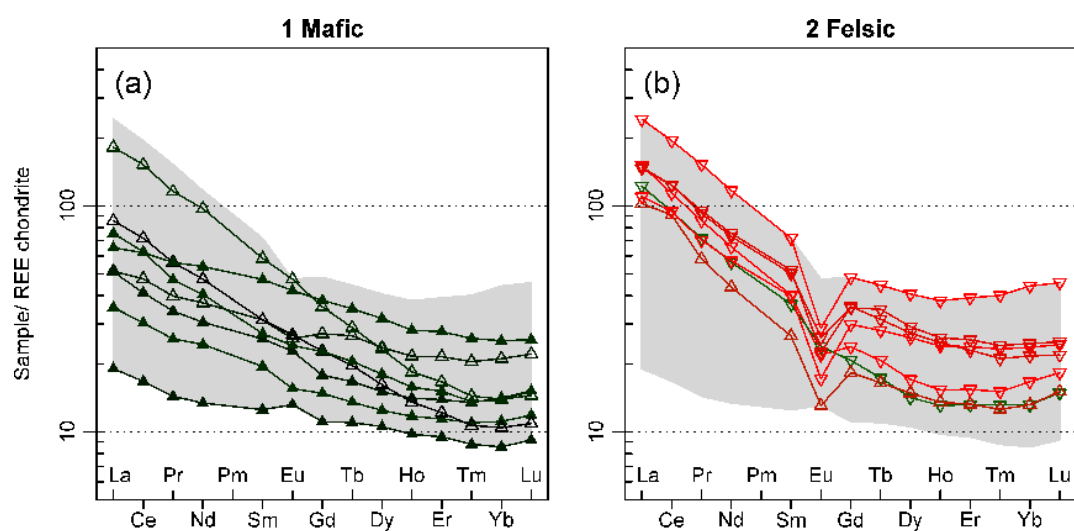


Figure 4.12: Chondrite-normalized (Boynnton 1984) REE patterns. The diagrams are colour-coded by silica, the grey field shows the overall variability in the whole dataset.

In geotectonic diagrams, the metarhyolites show a rather clear subduction affinity (Fig. 4.13a–c, f) but there may be also a feeble intraplate component (Fig. 4.13e). This does not require necessarily an origin in an active magmatic arc, as such felsic magmas could be also generated by remelting of pre-existing, arc-derived rocks (Förster et al. 1997; Konopásek et al. 2018; Pearce 1996b), for instance greywackes in an accretionary wedge (Jiang et al. 2016). The latter hypothesis would be in line with the observed detrital zircon ages, dominated by the ‘Ikh-Mongol Arc System’ derived grains.

The metabasalts appear to either having belonged to a continental arc (Fig. 4.13a) or to late- or post-orogenic settings, both compressive and distensive *sensu* Cabanis and Lecolle (1989) (Fig. 4.13b). In binary diagram Nb/Yb vs. Th/Yb (Pearce 2008) (Fig. 4.13c) the metabasalts range between OIB and arc-related, showing variable, but small shift above the ‘NMORB–OIB array’. The mantle melting generating the basaltic melts was probably shallow (spinel-stability field), as shown by relatively high HREE contents as well as the Nb/Yb vs. TiO₂/Yb discrimination diagram of Pearce (2008) (Fig. 4.12a, 4.13d). Overall, we assume that the studied metabasalt–metarhyolite association originated most likely in an overall extensional, possibly fore back-arc setting, where the ascending hot asthenosphere (OIB component) melted the overlying, subduction-modified lithospheric mantle and fertile metasediments of an older accretionary wedge.

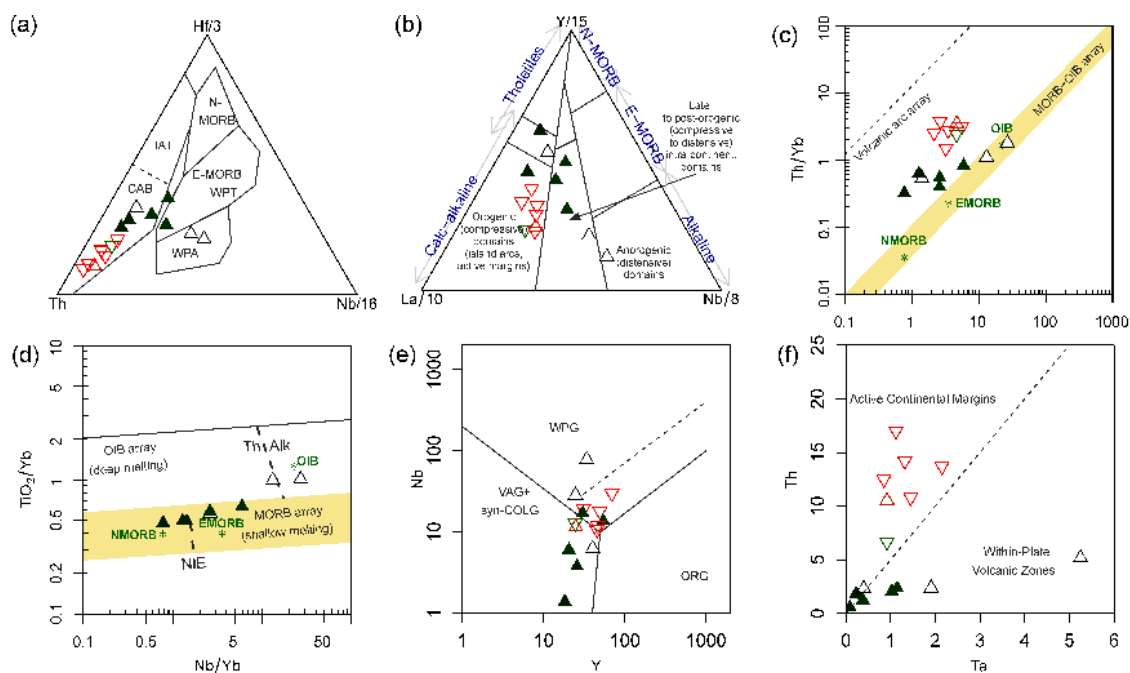


Figure 4.13: Geotectonic discrimination diagrams. (a) Th–Hf/3–Nb/16 triangular plot of Wood (1980). CAB = Calc-Alkaline Basalts, IAT = Island-Arc Tholeiites, WPT = Within-Plate Tholeiites, WPA = Within-Plate Alkaline basalts. (b) La/10–Y/15–Nb/8 plot of Cabanis and Lecolle (1989), where the Y/Nb serves as the “alkalinity index” and La/Y as the “calc-alkaline index”. (c) Nb/Yb vs. Th/Yb discrimination diagram of Pearce (2008). Compositions of average upper, bulk and lower continental crustal reservoirs (UCC, BCC and LCC respectively) are from Taylor and McLennan (1995). E- and N-MORB = Enriched and Normal Mid-Ocean Ridge Basalts; OIB = Oceanic Island Basalts. (d) Nb/Yb vs. TiO₂/Yb discrimination diagram of Pearce (2008). (e) Binary plot Y vs. Nb (Pearce et al. 1984) for determining the likely geotectonic setting of the granitoid rocks. VAG = Volcanic-Arc Granites, WPG = Within-Plate Granites, syn-COLG = Syn-Collisional Granites, ORG = Ocean Ridge Granites. (f) Binary plot Ta vs. Th (Schandl and Gorton 2002) for discrimination of the geotectonic setting of felsic igneous rocks.

Geochemistry of Tsogt high-grade core

The analysed rocks belong to three groups (Fig. 4.15): (1) amphibolites, (2) tonalites–granites and (3) diatexite. The tonalites–granites (Fig. 4.15a) and diatexite are subaluminous, relatively felsic rocks (Fig. 4.15b) that are calc-alkaline in character (Fig. 4.15d). As a consequence of the high-grade metamorphism, amphibolites suffered a strong loss of alkalis. Still, in the Nb/Y vs. Zr/Ti diagram of Winchester and Floyd (1977) modified by Pearce (1996a) they clearly correspond to alkali basalts (Fig. 4.15c).

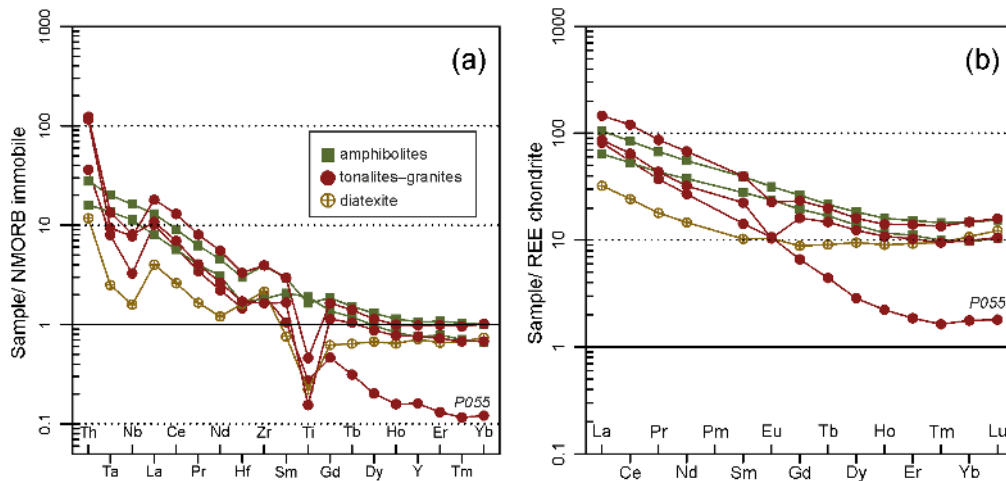


Figure 4.14: Multielement diagrams. (a) NMORB-normalized (S. S. Sun and McDonough 1989) spiderplot for presumably immobile elements (Pearce 2014). (b) – Chondrite-normalized (Boynton 1984) REE patterns.

The NMORB-normalized spiderplots (S. S. Sun and McDonough 1989) for the supposedly little mobile elements (Pearce 2014) in the amphibolites (Fig. 4.14a) show relatively smooth trends without any significant anomalies, except of inconspicuous hump for Zr–Hf. Patterns for the tonalites–granites on the other hand are characterized by strong enrichment of the lithophile elements, small negative anomalies of Ta–Nb and a deeper one for Ti. The tonalite P055 differs by its strong depletion in HREE and lack of negative Eu anomaly in the chondrite-normalized (Boynton 1984) spiderplot (Fig. 4.14b). The REE pattern of the diatexite is relatively flat, also without Eu anomaly.

In geotectonic diagrams, the amphibolites show an affinity to within-plate settings (Fig. 4.16a–b), with an overall geochemical character resembling Ocean-Island Basalts (OIB) (e.g., Fig. 4.16c–d) or transition between OIB and Enriched Mid-Ocean Ridge Basalts (EMORB) but still on the ‘NMORB–OIB array’ (Fig. 4.16e). The source of tonalites–granites with the diatexite seems to have had some affinity to magmatic arcs (Fig. 4.16a–d). In binary diagram Nb/Yb vs. Th/Yb (Pearce 2008) (Fig. 4.16e) they are progressively shifted above the ‘NMORB–OIB array’, into the region of arc-derived magmas or those strongly contaminated by, or largely derived from, the continental crust. The best explanation seems remelting of low-K mafic magmatic arc-related rocks rarely including tonalites (Fig. 4.16f). For the sample P055 this took place probably rather deep, in the presence of residual garnet. Overall, we assume that this rock association originated most likely in an incipient intra-continental rift setting, dissecting an older arc.

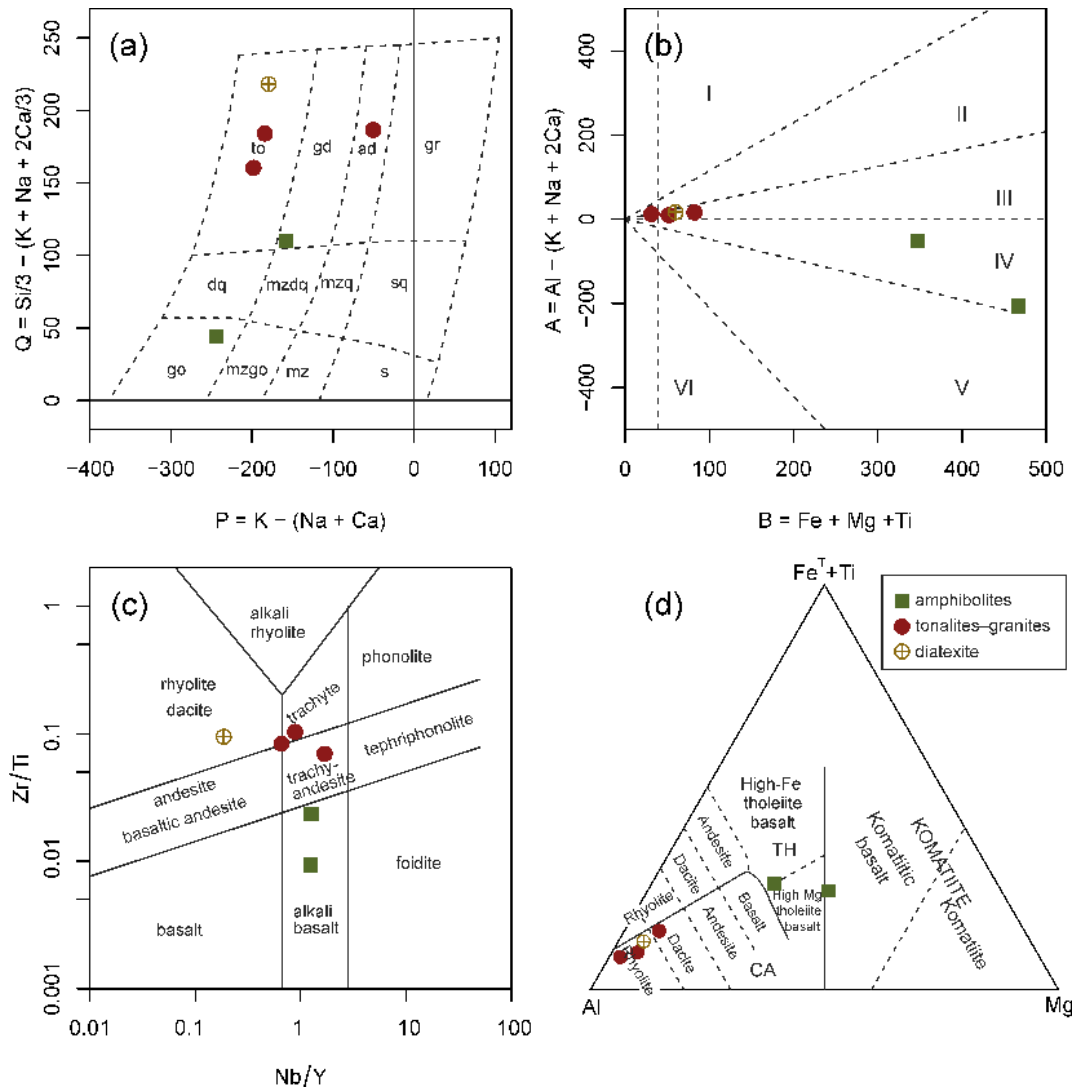


Figure 4.15: Classification diagrams for Tsogt magmatic and high-grade rocks. (a) Multicationic diagram P (balance of K feldspar to plagioclase) vs. Q (quartz) of Debon and Le Fort (1983). Abbreviations used: gr = granite, ad = adamellite, gd = granodiorite, to = tonalite, sq = quartz syenite, mzq = quartz monzonite, mzdq = quartz monzodiorite, dq = quartz diorite, s = syenite, mz = monzonite, mzgo = monzogabbro, go = gabbro. (b) Multicationic diagram B (maficity) vs. A (peraluminosity) of Debon and Le Fort (1983). The following domains and characteristic mineral assemblages are distinguished: Peraluminous domain: I – muscovite > biotite, II – biotite > muscovite, III – biotite (\pm minor amphibole); Metaluminous domain: IV – biotite, amphibole, \pm pyroxene, V – clinopyroxene, \pm amphibole, \pm biotite, VI – unusual mineral associations (carbonatites ...). (c) Nb/Y vs. Zr/Ti diagram of Winchester and Floyd (1977) modified by Pearce (1996a). (d) Cation plot Al-(Fe+Ti)-Mg of Jensen (1976): TH = tholeiitic, CA = calc-alkaline.

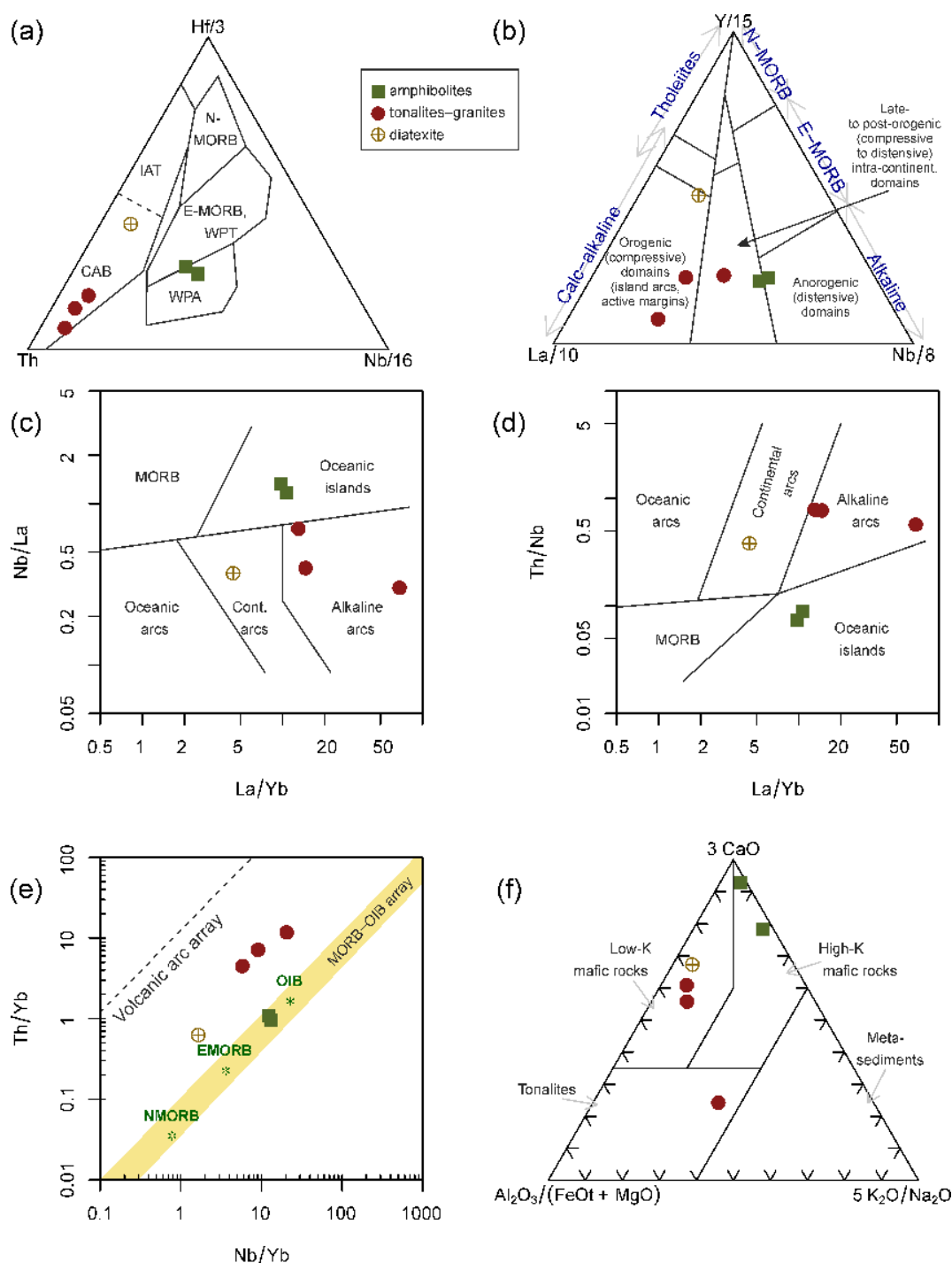


Figure 4.16: Geotectonic discrimination diagrams. (a) Th–Hf/3–Nb/16 triangular plot of Wood (1980). CAB = Calc-Alkaline Basalts; IAT = Island-Arc Tholeiites; WPT = Within-Plate Tholeiites; WPA = Within-Plate Alkaline basalts. (b) La/10–Y/15–Nb/8 plot of Cabanis and Lecolle (1989), where the Y/Nb ratio serves as the “alkalinity index” and La/Y as the “calc-alkaline index”. (c–d) La/Yb vs. Nb/La and La/Yb vs. Th/Nb plots of Hollocher et al. (2012). (e) Nb/Yb vs. Th/Yb discrimination diagram of Pearce (2008). Average upper, bulk and lower continental crustal reservoirs (UCC, BCC and LCC respectively) are from Taylor and McLennan (1995). E- and N-MORB = Enriched and Normal Mid-Ocean Ridge Basalts; OIB = Oceanic Island Basalts. (f) Ternary plot $\text{Al}_2\text{O}_3/(\text{FeO}_{\text{tot}} + \text{MgO}) - 3 \times \text{CaO} - 5 \times \text{K}_2\text{O}/\text{Na}_2\text{O}$ (wt.%) of Laurent et al. (2014, and references therein) discriminating possible sources of granitic melts based on compilation of the available experimental data.

Interpretation of Tsogt metamorphic dome evolution

Fundamental question is the age of the three deformation fabrics that are present in the studied section through the Tsogt dome. An attempt was made to date the felsic gneisses in the central part of the Tsogt dome as well as on the region close to transitional zone separating infra- from super-structure. In the first outcrop (Y081) we dated felsic orthogneiss and in the second one the leucosome filling lock up shear band affecting tonalitic orthogneiss sample (Y065). The two ages are providing mid-Devonian ~380 Ma U–Pb zircon ages (Fig. 4.17) which is interpreted as a timing of major melting event of the whole Cambro–Ordovician wedge (Hanžl et al. 2016; Jiang et al. 2016). In addition, the melting was most likely coeval with giant extensional event affecting the lower and middle crustal levels of the metamorphic edifice of the Tsogt dome.

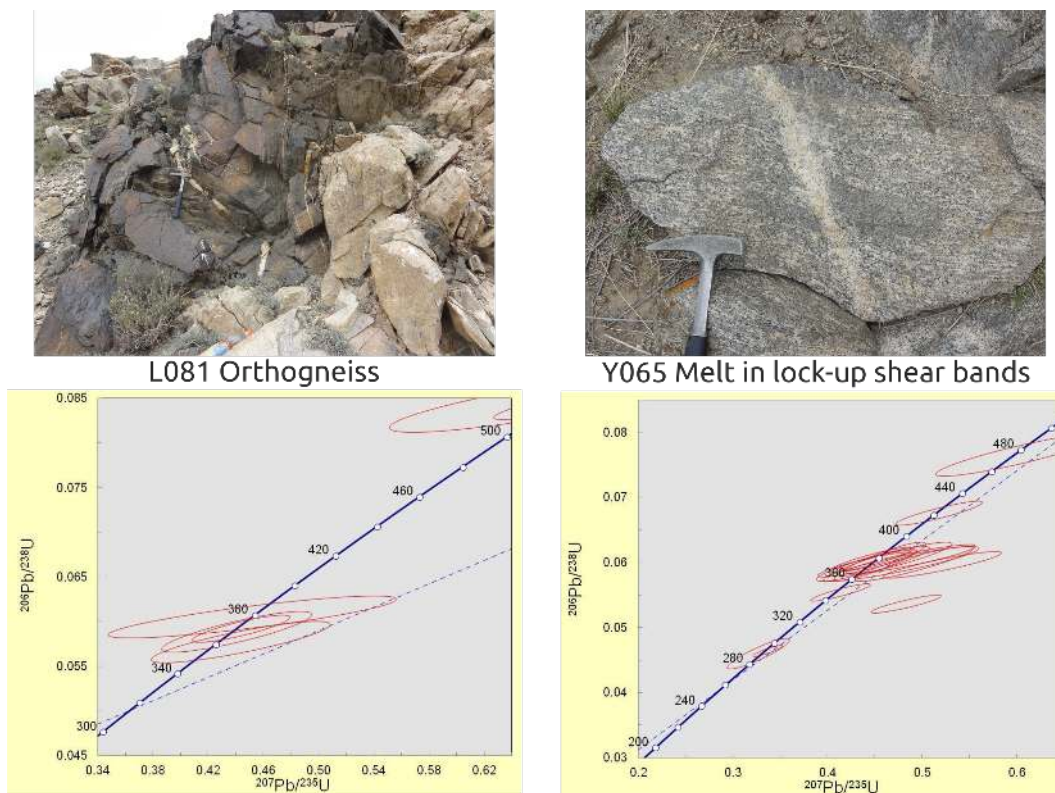


Figure 4.17: Geochronological data for granites - presently orthogneisses, emplaced in extensional fabrics S2 (with courtesy of Yingde Jiang).

The precise age of latest NNE–SSW shortening is difficult to determine keeping in mind general greenschist facies character of this deformation. However, the southern part of the Tsogt dome shows several leucocratic dykes or even leucosome layers that are parallel to WNW–ESE striking foliation. These dykes (sample Y062) and leucosomes (Y056a) were dated using U–Pb zircon method and yielded ages ranging from 300 to 290 Ma (Fig. 4.18). The dated rocks reveal also important Devonian and Early Ordovician inheritance. We can conclude that like in the Chinese Altai (Broussolle et al. 2018, 2019) the NNE–SSW shortening started during earliest Permian by extrusion of partially molten crust accompanied with intrusions of crustally derived melts in form of axial planar leucosomes and dykes of F3 folds.

All the presented data allow to propose a geodynamic model of the region that can be constrained from structural, petrological and geochronological point of views. This model is

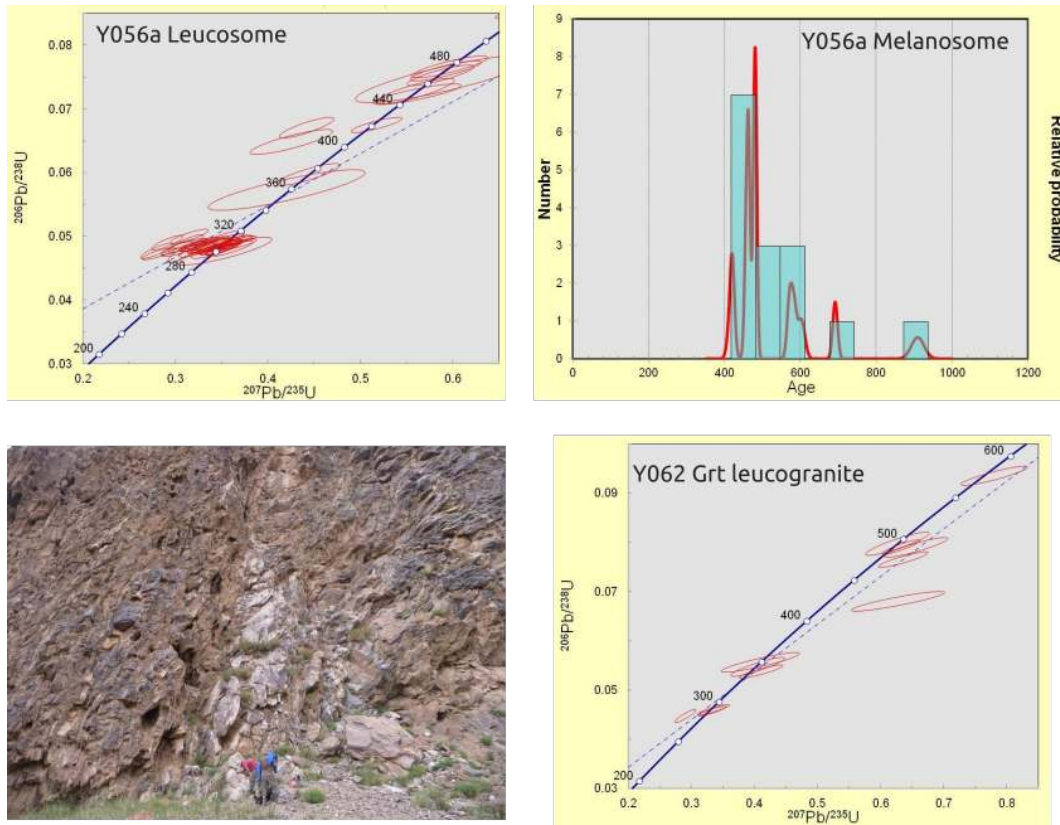


Figure 4.18: Geochronological data of leucogranites and axial planar leucosomes of F3 folds related to N–S shortening. (with courtesy of Yingde Jiang).

based on the fact, that we can identify, both in the upper crustal Tugrug Formation and deep crustal part of the Tsogt dome, earliest fabrics S1, that have been originally subvertical. We can also see, that metamorphic gradient related to this vertical fabric increases with depth. The upper - weakly metamorphosed part of the edifice is separated from deep high grade crustal part by a zone of mid-crustal horizontal fabric S2 and recumbent folds F2 that developed at high to medium temperatures. Both structures were reworked by new upright folds F3 and deformation zones S3 that heterogeneously reworked both the complexly deformed infrastructure of the Tsogt dome, subhorizontal infrastructure-superstructure transition zone (D2) and superstructure formed by the Tugrug Formation *sensu stricto*.

In our model, the first fabrics and metamorphism are related to the crustal thickening that affected the whole accretionary wedge. It can be shown that the metamorphism reached kyanite grade and pressure-temperature conditions of 10 kbar and 650°C (Fig. 4.19a–c). This metamorphism affects almost entire wedge and stretches from the Chinese Altai in the west (Jiang et al. 2019, 2015) to Mongolian Altai in the east. This event is probably of Late Silurian age (Soejono et al. 2018). Crustal thickening was followed soon after by giant extensional event that is responsible for the formation of crustal scale core complexes - such as the Tsogt dome. The detachments are associated to HT-LP metamorphism and important magmatism which is both mafic and felsic. It can be seen, that the granitoids intruded syntectonically with D2 extensional shearing - and the duration extensional shearing and crustal melting is estimated to 30 Ma from ca. 400 to 370 Ma (Hanžl et al. 2016; Jiang et al. 2016, 2019). The latest event is related to massive NNE–SSW shortening of the whole Altai system and was

responsible for amplification of Devonian core complexes, formation of network of NE–SW trending heterogeneous shear zones, upright folds and tabular domains of extruded migmatites and granitoids dated at 300–290 Ma (Burenjargal et al. 2016). The intensity of this Permian deformation gradually increases to the south implying existence of major collisional contact between the Trans-Altai Zone and Mongolian Altai. On the other hand the northern margin of the Mongolian Altai and the Lake Zone is massively reactivated as well as indicated by numerous E–W trending greenschist facies cleavage zones parallel to this principal tectonic boundary.

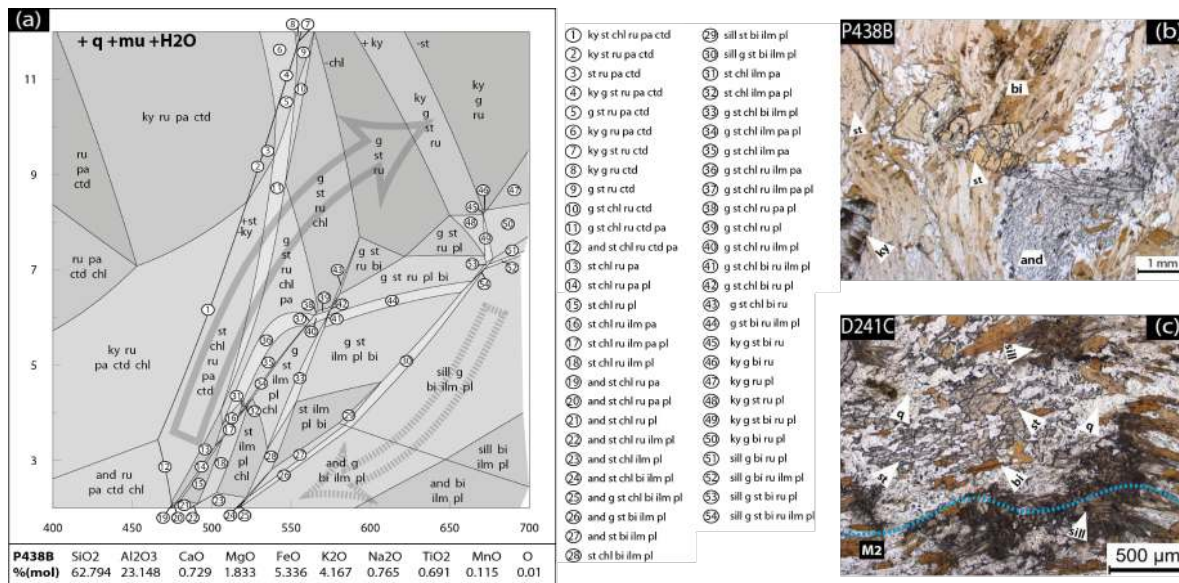


Figure 4.19: P–T pseudosection showing metamorphic evolution of metapelites of the Tsel and Tsogt domes. Unpublished data.

4.4 Variegated lithology and folding of the Tugrug Suite (6A)

N45°20' 38", E96°41' 30", rocks on the right bank of the Tugrug River 4 km E of Tsogt soum

The Tugrug Formation in the presented outcrop is mainly represented by volcano-sedimentary or volcanic rocks metamorphosed under lower greenschist conditions. Locally, some coarse-grained greywackes and metasandstones occur allowing detrital zircon analysis. The U–Pb ages of detrital zircons show clear Late Cambrian – Early Ordovician peak together with minor peaks of mid-Proterozoic ages (Figs. 4.20 and 4.21). Such zircon spectra are typically reported from the Habahe group metasediments in the Chinese Altai and other regions of Mongolian Altai in Mongolia and Russia. All that indicates the provenance of zircons from northerly Ikh Mongol Arc (Janoušek et al. 2018) and underlying Grenville-age basement.

In the studied outcrop occurs slates that reveal polyphase deformation pattern represented by complete transposition of bedding by sub-greenschist facies cleavage S1, development of syn-schistose isoclinal folds similar in geometry (Fig. 4.22a). The age of foliation and isoclinal folding is presently unknown but has to be older than mid-Devonian vertical shortening, which is well dated by syntectonic granitoids (Hanžl et al. 2016). This structural edifice is subsequently refolded by upright open to close chevron folds of buckles with WNW-ESE

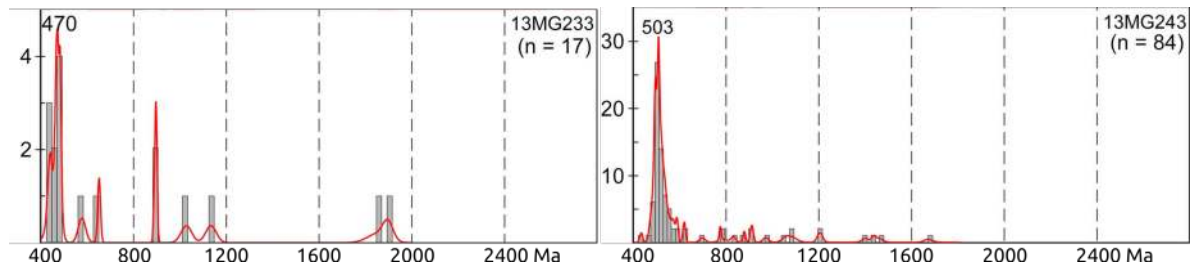


Figure 4.20: Relative probability plots for detrital zircon ages of terrigenous clastic sedimentary samples from the Ordovician succession (Jiang et al. 2017).



Figure 4.21: Field photograph and microphotographs showing the Ordovician sedimentary succession characterized by interbeds of terrigenous and volcanic layers.

trending hinges and sub-vertical axial planes (Fig. 4.22b). These folds are considered to be of Permian age in analogy to dated structural fabrics in the region.



Figure 4.22: (a) Relationship of S0 and S1, (b) superposed cleavages overprinting metamorphic foliation.

4.5 Contact of Tugrug Suite and Tsogt metamorphic core (6B)

N45°19' 11", E96°34' 27", 4.5 km NWW of Tsogt soum

This series of outcrops is characterized by transition from weakly metamorphosed Tugrug Formation slates and metavolcanics to amphibolite facies rocks of the Tsogt metamorphic core. This boundary is not characterized only by rather abrupt metamorphic jump but also by spectacular structural evolution, which is well exposed along visited transect. In the higher part of the section we can observe well preserved steep greenschist facies S1 fabric. Going structurally deeper one can observe progressive folding of of this foliation by recumbent F2 folds together with increasing metamorphic grade (Fig. 4.23). At the end of the section, the volcano-sedimentary sequence is replaced by mylonitic amphibolite facies orthogneiss that shows dominant flat S2 foliation only. This fabric is interpreted to result from vertical shortening of the whole sequence and forming a transition zone separating deep infrastructure of the core of the Tsogt dome from shallow crust superstructure represented by the Tugrug Formation.

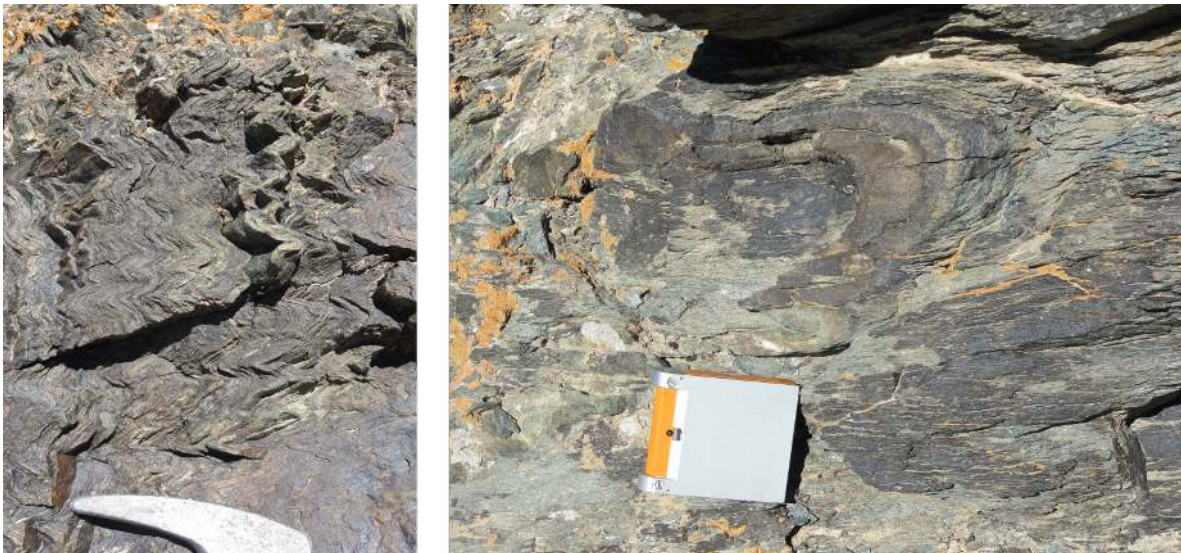


Figure 4.23: Development of S2 fabrics

4.6 High-grade rocks of Tsogt metamorphic core (6C)

N45°20' 45", E96°35' 35", 4.5 km SWW of Tsogt soum

The main rock type representing D2 transition zone are felsic to intermediate ortho-gneisses affected by amphibolite facies deformation (Fig. 4.24a). These rocks were interpreted by Hanžl et al. (2016) as syntectonic intrusions emplaced in mid-crustal levels during major vertical shortening event. The orthogneisses are intimately associated with garnetiferous amphibolites (Fig. 4.24b) or garnet bearing flaser-gabbros and sillimanite-garnet schists. The sample D241C (Fig. 4.19c) is a paragneiss with quartz, plagioclase, biotite, muscovite, sillimanite, garnet and staurolite. Staurolite occurs as corroded porphyroblasts in partial pseudomorphs, which has been partially to completely replaced by coarse-grained bioite, fibrolitic sillimanite, quartz and plagioclase. Therefore, staurolite is interpreted as relicts that are metastable with respect to the final phase assemblage sill-g-bi. The matrix is mainly composed of micas and fibrolitic sillimanite parallel to S2 foliation.



(a) HT foliation in orthogneiss



(b) Garnet amphibolites in Tsogt metamorphic core

Figure 4.24: High-grade rocks of Tsogt metamorphic core

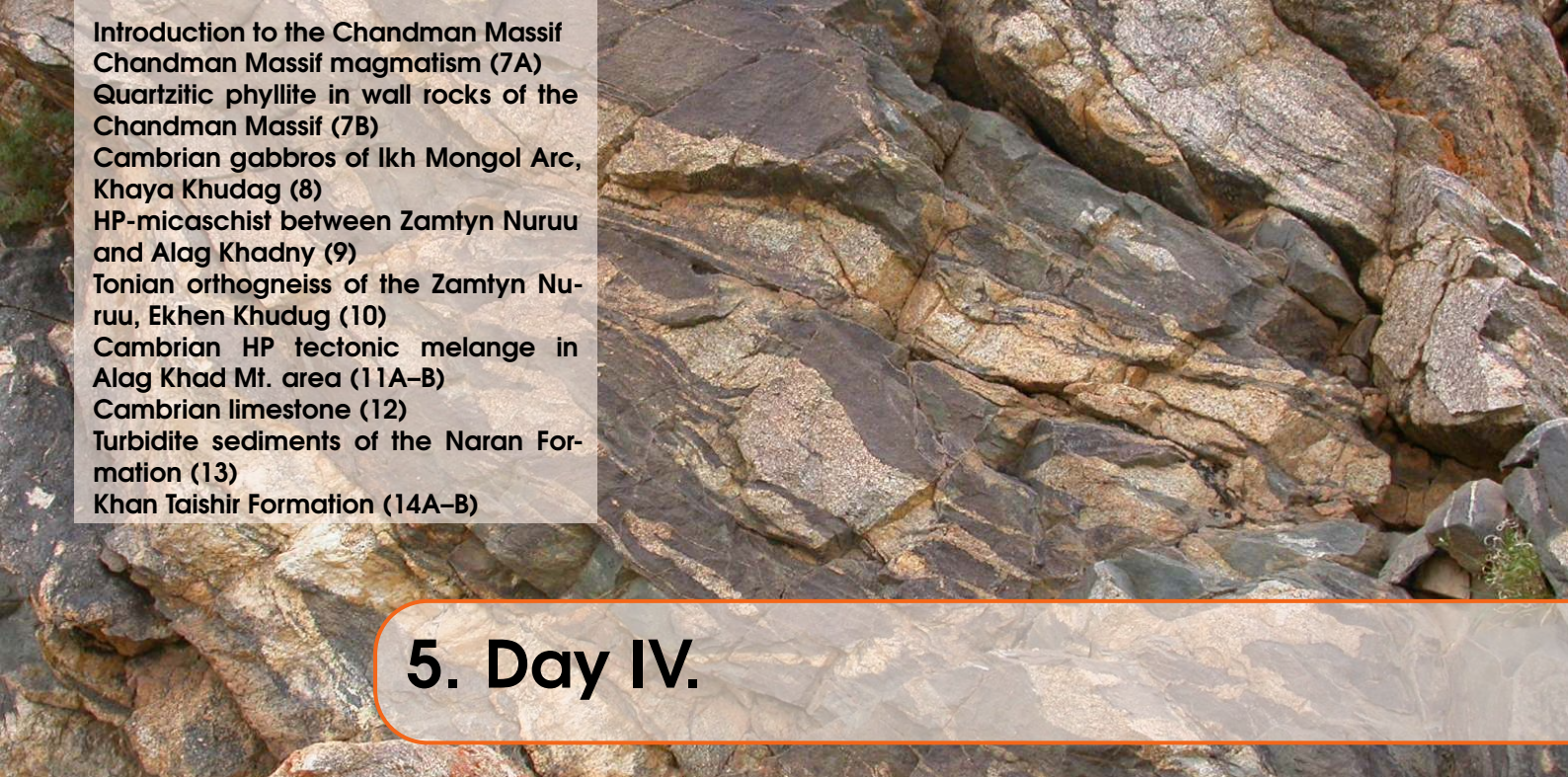
4.7 Migmatite of the Tsogt metamorphic core (6D)

N45°19'28", E96°35'1", 5.5 km SW of Tsogt soum

The core of the Tsogt dome shows a variety of rock types and structures reflecting complex and long-lasting magmatic and tectono-metamorphic evolution of the region. The alternating layers of felsic and intermediate gneisses, amphibolites and schists are characterized by ubiquitous S1 metamorphic schistosity and gneissosity that were primarily sub-vertical. These amphibolite facies fabrics are refolded by recumbent F2 folds, that is in many places characterized by formation of sub-horizontal axial planar foliation S2. This foliation may in places completely transpose early sub-vertical S1 fabric. The complexity of structural pattern is highlighted by development of late F3 folds, that are generally trending WNW-ESE. These structures may affect both S1 and S2, but differ from similar and syn-schistose F2 folds in shape being represented by chevron or asymmetric buckle folds. However, in some places they can be related to the formation of new schistosity S3, which makes structural successions of some outcrops difficult to interpret.



Figure 4.25: Polyphase folding recorded in Tsogt metamorphic core



Introduction to the Chandman Massif
Chandman Massif magmatism (7A)
Quartzitic phyllite in wall rocks of the
Chandman Massif (7B)
Cambrian gabbros of Ikh Mongol Arc,
Khaya Khudag (8)
HP-micaschist between Zamtyn Nuruu
and Alag Khadny (9)
Tonian orthogneiss of the Zamtyn Nu-
ruu, Ekhen Khudug (10)
Cambrian HP tectonic melange in
Alag Khad Mt. area (11A–B)
Cambrian limestone (12)
Turbidite sediments of the Naran For-
mation (13)
Khan Taishir Formation (14A–B)

5. Day IV.

5.1 Introduction to the Chandman Massif

The Chandman Massif represents a crustal-scale gneiss–migmatite–granite dome characteristic for a large region of Mongolian and Chinese Altai (Broussolle et al. 2015; Jiang et al. 2015; Lehmann et al. 2017). The Chandman Massif is located in the eastern part of the Mongolian Altai Mountains. It is a 35 km long and as much as 10 km wide an E–W elongated, oval-shaped body in the region of Chandman soum (Fig. 5.1). In the north crop out metamorphic rocks that show widespread migmatization while in the south crop out weakly metamorphosed rocks of the Tugrug Formation. The boundary between high-grade rocks and low-grade rocks is formed by granodiorites including septa of metasediments of the Tugrug Fm proving intrusive character of granitoids. This massif exhibits a lateral association of Devonian–Carboniferous granitoids and gneisses in the core, mantled by mid-crustal migmatites and peripheral medium- to low-grade metasedimentary sequences. Common xenoliths are meter to locally kilometre in size and consist of amphibolite, migmatized paragneiss and micaschist, rare quartzite, and calc-silicate lenses. Migmatites range from predominant metatexites to diatexites. The metamorphic envelope consists of non-migmatized medium- to low-grade metasedimentary rocks of Cambrian–Ordovician age (the Tugrug Formation) and Devonian to early Carboniferous very low-grade rocks. Reported crystallization ages of granitoids are 350.4 ± 1.7 Ma for a strongly foliated granite gneiss, 340.9 ± 2.5 Ma for a weakly deformed granite (both SHRIMP, sensitive high-resolution ion microprobe, U-Pb zircon Kröner et al. 2010), and 345 ± 2 Ma for a granodiorite (laser ablation–inductively coupled plasma–mass spectrometry U-Pb zircon Hrdličková et al. 2008). Migmatization was dated as 356 ± 1 Ma and subsolidus deformation reveals an age of 347 ± 4 Ma (both obtained using laser ablation–split stream, LASS, U-Pb monazite Broussolle et al. 2015). Radiometric Pb/U dating of zircon gave the Lower Carboniferous magmatic age. The $^{40}\text{Ar}/^{39}\text{Ar}$ ages of 350–340 Ma overlap with crystallisation ages and suggesting partly synchronous magmatism and cooling in the upper crust (Lehmann et al. 2017).

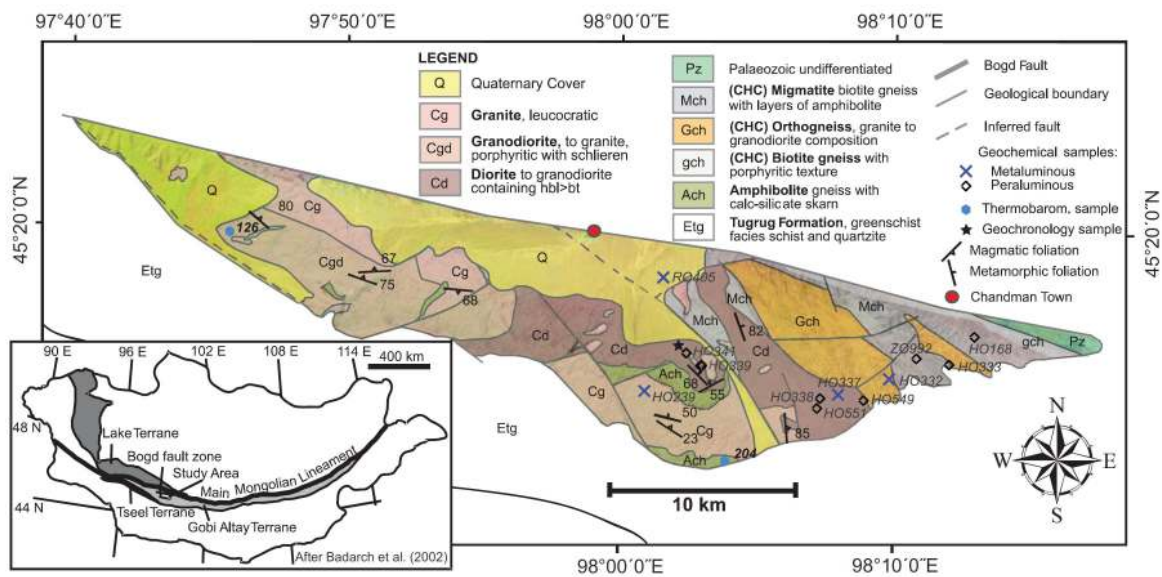


Figure 5.1: Map of the Chandman Massif (Economos et al. 2008).

5.2 Chandman Massif magmatism (7A)

N45° 13' 51", E98° 1' 0", valley 6.5 km SSW of Chandman

The Chandman Massif can be subdivided into two separate parts. Porphyritic, biotite granodiorite with anatectic textures and schlieren forms the southern part, whereas the biotite to biotite- amphibole granodiorite to tonalite varieties are situated in the northern part. The boundary is marked by a discontinuous belt of amphibolites and gneisses in roof pendants of the massif. The outcrop represents the N part of the pluton, the foliated amphibole-biotite granodiorite prevails. Schlierens are common, xenoliths of the wall rocks are rare.

Mineralogical composition of the granitoid rocks is rather uniform; variations exist in mineral contents and rock fabric. At outcrops, there is no sharp mineralogical or textural boundary between granodiorites and granites. The mafic rocks occasionally form layers and schlieren in foliated granitoid rocks. Deformation increases towards the NE and granitic rocks pass into orthogneisses. Preserved magmatic structures are overprinted by mild to moderate solid-state deformation (Economos et al. 2008).

Plutonic rocks (Fig. 5.2) are calc-alkaline, with potassium abundances corresponding to the high-K series for granites and medium-K series for tonalites to granodiorites (Economos et al. 2008). In the NMORB-normalized spider diagram, there is depletion in Ba, Nb, Sr, P and Ti, slight depletion in Zr and enrichment in Cs, Rb, Th, K, Pb and MREE. Samples fall mainly within the Volcanic Arc Granite (VAG) field and two samples into the Within Plate Granite (WPG) field of the classification by Pearce et al. (1984). Thermobarometry places constraints on the conditions of pluton emplacement to 11.5–13.7 km in the south, at least 15–20 km in the north and temperatures of 725–775°C (Economos et al. 2008).

The Chandman Massif rocks are affected by at least three main deformation events. The first one is associated with the formation of sub-horizontal foliation S1 developed mainly in deep crustal migmatites and granitoids and paragneisses. This sub-horizontal fabric is reworked by upright folds with sub-horizontal hinges and axial planar sub-vertical cleavage S2. This new foliation was originally oriented N–S as shown by structural reconstructions of

Lehmann et al. (2010, 2017). Finally, the whole structural edifice was reworked by large scale NNE–SSW oriented shortening leading to the development of kilometre-scale E–W trending fold with steeply plunging hinge and E–W trending axial plane. This fold is accompanied with a range of mesoscopic folds that affect both deep-seated and already exhumed rocks but also weakly metamorphosed envelope and un-metamorphosed Carboniferous cover.

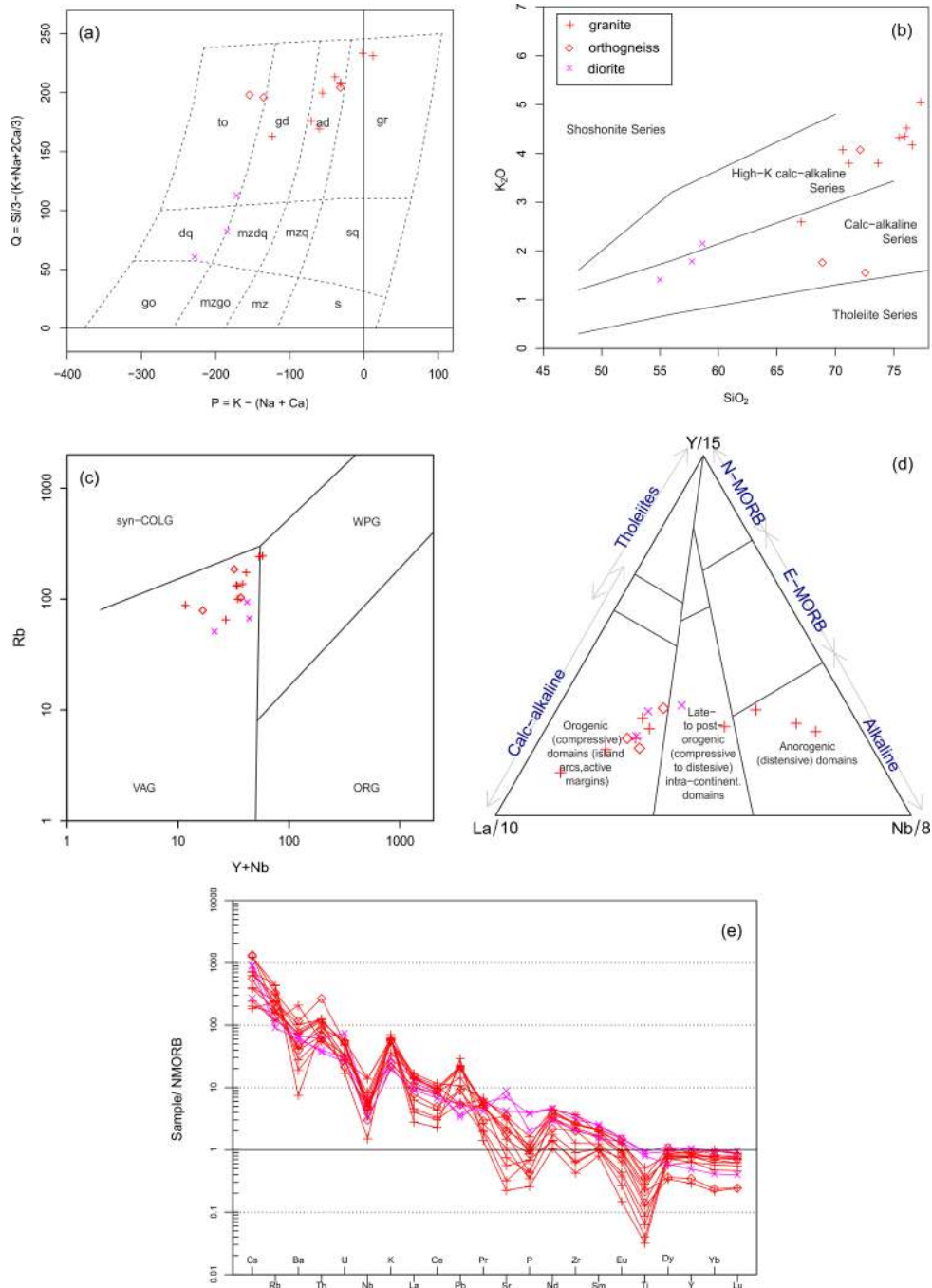


Figure 5.2: Geochemical classification of the plutonic rocks of the Chandman Massif. (a) Multicationic diagram P (balance of K feldspar to plagioclase) vs. Q (quartz) of Debon and Le Fort (1983); (b) SiO_2 - K_2O diagram of Peccerillo and Taylor (1976); geotectonic discrimination in diagrams of Pearce et al. (1984) (c) and Cabanis and Lecolle (1989) (d). (e) NMORB-normalized (S. S. Sun and McDonough 1989) spiderplot.

The granitoids and migmatites forming the core of the Chandman Massif show well developed horizontal fabric S1 that is reworked by syn-magmatic upright folding and development of still magmatic fabric S2.

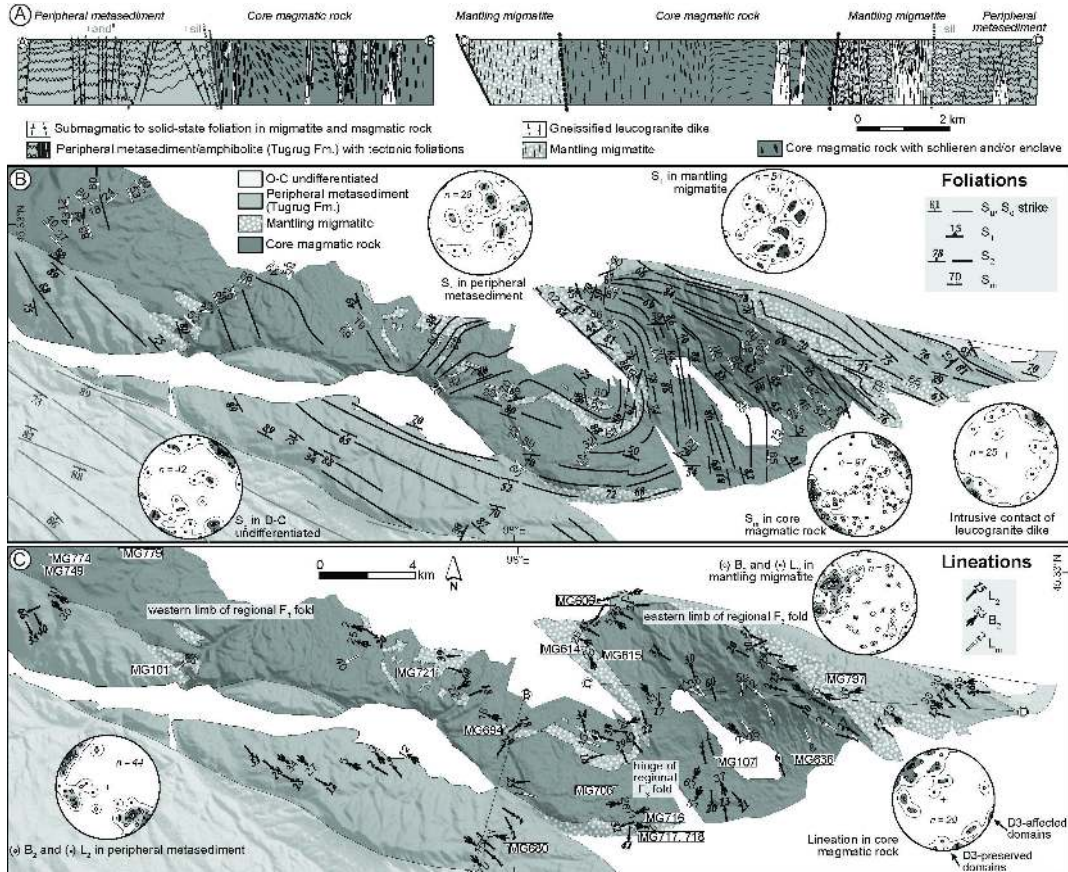


Figure 5.3: Structural map of the Chandman Massif showing the distribution of individual planar elements in various types of rocks. The core of large scale fold is formed by migmatites and granitoids. The envelope is developed mainly in the southern part of the area (with courtesy of Jeremie Lehmann).

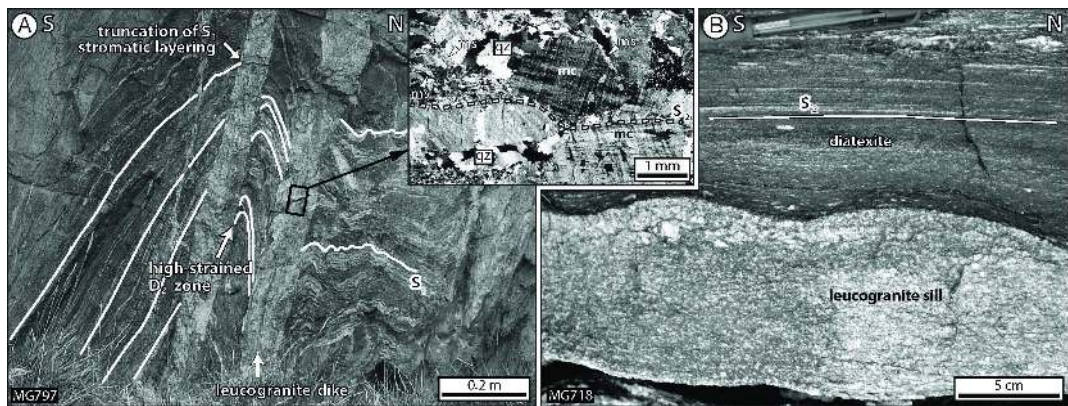


Figure 5.4: Field photograph of migmatitic sub-horizontal foliation affected by upright folding associated with intrusion of leucogranites dated at ~340 Ma (Lehmann et al. 2017).

5.3 Quartzitic phyllite in wall rocks of the Chandman Massif (7B)

N45°16' 37", E97°57' 32", flat ridge 11.8 km SSE of Chandman

In this outcrop Cambrian to Ordovician meta-sandstones and phyllites representing Tugrug Formation in the wall rocks of the Chandman Pluton are exposed (Fig. 5.5). These rocks more to the east revealing polyphase deformation and complex relationships of metamorphic fabrics to andalusite and cordierite porphyroblasts. The goal is to understand relationships of a sequence of structures and LP metamorphism affecting the metamorphic envelope. The principal feature is the development of metamorphic schistosity S0/1 that was originally subhorizontal and that was also reworked by two orthogonal folding events both related to the development of axial planar cleavage.



Figure 5.5: Examples of polyphase deformation where subhorizontal metamorphic foliation S1 is folded by upright folds.

Microstructural study of Broussolle et al. (2015) clearly shown growth of small andalusite and cordierite in subhorizontal foliation S1 and continuous growth of large andalusite porphyroblasts during the formation of S2 cleavage (Fig. 5.6). These features clearly demonstrate HT-LP metamorphic evolution (Fig. 5.7) affecting the upper crustal unit during both horizontal flow and upright folding.

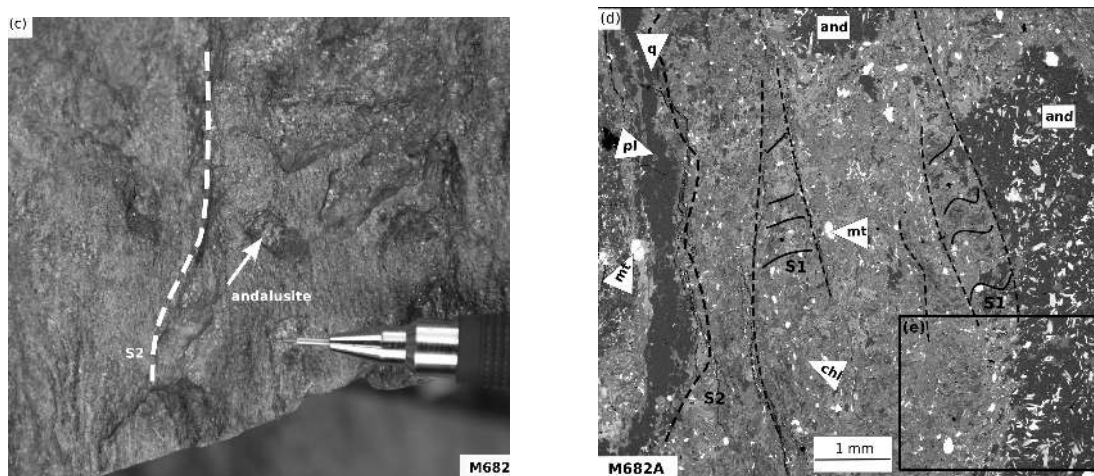


Figure 5.6: (a) The growth of andalusite formed during S2, (b) dominant S2 foliation marked by quartz ribbons, with relict domains where mica is oriented parallel to S1 fabric Broussolle et al. (2015).

Conclusions

This large scale crustal structure of the Chandman Massif allows understanding of processes related to melting of deep Altai crust and its exhumation during Late Devonian – Early Carboniferous extrusion. This event is associated with emplacement of granitoids, the formation of dome structure followed by intrusion of syn- compressional leucogranite dykes (Economos et al. 2008). The whole system is associated with LP-HT metamorphism affecting also adjacent upper crustal rocks buried in marginal synforms (Broussolle et al. 2015). The final exhumation stage and cooling of the whole system are constrained by numerous high-quality mineral (hornblende, biotite and muscovite) $^{40}\text{Ar}/^{39}\text{Ar}$ ages 340–350 Ma from granitoids, gneisses and metamorphic envelope (Lehmann et al. 2010, 2017). Detailed petrology of migmatite paragneiss from the core of the dome and slates from its envelope show contrasting but coeval evolution of the two crustal levels. In the deep crust, the horizontal fabric is associated with the growth of garnet and sillimanite, while the second vertical foliation bears sillimanite, cordierite and andalusite. On the other hand, supracrustal rocks show cordierite and andalusite in both horizontal and vertical fabrics.

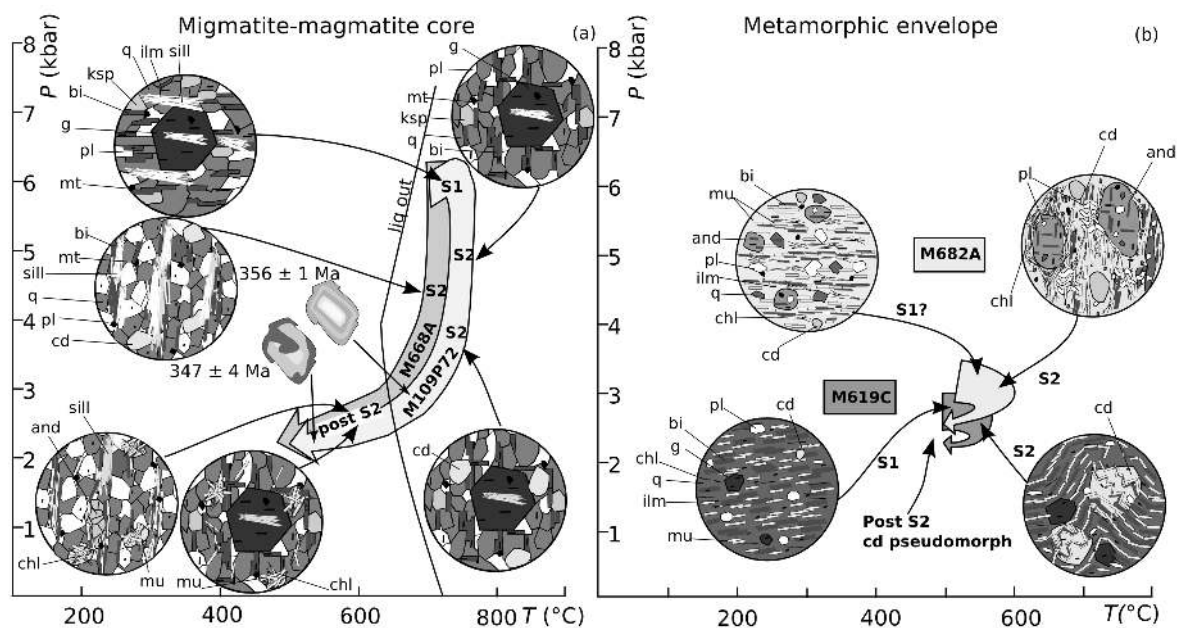


Figure 5.7: Microstructural, P-T and petro-chronological relationships from the Chandman Massif core and envelope (Broussolle et al. 2015).

The metamorphic, structural and geochronological relationships between granitoids, migmatites and low-grade metamorphic envelope allowed to propose a well constrained geodynamic model of this typical example of the granite-migmatite dome of the Mongolian Altai. This model shows that the high-grade rocks have been flowing horizontally at the depth of ca. 30–25 km and were extruded vertically to the depth level of around 5 km (Fig. 5.8). The heating of host rocks led to the development of narrow metamorphic aureole related to second steep cleavage and upright folding.

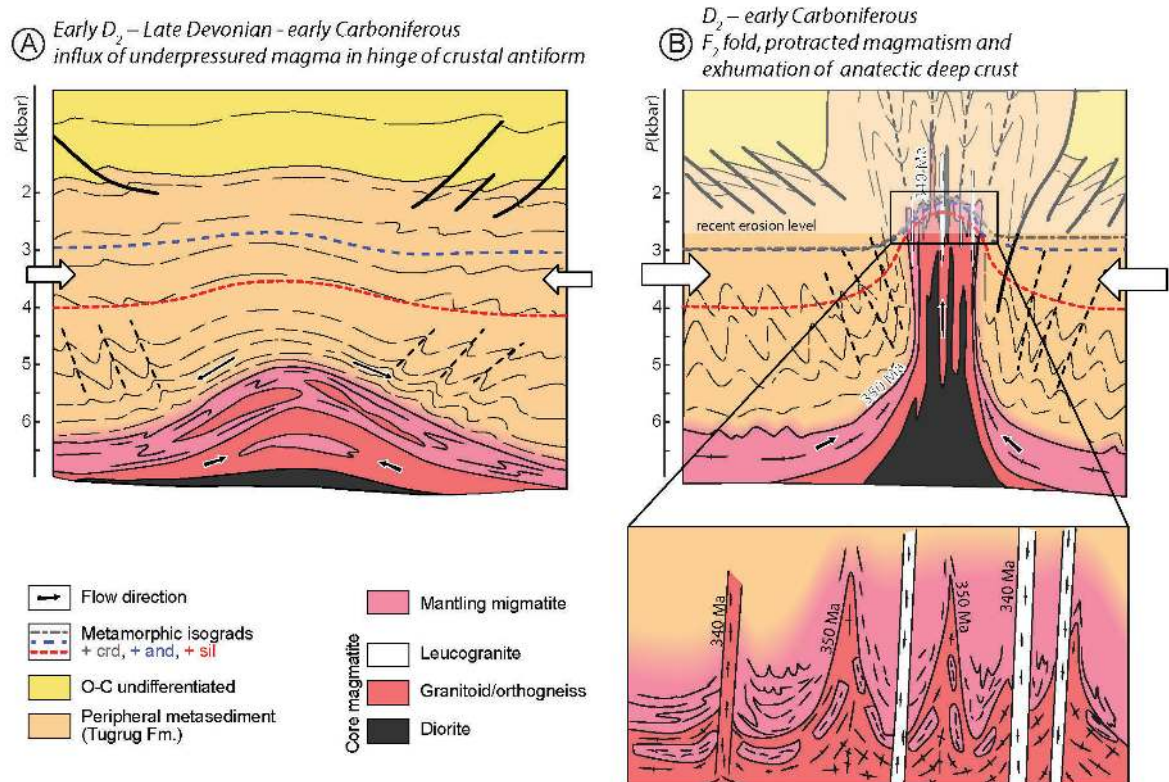


Figure 5.8: The model of the evolution of the Chandman dome in which weak and hot orogenic infrastructure is extruded to the shallow crustal depths. The last event is related to the formation of last leucogranite and pegmatite dykes that intruded the steep S_2 cleavage (Lehmann et al. 2017).

5.4 Cambrian gabbros of Ikh Mongol Arc, Khaya Khudag (8)

N45°23' 31", E98°8' 46", southern slopes of Ulaan Tsakhir Uul 10 km N of Chandman Khayrkan Uul

Syn-tectonic gabbros, gabbrodiorites and diorites are documented in the structurally deeper level of the Zamtyun Nuruu crystalline complex. They are usually strongly deformed. Magmatic fabrics as fractured aplite dyke, magmatic layering and foliation are commonly preserved (Fig 5.9).



Figure 5.9: Fragmented aplite dyke in gabbro with tonalite enclaves.

These metaluminous, amphibole-bearing gabbros–diorites (Fig. 5.10a–b) show a transitional tholeiitic to normal-K calc-alkaline character (Fig. 5.10c–d) and the dated sample from the visited locality yielded an U–Pb age of 542 ± 4 Ma interpreted as reflecting zircon crystallization (Buriánek et al. 2017). The ages of the studied gabbrodiorite and diorite are coeval with a thermal event at around 550 Ma recorded by the zircon rims of the coarse-grained orthogneiss from the Zamtyn Nuruu Complex. Hafnium isotope compositions of zircons from gabbros are close to that of depleted mantle ($\epsilon^{Hf}_t = +8.2$ to $+10.2$). The trace-element signatures (overall enrichment in incompatible elements, esp. in Ba, Th, U and K, with Pb and Sr spikes and Rb, Nb, P and Zr troughs in NMORB-normalized spider plots; Fig. 3) as well as whole-rock Sr–Nd isotopic data ($^{87}\text{Sr}/^{86}\text{Sr}_{540} \simeq 0.705$, $\epsilon^{Nd}_{540} \simeq +2$) point to a rather juvenile source, definitely not older than Grenvillian ($T_{DM,2stg}^{Nd} \simeq 1$ Ga).

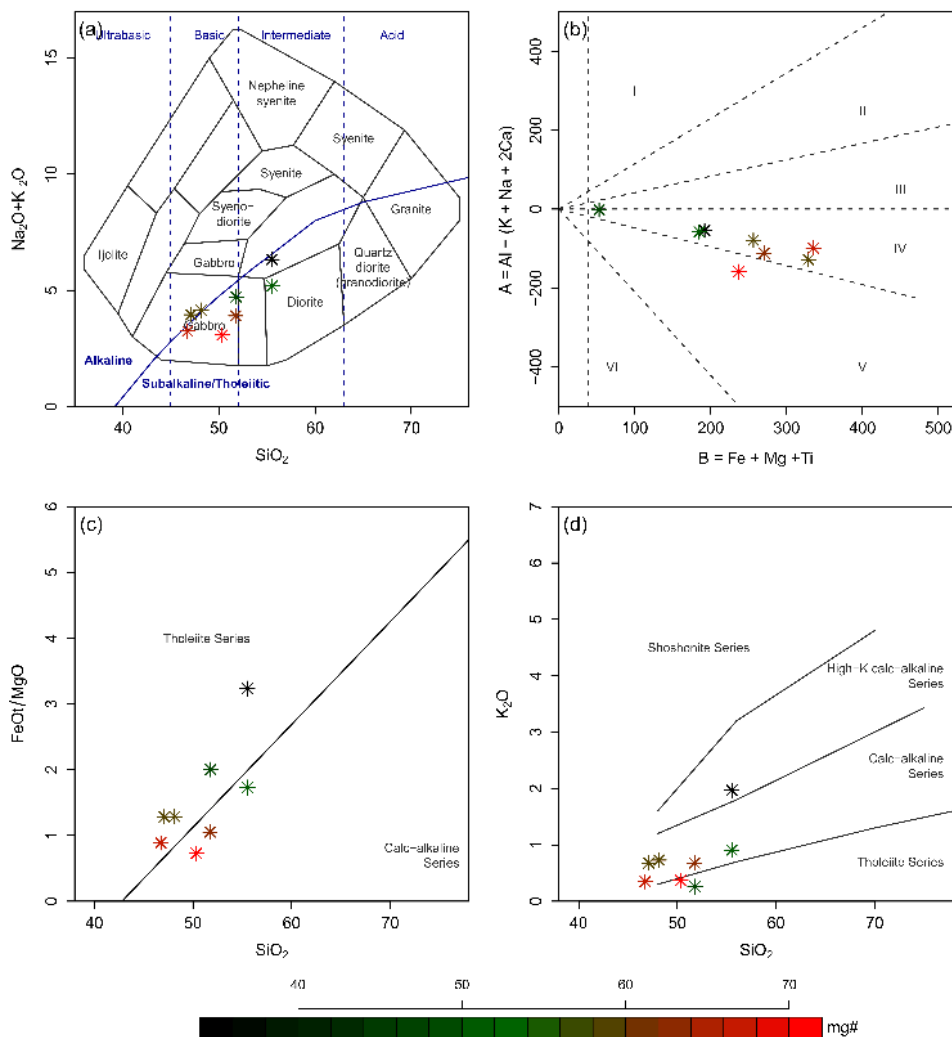


Figure 5.10: Classification diagrams for the Khaya Khudag gabbros–diorites. (a) Total alkalis–silica (TAS) diagram of Cox et al. (1979). (b) B vs. A diagram of Debon and Le Fort (1983). The following domains and characteristic mineral assemblages are distinguished: Peraluminous domain: I – muscovite > biotite, II – biotite > muscovite, III – biotite (\pm minor amphibole); Metaluminous domain: IV – biotite, amphibole, \pm pyroxene, V – clinopyroxene, \pm amphibole, \pm biotite, VI – unusual mineral associations (carbonatites ...). (c) SiO_2 vs. $\text{FeO}_{\text{tot}}/\text{MgO}$ plot of Miyashiro (1974) discriminating between calc-alkaline and tholeiitic series. (d) SiO_2 vs. K_2O plot of Peccerillo and Taylor (1976). All diagrams are colour-coded by mg# values.

Similar largely mafic, Cambrian subduction-related rock complexes can be found further west in the Dariv Range (Dijkstra et al. 2006) and in Western Mongolia. From the latter region, Rudnev et al. (2013) described island-arc peridotite–pyroxenite–gabbro–norite–plagiogranite and diorite–tonalite–plagiogranite plutons that evolved in the time span of 551–524 Ma. Thus, studied magmatic rocks likely reflect the development of an Early Cambrian active margin on the stabilized Baydrag microcontinent and date the ongoing oceanic subduction in the region. In fact, a belt of analogous Cambrian – Early Ordovician subduction-related magmatic complexes can be traced from Gobi and Mongolian Altai in the south to the south-western tip of the Siberian Craton in Russia in the north (Glorie et al. 2011; Kröner et al. 2011; Mongush et al. 2011; Soejono et al. 2016; Yarmolyuk et al. 2011). The spatiotemporal distribution, petrological character and whole-rock composition (including the radiogenic isotope data) are compatible with an idea that all these magmatic complexes once belonged together, forming the so-called ‘Ikh-Mongol’ Arc System (Janoušek et al. 2018). This enormous structure, almost two thousands kilometres long, decorated the outer margin of a chain of Precambrian ribbon continents (Erguna, Baydrag, Zabkhan and Tuva–Mongolian Continent Ribbon). Together with the Late Neoproterozoic passive margin (Lake Zone), it rims now the external part of the Mongolian Orocline (Xiao et al. 2015).

Most magmatism in the ‘Ikh-Mongol’ Arc System took place between c. 530 and 490 Ma. We assume that the character of subduction, and thus of the magma sources, changed dramatically along its strike (Fig. 5.11): from an Andean-type, where the magmatism recycled the mature Palaeoproterozoic continental crust (e.g., Zamtyr Nuruu Buriánek et al. 2017), through a primitive continental arc based on freshly accreted (Tonian) arc crust (Khan Taishir Magmatic Complex Janoušek et al. 2018) to an intraoceanic arc intruding the Cambrian sedimentary accretionary wedge (western Lake Zone Soejono et al. 2016).

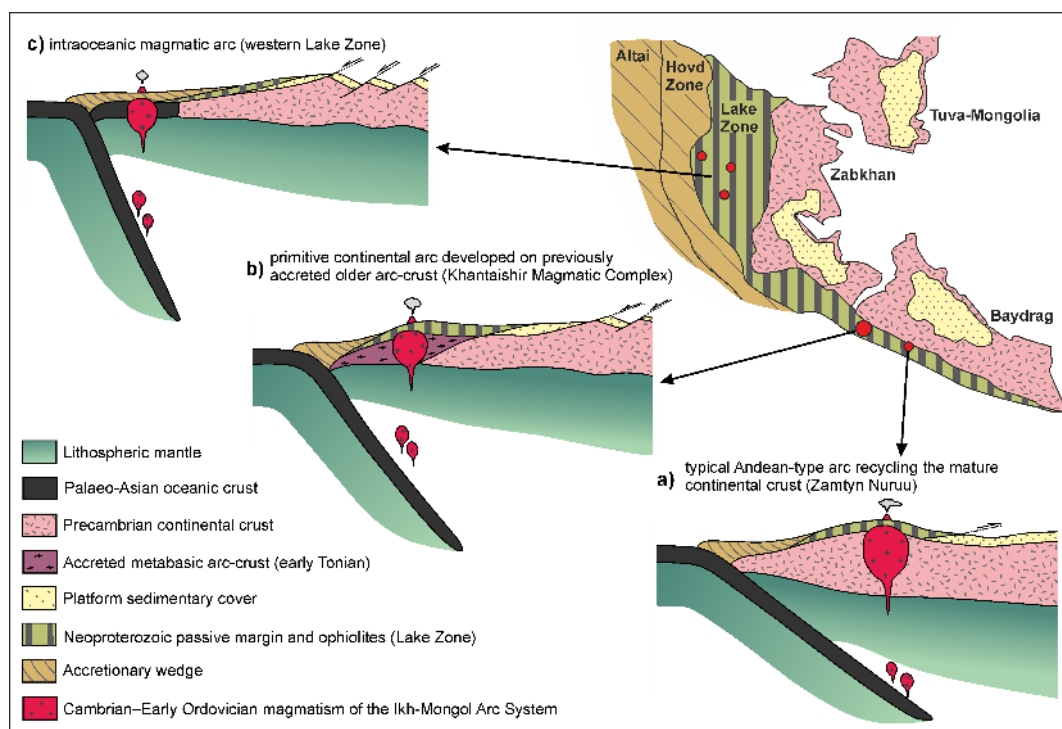


Figure 5.11: Idealized tectonic models for magmatism in three contrasting magmatic complexes along the Ikh-Mongol Arc System (Janoušek et al. 2018). For explanation, see the text.

5.5 HP-micaschist between Zamtyn Nuruu and Alag Khadny (9)

N45°23' 47", E98°18' 05", Dzoltyn Khundii, valley 13 km NE of Chandman Khayrkan Uul

The Maykhan Tsakhir Formation has been detached from the Lower Cambrian Tsakhir Uul Formation owing to its differing lithological character and grade of metamorphism. The unit is exposed in three geographically independent belts. The first one is E–W oriented between the Boomyn Khudag on the west and the Khuren Tsalugiin Khudag on the east between Alag Khadny Unit in the S and Khatashir Fm. in the N. The presented outcrop lies in the second belt forming a SW–NE trending belt between the Maykhan Tsakhir Tolgoi and the Bayan Tolgoi situated on the NW boundary of the Zamtyn Nuruu Complex south of the large serpentinite body of the Alag Khadny Unit (see map at locality 11). The third belt crops out in a NW–SE oriented belt on the NE slope of the Zamtyn Nuruu.

The footwall of the Maykhan Tsakhir Fm. is composed of high-grade metamorphic rocks and serpentinites of the Alag Khadny c. c. The tectonic character of the contact is suggested based on presence of mylonite zones parallel with the contact of units and on disintegration of the units into tectonic slices. The south and north contacts are unambiguously tectonic. The Khan Taishir Fm. is thrust over the Maykhan Tsakhir Fm. from the north and the metamorphites of the Zamtyn Nuruu Complex from the south.

The Maykhan Tsakhir Fm. is a primary sedimentary complex (Fig. 5.12) with predominant silty to sandy, often siliceous and graphitic carbonates and siliciclastic sediments, accompanied by minor bodies of volcanics. The sedimentary sequence typically starts with first meters thick layers or lenses of grey to dark grey chert. The whole complex is metamorphosed with increasing grade from NW to SE.



Figure 5.12: (a) Layers of limestone in siliceous shales (b) Folded schistose marbles.

Bedding is poorly preserved in the deformed and metamorphosed rocks. Bedding is steep, generally E–W trending with local undulation. In the area of Ikh Maykhan Tsakhir Tolgoi, large open folds with subhorizontal SW–NE oriented axis are preserved in chert layers (Fig 5.12a). The primary structures are overprinted by a foliation predominantly steeply dipping to the NNW (Fig. 5.12b).

The thick sequences of silty-sandy, often silicified and mostly recrystallized carbonates do not contain any determinable fossils. However, angular but also rounded possible algal crust fragments with locally perceptible lamination are quite common in locally developed breccia layers or form thin lenses to layers. Indeterminable fragments of tube-shaped organic remnants resemble rather recrystallized massive crinoids than archaeocyathids. Especially the remnants of white, circular bioclasts in the red marble are very convincing and may indicate heterogeneous,

tectonically limited trench within the Neoproterozoic – Lower Palaeozoic depositional area, although its tectonic origin should be considered obscure. The rocks of the Maykhan Tsakhir Fm. point to the existence of carbonate platform formed at relatively deep-water environment during Neoproterozoic to Early Cambrian. Sedimentary rocks are associated with rare island-arc basalts which may indicate initiation of subduction and subduction-related volcanism already in Early Cambrian.

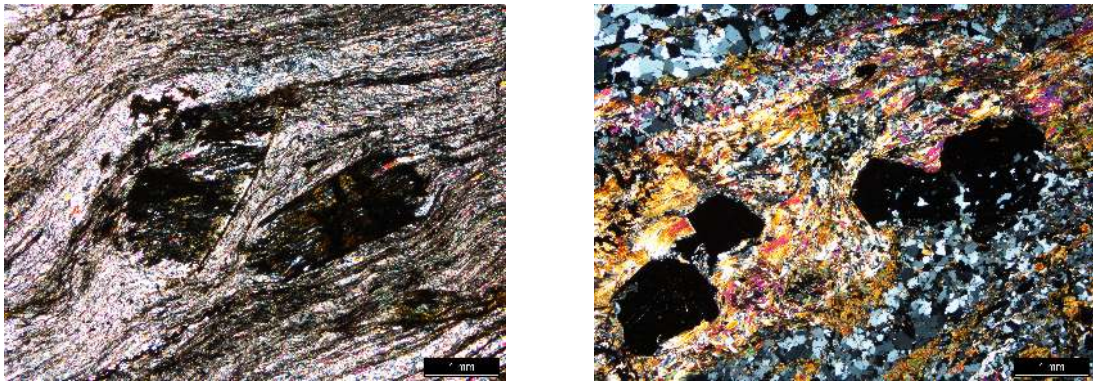


Figure 5.13: (a) Microphotograph of chloritoid schist, (b) microphotograph of garnet-staurolite schist.

Muscovite to biotite-muscovite micaschists, locally with garnet and/or staurolite are exposed mainly along the boundary with the Zamtyn Nuruu c.c. The rocks exhibit lepidoblastic to nematolepidoblastic textures, locally with crenulation folds. They are fine-grained, or porphyroblastic with fine-grained matrix and porphyroblasts of garnet, whose size does not exceed a few mm. The major components of these rocks are Qtz, Ms \pm Pl \pm Kfs \pm Bt and/or Chl \pm Grt \pm St.

Among metapelites of the northern belt dominate garnet-chloritoid schists that consist mainly of garnet, Fe-rich chloritoid, phengite, chlorite (Mg-rich and Fe-rich) and quartz, with minor amounts of kyanite, rutile, ilmenite, zircon and carbonaceous matter. Small lenticular bodies of kyanite-bearing garnet-chloritoid schists (1–2 m in length and 0.5 m in width) within recrystallized carbonates are located close to the contact with the eclogite body in the boundary zone between Maykhan Tsakhir Fm. and Alag Khadny Unit. The peak mineral assemblage of the rim of Grt + Fe-rich Cld + Ph + Mg-rich Chl + Ky + Qz indicates HP intermediate metamorphism of 560–590°C and 10–11 kbar (Javkhlan et al. 2013). $^{40}\text{Ar}/^{39}\text{Ar}$ muscovite plateau ages of 540 Ma from the garnet-chloritoid schist have been reported by Lehmann et al. (2010) and Štípská et al. (2010).

Reconstruction of metamorphic evolution of the metapelites is complicated by the broad chemical heterogeneity displayed not only by the variability of rock types but within the frame of the same rock. Chloritoid schists with mineral assemblage Qtz + Chl + Cld + Ms (Phg) \pm Grt \pm Ky \pm Pl \pm Bt \pm Grt indicate PT conditions $590 \pm 60^\circ\text{C}$ and 11 ± 3 kbar (Fig. 5.14). These results are consistent with the P-T calculations of Javkhlan et al. (2013). For the muscovite-biotite micaschists near the contact of the Zamtyn Nuruu Complex pre-peak P-T conditions were calculated from the mineral inclusions (Phg + Qtz + Chl \pm Pl \pm Bt \pm Cld) in the core of garnet to 560–600°C and 6–8 kbar, with uncertainties usually about $\pm 30^\circ\text{C}$ and 1 kbar. These HP-MT conditions reflect likely the pressure event of thrusting of the Zamtyn Nuruu Complex over the rocks of the Maykhan Tsakhir Fm. (Hanžl et al. 2007).

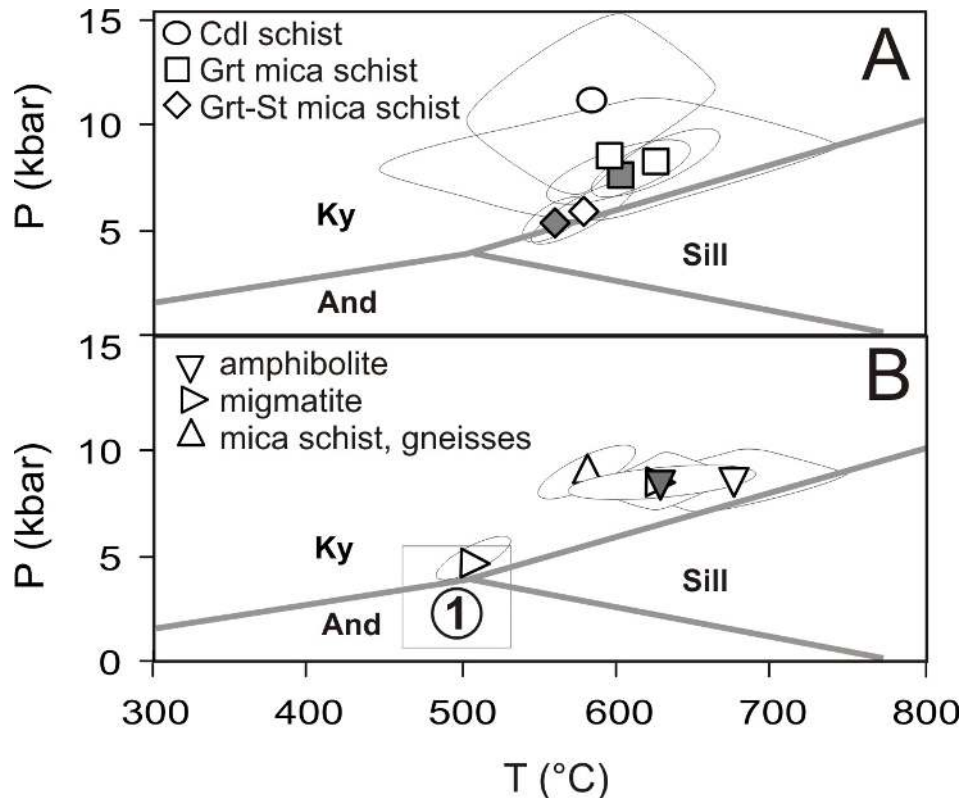


Figure 5.14: The metamorphic P-T condition of Maykhan Tsakhir Fm. (a) and Zamtyun Nuruu c. c. (b): (1) retrograde migmatite assemblage, symbols grey filling represent garnet core PT conditions.

5.6 Tonian orthogneiss of the Zamtyun Nuruu, Ekhen Khudug (10)

N45°24' 21", E98°20' 16", valley S–N trending valley 19 km NE of Chandman Khayrkhan Uul

The Zamtyun Nuruu Complex was defined in the report of Hanžl et al. (2007). This unit was distinguished from the Khan Taishir Fm. because of its different geological position, lithology and metamorphic character. The unit is exposed mainly in the mountain range of the Zamtyun Nuruu in NW–SE oriented belt between Alag Khadyun in the W and western slopes of the Bayan Tsagaan The Zamtyun Nuruu Complex is represented by variegated metamorphic rocks subdivided according to characteristic lithology into lower and upper parts.

The core and the S part of the Zamtyun Nuruu Complex are mostly built of orthometamorphites, which are designated as the "**Lower part**" of the formation. They consist of orthogneiss, amphibolite, metadiorite and metagabbro, strongly metamorphosed and migmatized. The variegated metasedimentary rocks – paragneisses to micaschists with layers and lenses of calc-silicate rocks with frequent metavolcanic rocks (greenschist, metatuff) and sills and dykes of volcanics prevailing in the area of Kharaatyn Uul are denoted as the "**Upper part**" of the Zamtyun Nuruu Complex.

Coarse-grained porphyroclastic orthogneiss (Fig. 5.15) consists of fine- to medium-grained quartzo-feldspathic matrix containing pronounced phenocrysts of alkali-feldspars. They are of light grey, grey, pink to reddish grey and red colour shades and exhibit monotonous mineral composition. They consist of quartz, mostly recrystallized, plagioclase, K-feldspar and less abundant micas. Biotite is rare, muscovite forms idioblastic flakes as well as sericitic melange. Zircon, apatite, rare monazite, allanite and unique garnet are accessories. Zoisite, epidote



Figure 5.15: Orthogneiss of the Zamtyn Nuruu complex is characteristic by σ -porphyroblasts of feldspar reaching a size up to three cm.

and chlorite are products of secondary processes. Microstructures reflect the stage of brittle deformation documented by cataclasis, crushing of grain margins. Kink bands in plagioclase lamellae may locally be observed. The characteristic metamorphic feature in these rocks is partial melting and migmatization, most likely caused by decompression melting during fast exhumation.

Protoliths of orthogneisses are of granodiorite–granite composition (Middlemost 1994, $\text{SiO}_2 = 63.5\text{--}70.7$ wt.%), and are subaluminous ($A/\text{CNK} = 1.0\text{--}1.1$) with variable $\text{K}_2\text{O}/\text{Na}_2\text{O}$ ratios (0.6–1.5). The trend is likely calc-alkaline, whereby the K_2O contents are high (2.5–4.8 wt.%), and thus the orthogneisses classify as high-K calc-alkaline to shoshonitic rocks (Fig. 5.16). The orthogneiss shows clearly a pre-collisional, subduction-related setting, or at least an arc-related source (Buriánek et al. 2017).

The age of Zamtyn Nuruu c. c. was considered to be Neoproterozoic in the concept by Rauzer et al. (1987). Several samples of orthogneiss and metadiorite were newly dated using the laser ablation method on single zircon grains (Buriánek et al. 2017). The results range from 514 ± 7.4 Ma in orthogneisses to 517 ± 5.3 Ma in metadiorites. These ages coincide rather with the later metamorphic overprint, which is evident and can be derived from the age estimated for diorite body (541.8 ± 4.4 Ma) that intruded rocks of the Zamtyn Nuruu Complex. However, inherited zircon cores in the same orthogneiss sample yielded an age of 941 ± 11 Ma, which is likely to correspond to magmatic age of the protolith.

The mentioned crystallization ages (933–947 Ma) do not fit Archaean to Neoproterozoic ages of the Baydrag and Dzavkhan microcontinents (e.g. Demoux et al. 2009b; Kozakov et al. 2014; Levashova et al. 2010). However, similar ages were reported by Demoux et al. (2009b) from metagranitoids of Baga Bogd Uul east of the studied area. These authors interpreted ages in a range of 954–983 Ma as timing the emplacement of the protolith. Similar protolith ages are known from metamorphosed granitic rocks in the South Gobi microcontinent (916 ± 16 Ma and 952 ± 8 Ma Wang et al. 2001; Yarmolyuk et al. 2005).

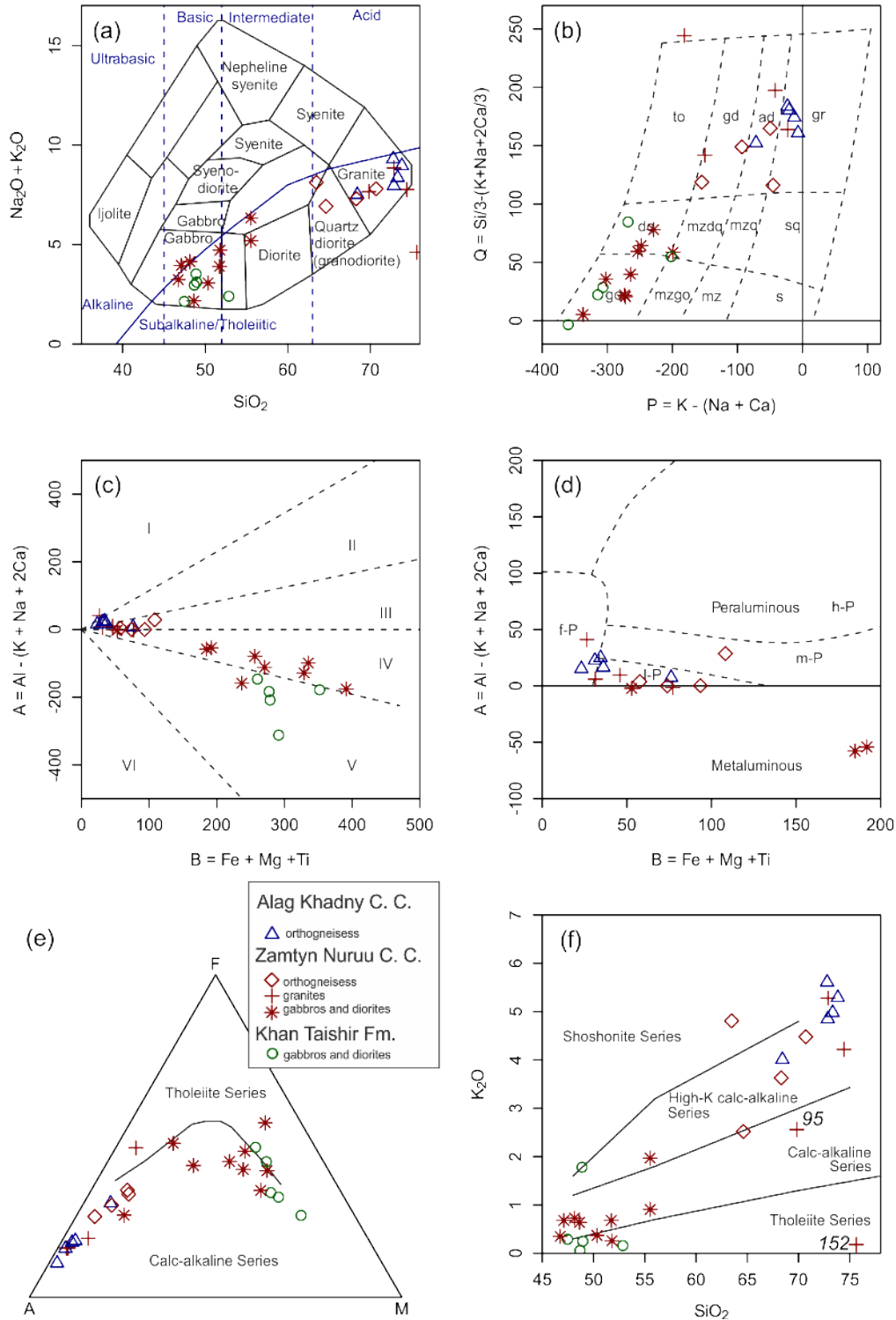


Figure 5.16: Discrimination diagrams for orthogneisses, granites, gabbros and diorites from the Zamtyn Nurru Complex and adjacent units: (a) Total alkalis–silica (TAS) diagram of Cox et al. (1979). (b) P vs. Q diagram of Debon and Le Fort (1983); (c) B vs. A diagram of Debon and Le Fort (1983) and (d) its modification by Villaseca et al. (1998). (e) AFM plot of Irvine and Baragar (1971) with solid line discriminating between calc-alkaline and tholeiitic series. (f) SiO_2 vs. K_2O plot of Peccerillo and Taylor (1976). According to Buriánek et al. (2017).

5.7 Cambrian HP tectonic melange in Alag Khad Mt. area (11A–B)

N45°24' 59", E98°13' 55", eastern termination of Alag Khadny range, 21 km SE from Erdene Uul

The newly defined Alag Khadny crystalline complex (Hanžl et al. 2007) is exposed in a E–W oriented about 10 km long and up to 4 km wide belt the Khan Taishir Fm. in the north and the Zamtyn Nuruu in the south (Fig. 5.17). Contacts of all these units are tectonic or tectonized. A series of steep faults separates this complex from the Zamtyn Nuruu c. c., whereas the Khan Taishir Fm. is thrust over the Alag Khadny c. c. Metamorphic complex is interpreted as a tectonic mélange, which can be subdivided into the three different parts:

- High pressure and high temperature (HP-HT) part. Main constituents are orthogneisses with intercalations of micaschists and paragneisses. This sequence contains lenses or layers of eclogite and rare, thin layers of marble.
- Amphibolite bodies tectonically incorporated in marbles and micaschist of the Maykhan Tsakhir Fm.
- Serpentinite body.

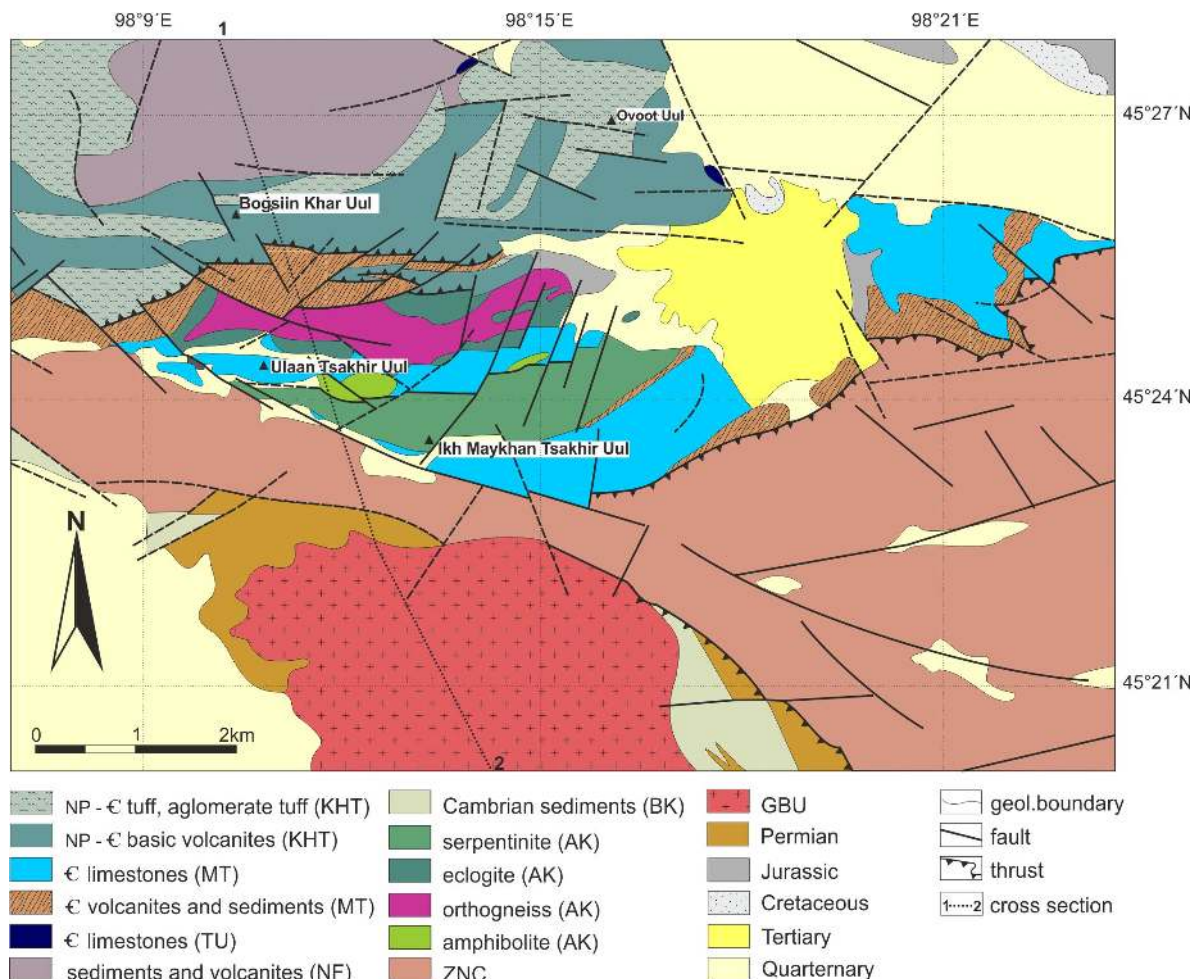


Figure 5.17: Geological map with position of eclogite boudins in Alag Khadny Belt (Buriánek et al. 2017).

Eclogites, early Cambrian carbonates and chloritoid-bearing metapelites is exposed in form of the accretionary wedge (Fig. 5.18), which was thrust during the early Cambrian over the Mesoproterozoic Dzabkhan-Baydrag continent (Fig. 5.20). The rock association of the

wedge forms a tectonic window emerging through the hanging-wall Khan Taishir ophiolite unit, which preserves a typical Tethyan-type ophiolitic sequence. The eclogites described by Štípská et al. (2010) are composed of garnet, omphacite, amphibole, rutile, \pm muscovite, \pm quartz, \pm epidote, and exhibit well-equilibrated matrix textures (Fig. 5.19). Jadeite content of the omphacite reaches up to 45 mol. %, the Si content of muscovite is between 3.40 and 3.45 p.f.u., amphibole is winchite to barroisite, but reaches tschermakitic composition at some rims, and garnet composition is $\text{grs}_{0.24-0.36}$, $\text{alm}_{0.43-0.56}$, $\text{py}_{0.05-0.18}$, $\text{sps}_{0.00-0.18}$, $\text{XFe}_{0.75-0.91}$. The peak assemblage, together with the composition of garnet rims, omphacite, amphibole and muscovite, correspond in a pseudosection to 20–22.5 kbar and 590–610°C. The tschermakitic rim of amphibole is interpreted as partial reequilibration on decompression below 16 kbar and around 600–630°C. Other eclogite varieties may contain also other assemblages with porphyroblastic garnet, clinopyroxene (omphacite, aegirine-augite), sodic, sodic-calcic, and calcic amphiboles (glaucophane, taramite, barroisite, winchite, pargasite, tschermakite, Fe/Mg-hornblende, and actinolite) with minor amounts of epidote, phengite, paragonite, plagioclase, biotite, K-feldspar, rutile, titanite, quartz, calcite, hematite, ilmenite and zircon. Further detailed study of mineral inclusions and mineral assemblages revealed that the eclogites were subjected to blueschist facies metamorphism before the peak eclogite facies stage (Javkhlan et al. 2013).

Two muscovite separates from the eclogite yielded an Ar-Ar plateau age of 543.1 ± 3.9 Ma and a mean age of 547.9 ± 2.6 Ma, whereas muscovite from an interbedded garnet-chloritoid micaschist yielded an Ar-Ar plateau age of 536.9 ± 2.7 Ma; these ages are interpreted as cooling ages (Štípská et al. 2010). K-Ar ages (amphibole and phengite) of amphibole-rich veins developed in the eclogite bodies show c. 600 Ma (Javkhlan et al. 2013).

Amphibolites and eclogites in the unit have tholeiite-basalt composition and trace elements data suggest MORB and island arc tectonic affinities. The eclogites have relatively narrow range of mostly radiogenic $\epsilon\text{Nd}(T)$ values (+2.3 to +3.7 as back-calculated for 550 Ma) and model age T_{DM} of 1.47–1.77 Ga at a wide range of initial $^{87}\text{Sr}/^{86}\text{Sr}$ ratio due to variable LILE mobilization in pre- or synmetamorphic processes. The geochemical and isotope data indicate the variably enriched MORB-like protolith for eclogites that have their variable composition through differentiation of precursor melts, slightly enriched mantle source and/or variable degree of crustal contamination (Skuzovatov et al. 2018).

The P-T data, geochemistry of eclogites and cooling ages suggest an affinity to the north Mongolian blueschist belt, which are believed typical for subduction of warm oceanic lithosphere and closure of small oceanic basins (Fig. 5.21). Thus, the discovery of the eclogites in this area represents an important finding suggesting extension of the early Cambrian subduction system of the Central Asian Orogenic Belt far to the east in a region where it was not expected (Štípská et al. 2010).

Orthogneisses of alkali feldspar granite to granite protolith and subaluminous composition ($A/\text{CNK} = 1.0\text{--}1.1$) correspond to high-K calc-alkaline to shoshonite series ($\text{K}_2\text{O} = 4.0\text{--}5.6$; $\text{K}_2\text{O}/\text{Na}_2\text{O} = 1.1\text{--}1.6$). The NMORB-normalized multielement patterns are characterized by a strong enrichment of Cs, Rb, Th, U and Pb over HREE, whose normalized contents are close to unity. Superimposed are troughs in Ba, Nb, Sr, P and Ti. Chondrite-normalized patterns are strongly fractionated with pronounced negative Eu anomalies ($\text{La}_N/\text{Yb}_N = 9.4\text{--}34.4$; $\text{Eu}/\text{Eu}^* = 0.26\text{--}0.56$). The position in the geotectonic diagram of Pearce et al. (1984) apparently corresponds to syn-collisional granites. However, as pointed out by the original authors, this classification scheme is not suitable for discrimination of post-collisional suites and the same



Figure 5.18: (a) Eclogite boudins form morphological pronounced knolls in orthogneiss and micaschist, (b) tectonic melange with eclogite boudins in micaschist.

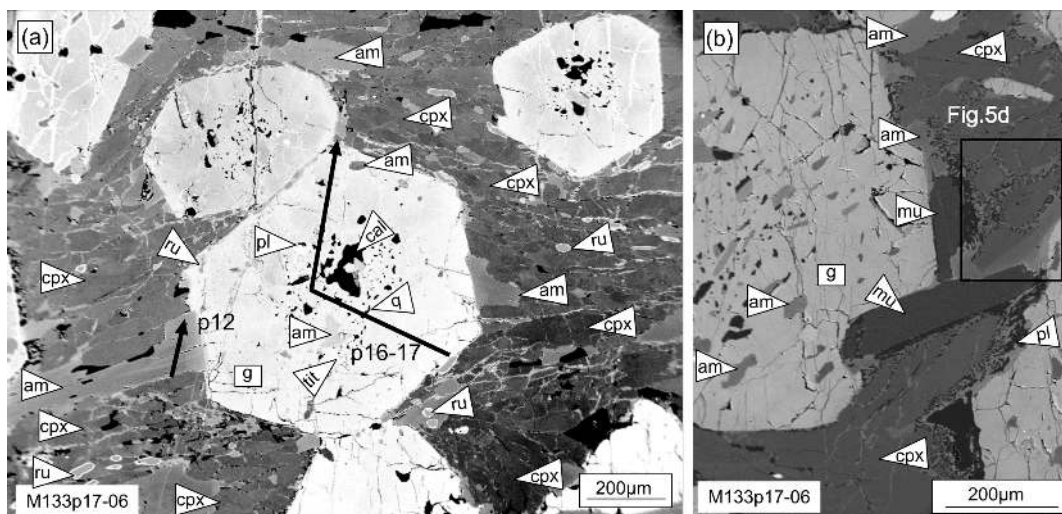


Figure 5.19: Backscattered electron (BSE) images of muscovite-bearing eclogite (a) Garnet with profile indicated, containing inclusions of calcite, quartz, titanite, amphibole, plagioclase and rutile. Matrix of clinopyroxene, rutile and amphibole, (b) muscovite in the matrix of clinopyroxene. Plagioclase-clinopyroxene-amphibole symplectites around clinopyroxene, garnet and muscovite (Štípská et al. 2010).

applies to the scheme of Schandl and Gorton (2002). Indeed, the diagram of Harris et al. (1986) indicates that the granites have elevated Ta contents compared with Hf and Nb, that is a hallmark of late- to post-collisional, calc-alkaline intrusions (Buriánek et al. 2017).

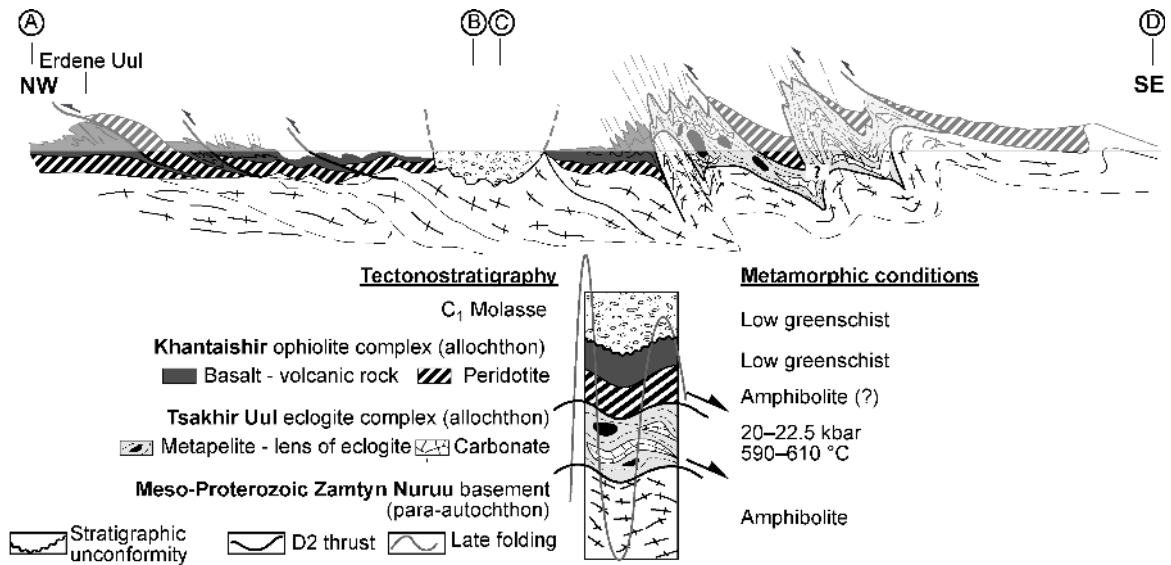


Figure 5.20: Interpretative geological cross-section and associated simplified stratigraphic column show structural relationships between the early Devonian molasse, Khan Taishir ophiolitic domain, Tsakhir Uul accretionary complex and underlying basement (Štípská et al. 2010).

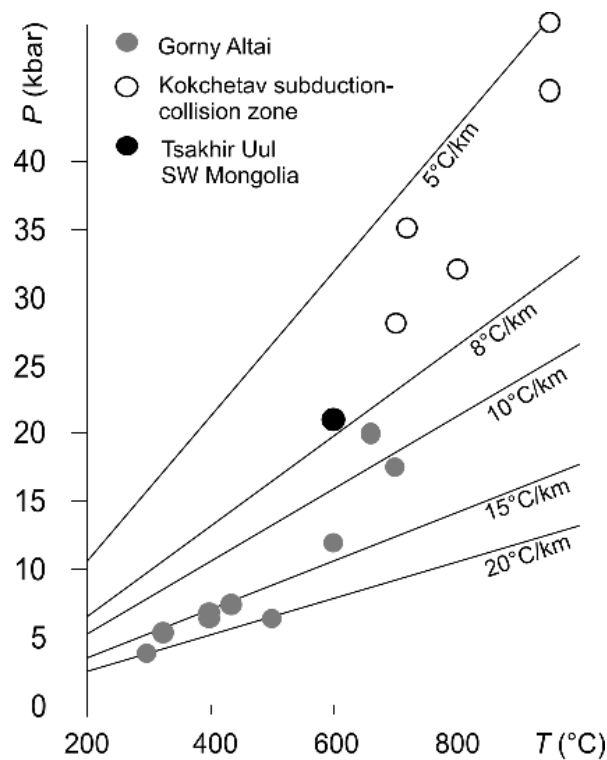


Figure 5.21: Recorded P-T conditions of about 21 kbar and 600 °C and mineral assemblage of the Tsakhir Uul eclogites are similar to eclogites associated with serpentinite mélanges of the Gorny Altai and plot on a P-T gradient of about 8 °C/km. These data suggest that the Tsakhir Uul accretionary wedge eclogites originated by subduction of a young and "warm" oceanic crust (Volkova et al. 2005). It is suggested that the eclogites of the SW Mongolia are connected to the same closure of small oceanic basins typical for the Gorny Altai subduction system, while the major subduction system operated to the west in the region of Kokchetav subduction-collision zone (Štípská et al. 2010).

5.8 Cambrian limestone (12)

N45°27' 32", E98°13' 58", 18 km SEE of Erdene Uul

Lenses of white recrystallized and foliated limestones south of the Notgon Uul between the Khan Taishir Fm. in its hanging wall and in the footwall of the Naran Fm. Contacts are steep (Fig. 5.22a). At boundary with the underlying metabasalts and agglomerates of the Khan Taishir Fm., the layers of the red-coloured cherts were developed (Fig. 5.23). Contact seems to be transgressive, tectonically reworked. The unit was considered by Markova (1975) to be a part of the Khan Taishir Formation. Later Rauzer et al. (1987) have distinguished the Tsakhir Uul Formation as an independent geological unit.



Figure 5.22: (a) Narrow syncline? of the Cambrian limestones between Khan Tashir Fm. (right E) and Naran Fm. (left W), (b) cut through the archaeocyathid rich limestone (with courtesy of Petr Budil).

Grey-brown limestone is formed by subangular clasts of carbonates up to tens of centimetres in size cemented by carbonate cement. Limestone clasts contain grains of quartz and opaque minerals. Limestones are sparitic, often recrystallized, fine- to medium-grained, locally also bioclastic. They contain rare grains of ore minerals. Locally, they have a character of red recrystallized limestones. Determinable remains of marine fauna and flora (including fragments of stromatolites, expressively laminated limestones and algal crusts) are quite rare in the grey-white limestones affiliated also to this formation, which are only locally abundant; but this may be caused by ubiquitous recrystallization of the rocks (perhaps also because of the original taphonomical conditions?). Nevertheless, locally very rich (by species diversity and morphological disparity) and surprisingly well-preserved (Fig. 5.22b) shallow-water archaeocyathid associations with common microbialites forming even shallow-water biostromes to bioherms were documented at several outcrops. The generic composition (archaeocyathid remains were preliminarily determined as *Inessocyathus?* sp., *Urcyathus?* sp., *Coscinocyathus?* sp., *Erismatocoscinus?* sp., *Nochroicyathus?* sp. and *Degeletticyathus?* sp.) indicates *Tommotian* to *Botomian* ages (Lower Cambrian); with this age, also relatively simple morphology of archaeocyathids corresponds well.

The age of the Tsakhir Uul Fm. is established relatively exactly basing on above-mentioned archaeocyathid fauna, which indicates Lower Cambrian, Tommotian to Botomian stages. The fossil associations indicate a marine shallow-water environment (in the photic zone). The considerable morphological disparity of archaeocyathids (the simple, conic forms prevail but these are accompanied also by branching forms) indicates probably a relatively quiet (protected shelf but not lagoons) to the medium-dynamic environment. Limestones likely represent the dumps of a ramp of calciturbidite current in its proximal part.

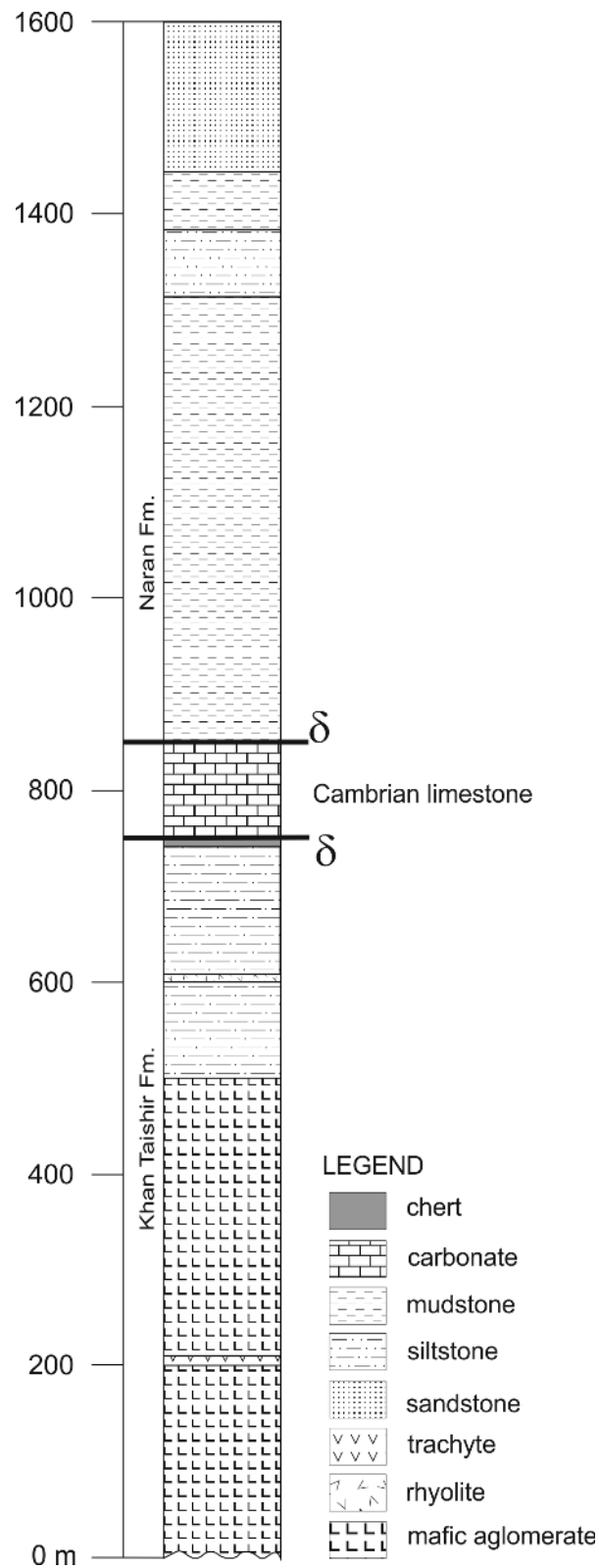


Figure 5.23: Schematic lithologic profile on the boundary of the Cambrian limestones with Khan Taishir and Naran formations.

5.9 Turbidite sediments of the Naran Formation (13)

N45°27' 2", E98°12' 49" cliff in dry valley meander, 17.5 km SEE of Erdene Uul

The Naran Formation was originally described by Markova (1975). The unit forms syncline in area of Erdene Uul – Zamtyn Nuruu on the Khan Taishir Formation. Rauzer et al. (1987) described discordant contact of the formation with the underlying Khan Taishir and Tsakhir Uul formations and suggested the Lower to Middle Cambrian age for the unit. Dergunov (2001) described the Naran Fm. as a Vendian – Cambrian sequence made up of greywacke turbidite. SHRIMP II analyses of ten clastic zircons from this sequence resulted in three groups of which are ca. 400, 810 and 2560 Ma and which indicates much younger (Devonian?) age of sedimentation and old, even Archean, probably Baydrag block source (Kröner et al. 2010).

Sandstones and slaty siltstones with tuffaceous admixture alternate in a rhythmic sequence (Fig. 5.24a) in cycles with thin layers of green-grey pea gravel conglomerates at the base. They gradually pass into green, grey or variegated siltstones to mudstones alternating in cm thick layers. Sandstones are fine- to medium-grained with psammitic texture, they are arkosic with angular to subangular grains of quartz and feldspars. The basal cement is slightly recrystallized and composed of a mixture of quartz, albite and sericite. In samples with tuffaceous admixture lithic fragments are present, the matrix is weakly chloritised and epidotised. Grains of zircon and titanite are accessory. Siltstones, shales and muddy slates gradually pass into each other, they have a variable amount of tuffaceous admixture. They are grey, grey-green or variegated. Muddy slates contain locally thin layers of dark grey carbonate rocks. Oval slightly flattened nodules are locally present in the mudstones (Fig. 5.24b). These fine-grained rocks are composed of clasts of feldspars, quartz and altered volcanics. Fragments float in the argillaceous or siliceous matrix which is locally coloured by iron oxides. The cement is usually recrystallized with overgrowths of sericite and chlorite. There is common epidote and carbonate in rocks with tuffaceous admixture. There are common cubes of pyrite up to 1 cm in size in these fine-grained rocks. Crystals are syn-deformational with pressure shadows filled by chlorite along them.



Figure 5.24: (a) Rhythmic alternation of fine-grained sandstones and siltstones. Steep bedding is little oblique to cleavage, (b) calcareous nodules in mudstone.

Rhythmic lamination is the dominant feature of the sequence, the beds are steep-folded with predominant orientation NEN–SWS in both limbs of the syncline and are accompanied by a steep cleavage. The rhythmic turbidite sediments as shales, siltstones and fine-grained greywackes up to sandstones predominate in the sequence. Volcanic rocks of overwhelmingly

acid composition are exposed in the centre of the syncline. Basaltic rocks are exposed on the bottom of the sequence in the form of flat-lying bodies or as sills. The volcanic rocks are calc-alkaline, basalts have a tholeiitic affinity. The unit is sporadically crosscut by porphyry dykes of trachyandesite affinity or rhyolites. Sediments have a flysch character having been developed in distal parts of turbidite currents. The common pyrite could indicate the anoxic environment in deeper water settings. The presence of volcanic material in upper parts of the sequence indicates possible rising of a volcanic arc in the area adjacent to the sedimentary basin.

5.10 Khan Taishir Formation (14A–B)

A: N45°26' 1", E98°11' 40", B: N45°25' 41", E98°11' 36", Uldzii Bulgiin Arag valley, 16 km SE from Erdene Uul

Volcaniclastic rocks and deformed pillow lavas of the Khan Taishir formation are exposed in southern part of valley Uldzii Bulgiin Arag. The locality represents volcanic part of the Khan Taishir Formation. It forms large syncline here with turbidite of Naran Formation in hanging wall. Units is steeply thrust to the S over the high grade rocks of the Alag Khadny Unit.

Khan Taishir Formation extend from the Altai City (Khan Taishir ophiolite of Zonenshain and Kuzmin 1978) in the NW and Erdene Uul ophiolite in the SE (Tomurtogoo 1980). It continues further to the E to area of the Khar Argalantyn Nuruu. This volcano-sedimentary sequence consists Ediacaran ophiolites (Tomurtogoo 1980) and products of massive volcanism. U–Pb zircon age of plagiogranites from the Khan Taishir ophiolite is 568 ± 4 Ma (Gibsher et al. 2001), 565 ± 7 Ma and 573 ± 8 Ma (Jian et al. 2014) and surprisingly old gabbro from Erdene Uul Ophiolite yielding age 973 ± 12 Ma (Buriánek et al. 2017).

Strongly altered (epidotization, chloritization, silicification, albitization) mafic to intermediate volcanic and volcaniclastic rocks are locally interlayered with beds and lenses up to 20 cm thick of grey laminated limestones. Individual pillows (Fig. 5.25a) are mostly up to 0.5 meter in diameter and almost entirely composed of aphanitic or porphyritic massive basalts small calcite-rich amygdalae are visible mainly along margins of the pillow. On the locality they are strongly deformed. Volcaniclastic deposits includes crystal tuffs (Fig. 5.25b) with pronounced columns of amphibole, medium to coarse grained hyaloclastites and autoclastic breccia with angular clasts amygdaloidal and massive basalts.

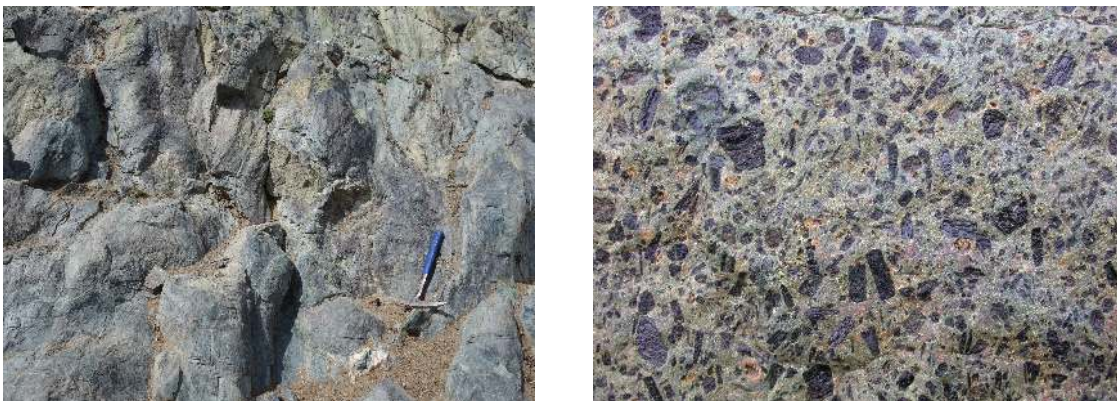


Figure 5.25: (a) Deformed pillow lava, (b) crystal tuff of andesite composition, hornblende columns reach up to 2 cm.

Volcanic and volcanoclastic rocks correspond to the subalkaline basalt, basaltic-andesite and andesite in the classification diagrams (Fig. 5.26). They are mostly of tholeiitic character, with some overlap to a low-K calc-alkaline domain. Some samples show high SiO_2 , MgO and low TiO_2 contents. In this respect they approach the boninites even though they do not yet fulfil the IUGS definition ($\text{SiO}_2 > 52$, $\text{MgO} > 8$, $\text{TiO}_2 < 0.5$ wt.% Le Bas 2000). The volcanic rocks show a clear subduction-related signature in many geotectonic diagrams (Fig. 5.27), including those of Meschede (1986) and Pearce (2008). Often low Zr/Th, as well as low Nb/Yb and Th/Yb ratios point to intra-oceanic arc (Buriánek et al. 2017). This is in line with the evidence for a shallow-mantle melting in the Nb/Yb vs. TiO_2/Yb diagram of Pearce (2008).

Geological, petrographical and geochemical data from the Khan Taishir Fm. point to the oceanic character of rocks with prevailing basaltic lavas, deep oceanic sediments and represent dismembered members of the ophiolite sequence and is accompanied by huge volcanic activity on adjacent island arc.

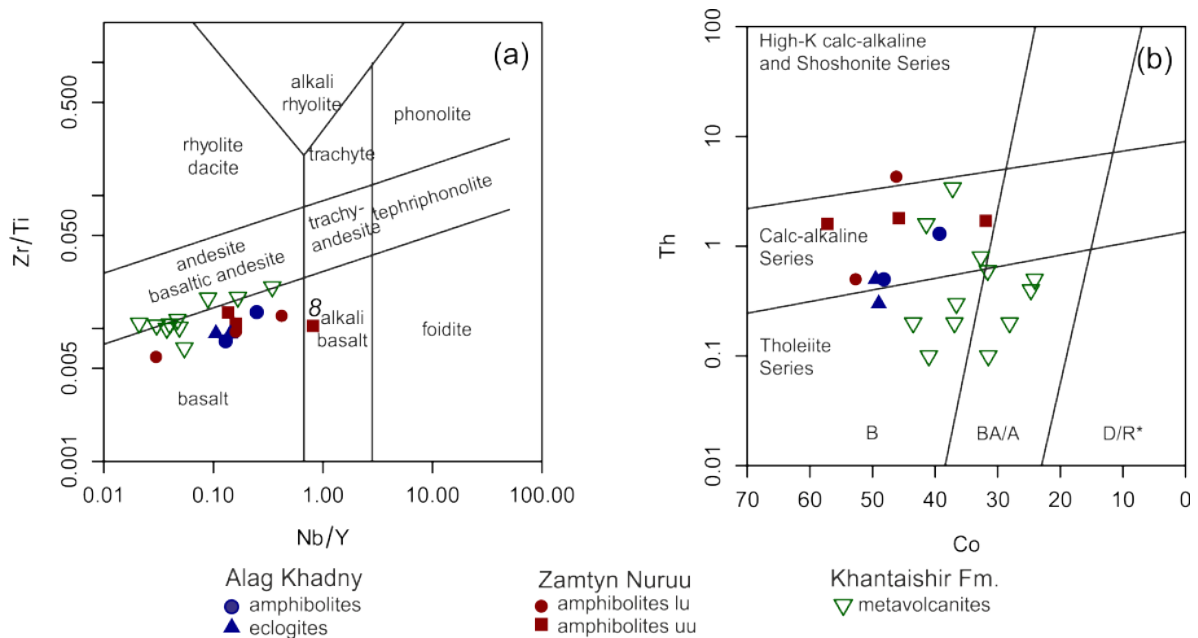


Figure 5.26: Classification of (meta)volcanic rocks from the selected geological units of the Zamtyn Nurru area. (a) Nb/Y vs. Zr/Ti diagram of Pearce (1996b); (b) Co vs. Th diagram of Hastie et al. (2007). Modified from Buriánek et al. (2017).

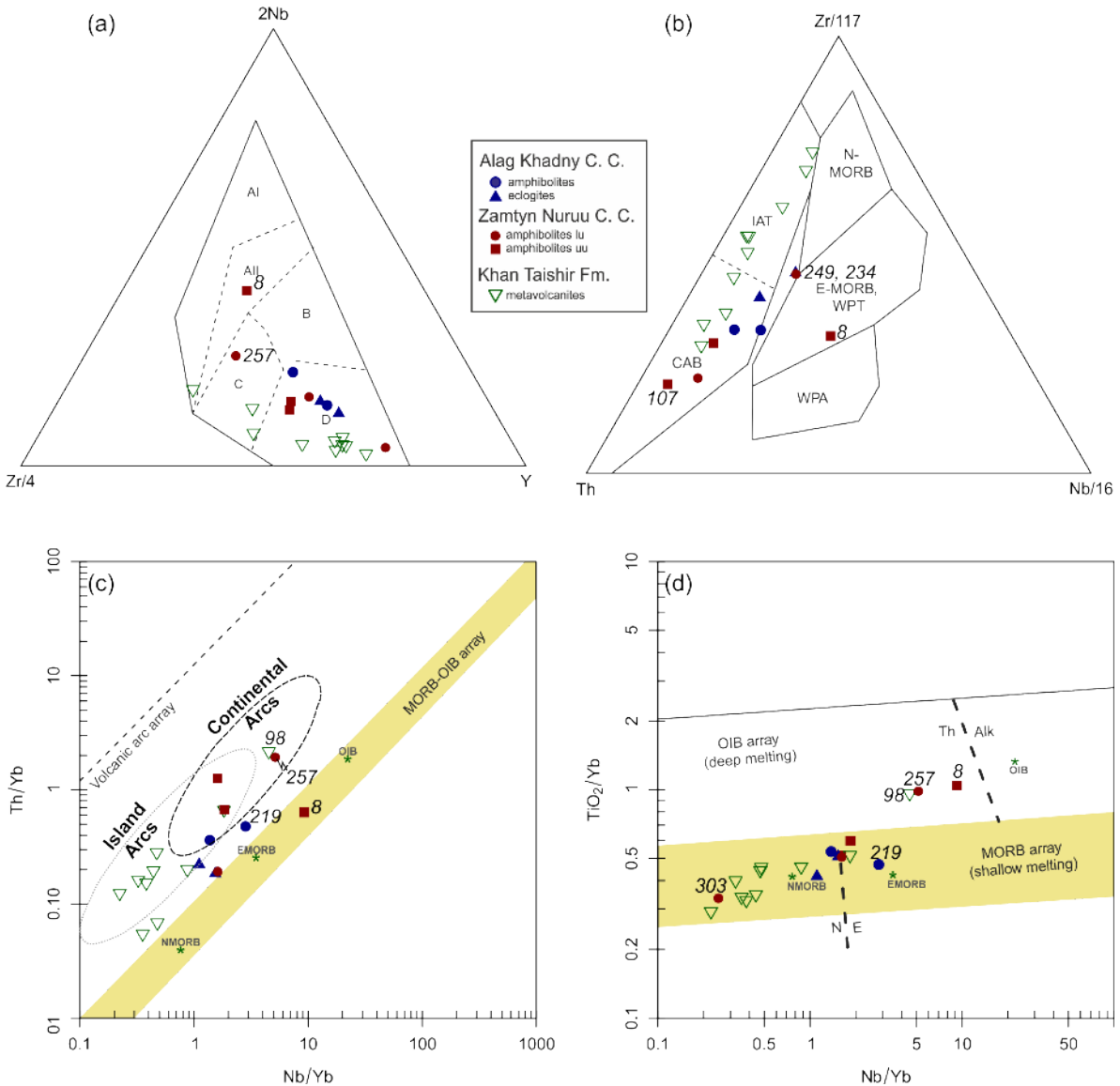


Figure 5.27: Geotectonic discrimination diagrams for the amphibolites, eclogites and low-grade metavolcanic rocks from the studied units: (a) $Zr/4-2 \times Nb-Y$ diagram of Meschede (1986): AI = within-plate alkaline basalts, AII = within-plate tholeiites and within-plate alkaline basalts, B = plume mid-ocean ridge basalts, C = within-plate tholeiites and volcanic arc basalts, D = normal mid-ocean ridge basalts and volcanic arc basalts. (b) Ternary diagram $Th-Zr/117-Nb/16$ of Wood (1980); IAT = island-arc tholeiites, CAB = calc-alkaline basalts, WPT = within-plate tholeiites, WPA = within-plate alkaline basalts. (c) $Nb/Yb-Th/Yb$ discrimination diagram (Pearce 2008). (d) $Nb/Yb-TiO_2/Yb$ discrimination diagram (Pearce 2008). Modified from Buriánek et al. (2017).



References

- Badarch, G., Cunningham, D., & Windley, B. F. (2002). A new terrane subdivision for Mongolia: Implications for the Phanerozoic crustal growth of Central Asia. *Journal of Asian Earth Sciences*, 21, 87–110.
- Bold, U., Crowley, J. L., Smith, E. F., Sambuu, O., & Macdonald, F. A. (2016). Neoproterozoic to early Paleozoic tectonic evolution of the Zavkhan terrane of Mongolia: Implications for continental growth in the Central Asian orogenic belt. *Lithosphere*, 8(6), 729–750.
- Borzakovskii, Y. A. (1985). *Making of geological map and map of raw deposits of the western Mongolia (W of meridian 102) on the scale 1: 500,000 with explanatory text, Period I, maps M-46B, L-47A, B, V, G*. Moscow.
- Boynton, W. V. (1984). Cosmochemistry of the rare earth elements: Meteorite studies. In *Developments in geochemistry* (Vol. 2, pp. 63–114). Elsevier.
- Bridge, J. S. (1993). Description and interpretation of fluvial deposits: a critical perspective. *Sedimentology*, 40(4), 801–810.
- Broussolle, A., Aguilar, C., Sun, M., Schulmann, K., Štípská, P., Jiang, Y., Yu, Y., Xiao, W., Wang, S., & Míková, J. (2018). Polycyclic Palaeozoic evolution of accretionary orogenic wedge in the southern Chinese Altai : Evidence from structural relationships and U – Pb geochronology. *Lithos*, 315, 400–424.
- Broussolle, A., Štípská, P., Lehmann, J., Schulmann, K., Hacker, B. R., Holder, R., Kylander-Clark, A. R. C., Hanžl, P., Racek, M., Hasalová, P., Lexa, O., Hrdličková, K., & Buriánek, D. (2015). P-T-t-D record of crustal-scale horizontal flow and magma-assisted doming in the SW Mongolian Altai. *Journal of Metamorphic Geology*, 33, 359–383.
- Broussolle, A., Sun, M., Schulmann, K., Guy, A., Aguilar, C., Štípská, P., Jiang, Y., Yu, Y., & Xiao, W. (2019). Are the Chinese Altai “terrane” the result of juxtaposition of different crustal levels during Late Devonian and Permian orogenesis? *Gondwana Research*, 66, 183–206.
- Buchan, C., Pfänder, J., Kröner, A., Brewer, T. S., Tomurtogoo, O., Tomurhuu, D., Cunningham, D., & Windley, B. F. (2002). Timing of accretion and collisional deformation in the Central Asian Orogenic Belt: Implications of granite geochronology in the Bayankhongor Ophiolite Zone. *Chemical Geology*, 192, 23–45.

- Burenjargal, U., Okamoto, A., Kuwatani, T., Sakata, S., Hirata, T., & Tsuchiya, N. (2014). Thermal evolution of the Tseel terrane, SW Mongolia and its relation to granitoid intrusions in the Central Asian Orogenic. *Journal of Metamorphic Geology*, *32*, 765–790.
- Burenjargal, U., Okamoto, A., Tsuchiya, N., Uno, M., Horie, K., & Hokada, T. (2016). Contrasting geochemical signatures of Devonian and Permian granitoids from the Tseel Terrane, SW Mongolia. *Journal of Geosciences*, *61*, 51–66.
- Buriánek, D., Schulmann, K., Hrdličková, K., Hanžl, P., Janoušek, V., Gerdes, A., & Lexa, O. (2017). Geochemical and geochronological constraints on distinct Early-Neoproterozoic and Cambrian accretionary events along southern margin of the Baydrag Continent in western Mongolia. *Gondwana Research*, *47*, 200–227.
- Cabanis, B. & Lecolle, M. (1989). The La/10-Y/15-Nb/8 diagram: A tool for distinguishing volcanic series and discovering crustal mixing and/or contamination. *Comptes Rendus de l'Academie des Sciences, serie 2*, *309*, 2023–2029.
- Cocks, L., Robin, M., & Torsvik, T. H. (2007). Siberia, the wandering northern terrane, and its changing geography through the Palaeozoic. *Earth-Science Reviews*, *82*, 29–74.
- Cox, K., Bell, J., & Pankhurst, R. (1979). *77ie interpretation of igneous rocks*. George Allen & Unwin, 450pp.
- Debon, F. & Le Fort, P. (1983). A chemical–mineralogical classification of common plutonic rocks and associations. *Earth and Environmental Science Transactions of the Royal Society of Edinburgh*, *73*(3), 135–149.
- Demoux, A., Kroner, A., Hegner, E., & Badarch, G. (2009a). Devonian arc-related magmatism in the Tseel terrane of SW Mongolia: chronological and geochemical evidence. *Journal of the Geological Society*, *166*, 459–471.
- Demoux, A., Kröner, A., Badarch, G., Jian, P., Tomurhuu, D., & Wingate, M. T. D. (2009b). Zircon Ages from the Baydrag Block and the Bayankhongor Ophiolite Zone: Time Constraints on Late Neoproterozoic to Cambrian Subduction- and Accretion-Related Magmatism in Central Mongolia. *The Journal of Geology*, *117*(4), 377–397.
- Dergunov, A. B. (2001). *Tectonics, magmatism, and metallogeny of mongolia*. Psychology Press.
- Dijkstra, A. H., Brouwer, F. M., Cunningham, W. D., Buchan, C., Badarch, G., & Mason, P. R. (2006). Late Neoproterozoic proto-arc ocean crust in the Dariv Range, Western Mongolia: a supra-subduction zone end-member ophiolite. *Journal of the Geological Society*, *163*(2), 363–373.
- Donskaya, T., Sklyarov, E., Gladkochub, D., Mazukabzov, A., Saľnikova, E., Kovach, V., Yakovleva, S., & Berezhnaya, N. (2000). The pribaikalian collisional metamorphic belt. *Doklady Akademii Nauk-Rossijskaya Akademiya Nauk*, *374*(1), 79–83.
- Economos, R. C., Hanžl, P., Hrdličková, K., Buriánek, D., Said, L. O., Gerdes, A., & Paterson, S. R. (2008). Geochemical and structural constraints on the magmatic history of the Chandman Massif of the eastern Mongolian Altay Range, SW Mongolia. *Journal of Geosciences*, *53*(3-4), 335–352.
- Förster, H.-J., Tischendorf, G., & Trumbull, R. B. (1997). An evaluation of the Rb vs. (Y+ Nb) discrimination diagram to infer tectonic setting of silicic igneous rocks. *Lithos*, *40*(2-4), 261–293.
- Gibsher, A. S., Khain, E. V., Kotov, A. B., Saľnikova, E. B., Kozakov, I. K., Kovach, V. P., Yakovleva, S. Z., & Fedoseenko, A. M. (2001). Late Vendian age of the Khan-Taishiri

- ophiolite complex in western Mongolia. *Russian Geology and Geophysics*, 42(8), 1179–1185.
- Gladkochub, D. P., Donskaya, T. V., Wingate, M. T., Poller, U., Kröner, A., Fedorovsky, V. S., Mazukabzov, A. M., Todt, W., & Pisarevsky, S. A. (2008). Petrology, geochronology, and tectonic implications of c. 500 Ma metamorphic and igneous rocks along the northern margin of the Central Asian Orogen (Olkhon terrane, Lake Baikal, Siberia). *Journal of the Geological Society*, 165(1), 235–246.
- Glorie, S., De Grave, J., Buslov, M. M., Zhimulev, F. I., Izmer, a., Vandoorne, W., Ryabinin, a., Van den haute, P., Vanhaecke, F., & Elburg, M. a. (2011). Formation and palaeozoic evolution of the gorny-altai-altai-mongolia suture zone (south siberia): Zircon u/pb constraints on the igneous record. *Gondwana Research*, 20(2-3), 465–484.
- Hanžl, P., Aichler, J., Bolormaa, K., Byambasuren, D., Budil, P., Buriánek, D., Hrdličková, K., Erban, V., Gerdes, A., Gilíková, H. et al. (2007). *Geological Survey of the Mongolian Altay at a scale 1: 50,000 (Zamtyin Nuruu–50)* (P. Hanžl & J. Aichler, Eds.). Ulaanbaatar: Czech Geological Survey, Brno and MPRAM.
- Hanžl, P., Altanbaatar, B., Guy, A., Buriánek, D., Lexa, O., Schulmann, K., Kuncová, E., Hrdličková, K., Janoušek, V., Krejčí, Z., & Jiang, Y. (2018). *Geological map at a scale 1:500 000 along contacts of the Lake, Gobi-Altai and and Trans Altai Zones, map sheet L-47-V, SW Mongolia*. National University of Mongolia, School of Arts and Sciences. Ulaanbaatar.
- Hanžl, P., Guy, A., Altanbaatar, B., Lexa, O., Schulmann, K., Kuncová, E., Hrdličková, K., Janoušek, V., Buriánek, D., Krejčí, Z., Jiang, Y., & Otgonbaatar, D. (2019). Geology of the Gobi and Mongol Altai junction: a key for understanding of the Mongolian Altaides. *Journal of Maps*, submitted.
- Hanžl, P., Krejčí, Z., Altanbaatar, B., Lexa, O., Buriánek, D., Janoušek, V., Schulmann, K., Jiang, Y., & Hrdličková, K. (2017). Geology of the Gobi Altai and Tsel terranes in the central part of the Sagsai River Watershed, SE Mongolian Altai. *Journal of Maps*, 13(2), 270–275.
- Hanžl, P., Schulmann, K., Janoušek, V., Lexa, O., Hrdličková, K., Jiang, Y., Buriánek, D., Altanbaatar, B., Ganchuluun, T., & Erban, V. (2016). Making continental crust : origin of Devonian orthogneisses from SE Mongolian Altai. *Journal of Geosciences*, 61, 25–50.
- Harris, N. B., Pearce, J. A., & Tindle, A. G. (1986). Geochemical characteristics of collision-zone magmatism. *Geological Society, London, Special Publications*, 19(1), 67–81.
- Hastie, A. R., Kerr, A. C., Pearce, J. A., & Mitchell, S. (2007). Classification of altered volcanic island arc rocks using immobile trace elements: development of the Th–Co discrimination diagram. *Journal of Petrology*, 48(12), 2341–2357.
- He, Y., Sun, M., Cai, K., Xiao, W., Zhao, G., Long, X., & Li, P. (2015). Petrogenesis of the Devonian high-Mg rock association and its tectonic implication for the Chinese Altai orogenic belt, NW China. *Journal of Asian Earth Sciences*, 113, 61–74.
- Helo, C., Hegner, E., Kröner, A., Badarch, G., Tomurtogoo, O., Windley, B. F., & Dulski, P. (2006). Geochemical signature of Paleozoic accretionary complexes of the Central Asian Orogenic Belt in South Mongolia: constraints on arc environments and crustal growth. *Chemical Geology*, 227(3-4), 236–257.
- Hollocher, K., Robinson, P., Walsh, E., & Roberts, D. (2012). Geochemistry of amphibolite-facies volcanics and gabbros of the Støren Nappe in extensions west and southwest of

- Trondheim, Western Gneiss Region, Norway: a key to correlations and paleotectonic settings. *American Journal of Science*, 312(4), 357–416.
- Hrdličková, K., Bolormaa, K., Buriánek, D., Hanžl, P., Gerdes, A., & Janoušek, V. (2008). Petrology and age of metamorphosed rocks in tectonic slices inside the Palaeozoic sediments of the eastern Mongolian Altay, SW Mongolia. *Journal of Geosciences*, 53(2), 139–165.
- Hrdličková, K., Gerdes, A., Gilřková, H., Bat-Ulzii, D., & Hanžl, P. (2010). Burd gol granite massif as a product of the late cambrian post- -orogenic magmatism in the SE part of the Lake Zone, Gobi Altay, SW Mongolia. *Journal of Geosciences*, 55(4), 369–386.
- Irvine, T. N. J. & Baragar, W. R. A. (1971). A guide to the chemical classification of the common volcanic rocks. *Canadian Journal of Earth Sciences*, 8(5), 523–548.
- Jahn, B. M. (2004). The Central Asian Orogenic Belt and growth of the continental crust in the Phanerozoic. *Geological Society, London, Special Publications*, 226(1), 73–100.
- Janoušek, V., Jiang, Y., Buriánek, D., Schulmann, K., Hanžl, P., Soejono, I., Kröner, A., Altanbaatar, B., Erban, V., Lexa, O. et al. (2018). Cambrian–Ordovician magmatism of the Ikh-Mongol Arc System exemplified by the Khantaishir Magmatic Complex (Lake Zone, south–central Mongolia). *Gondwana Research*, 54, 122–149.
- Javkhlan, O., Takasu, A., Bat-Ulzii, D., & Kabir, M. F. (2013). Metamorphic pressure-temperature evolution of garnet-chloritoid schists from the Lake Zone, SW Mongolia. *Journal of Mineralogical and Petrological Sciences*, 108(5), 255–266.
- Jensen, L. (1976). A new plot for classifying subalkalic volcanic rocks. *Ontario Division of Mines, Miscellaneous Paper*, 66, 1–22.
- Jian, P., Kröner, A., Jahn, B. M., Windley, B. F., Shi, Y., Zhang, W., Zhang, F., Miao, L., Tomurhuu, D., & Liu, D. (2014). Zircon dating of Neoproterozoic and Cambrian ophiolites in West Mongolia and implications for the timing of orogenic processes in the central part of the Central Asian Orogenic Belt. *Earth-Science Reviews*, 133, 62–93.
- Jian, P., Kröner, A., Windley, B. F., Shi, Y., Zhang, F., Miao, L., Tomurhuu, D., Zhang, W., & Liu, D. (2010). Zircon ages of the Bayankhongor ophiolite mélangé and associated rocks: time constraints on Neoproterozoic to Cambrian accretionary and collisional orogenesis in Central Mongolia. *Precambrian Research*, 177(1-2), 162–180.
- Jian, P., Liu, D., Kröner, A., Windley, B. F., Shi, Y., Zhang, F., Shi, G., Miao, L., Zhang, W., Zhang, Q., Zhang, L., & Ren, J. (2008). Time scale of an early to mid-Paleozoic orogenic cycle of the long-lived Central Asian Orogenic Belt, Inner Mongolia of China: Implications for continental growth. *Lithos*, 101(3-4), 233–259.
- Jiang, Y., Schulmann, K., Sun, M., Štípská, P., Guy, A., Janoušek, V., Lexa, O., & Yuan, C. (2016). Anatexis of accretionary wedge, Pacific-type magmatism, and formation of vertically stratified continental crust in the Altai Orogenic Belt. *Tectonics*, 35(12), 3095–3118.
- Jiang, Y., Schulmann, K., Kröner, A., Sun, M., Lexa, O., Janoušek, V., Buriánek, D., Yuan, C., & Hanžl, P. (2017). Neoproterozoic-Early Paleozoic Peri-Pacific Accretionary Evolution of the Mongolian Collage System: Insights From Geochemical and U-Pb Zircon Data From the Ordovician Sedimentary Wedge in the Mongolian Altai. *Tectonics*, 36(11), 2305–2331.
- Jiang, Y., Schulmann, K., Sun, M., Weinberg, R. F., Štípská, P., Li, P. F., Zhang, J., Chopin, F., Wang, S., Xia, X. P., & Xiao, W. J. (2019). Structural and Geochronological Constraints

- on Devonian Suprasubduction Tectonic Switching and Permian Collisional Dynamics in the Chinese Altai, Central Asia. *Tectonics*, 38(1), 253–280.
- Jiang, Y., Štípská, P., Sun, M., Schulmann, K., Zhang, J., Wu, Q. H., Long, X. P., Yuan, C., Racek, M., Zhao, G. C., & Xiao, W. (2015). Juxtaposition of barrovian and migmatite domains in the Chinese Altai: A result of crustal thickening followed by doming of partially molten lower crust. *Journal of Metamorphic Geology*, 33(1), 45–70.
- Jiang, Y., Sun, M., Kröner, A., Tumurkhuu, D., Long, X., Zhao, G., Yuan, C., & Xiao, W. (2012). The high-grade Tsel Terrane in SW Mongolia: An Early Paleozoic arc system or a Precambrian sliver? *Lithos*, 142–143, 95–115.
- Kepezhinskas, P. K., Kepezhinskas, K., & Puchtel, I. S. (1991). Lower Paleozoic oceanic crust in Mongolian Caledonides: SM - ND isotope and trace element data. *Geophysical Research Letters*, 18(7), 1301–1304.
- Khain, E. V., Bibikova, E. V., Salnikova, E. B., Kröner, A., Gibsher, A. S., Didenko, A. N., Degtyarev, K. E., & Fedotova, A. A. (2003). The Palaeo-Asian ocean in the Neoproterozoic and early Palaeozoic: New geochronologic data and palaeotectonic reconstructions. *Precambrian Research*, 122, 329–358.
- Khain, E. V., Neimark, L. A., & Amelin, Y. V. (1995). The Caledonian stage of remobilization of the Precambrian basement of the Gargan block, the Eastern Sayan (isotopic geochronological data). In *Doklady an* (Vol. 342, 6, pp. 776–780).
- Konopásek, J., Janoušek, V., Oyhantçabal, P., Sláma, J., & Ulrich, S. (2018). Did the circum-Rodinia subduction trigger the Neoproterozoic rifting along the Congo–Kalahari Craton margin? *International Journal of Earth Sciences*, 107(5), 1859–1894.
- Kovach, V. P., Dzhen, P., Yarmolyuk, V. V., Kozakov, I. K., Lyu, D., Terenteva, L. B., Lebedev, V. I., & Kovalenko, V. I. (2005). Magmatism and geodynamics of early stage of the paleo-Asian ocean formation: geochronological and geochemical data of the ophiolites of the Bayan-Khongor zone. *Doklady Akademii Nauk-Rossijskaya Akademiya Nauk*, 404(2), 229–234.
- Kovach, V. P., Yarmolyuk, V. V., Kovalenko, V. I., Kozlovskiy, A. M., Kotov, A. B., & Terenteva, L. B. (2011). Composition, sources, and mechanisms of formation of the continental crust of the Lake Zone of the Central Asian Caledonides. II. Geochemical and Nd isotope data. *Petrology*, 19(4), 399–425.
- Kovalenko, V. I., Yarmolyuk, V. V., Kovach, V. P., Kotov, A. B., Kozakov, I. K., Salnikova, E. B., & Larin, A. M. (2004). Isotope provinces, mechanisms of generation and sources of the continental crust in the Central Asian mobile belt: Geological and isotopic evidence. *Journal of Asian Earth Sciences*, 23, 605–627.
- Kozakov, I. K., Kovach, V. P., Bibikova, E. V., Kirnozova, T. I., Lykhin, D. A., Plotkina, Y. V., Tolmacheva, E. V., Fugzan, M. M., & Erdenezhargal, C. (2014). Late Riphean episode in the formation of crystalline rock complexes in the Dzabkhan microcontinent: geological, geochronologic, and Nd isotopic-geochemical data. *Petrology*, 22(5), 480–506.
- Kozakov, I. K., Sal, E. B., Wang, T., Didenko, A. N., Plotkina, Y. V., & Podkovyrov, V. N. (2007). Early Precambrian Crystalline Complexes of the Central Asian Microcontinent: Age, Sources, Tectonic Position. *Stratigraphy and Geological Correlation*, 15(2), 121–140.
- Kozakov, I. K., Salnikova, E. B., Khain, E. V., Kovach, V. P., Berezhnaya, N. G., Yakovleva, S. Z., & Plotkina, Y. V. (2002). Early Caledonian crystalline rocks of the Lake zone in

- Mongolia: formation history and tectonic settings as deduced from U-Pb and Sm-Nd datings. *Geotectonics*, 36(2), 156–166.
- Kozakov, I. K., Saĭnikova, E. B., Yarmolyuk, V. V., Kozlovsky, A. M., Kovach, V. P., Azimov, P. Y., Anisimova, I. V., Lebedev, V. I., Enjin, G., Erdenejargal, C., Plotkina, Y. V., Fedoseenko, A. M., & Yakovleva, S. Z. (2012a). Convergent boundaries and related igneous and metamorphic complexes in caledonides of Central Asia. *Geotectonics*, 46(1), 16–36.
- Kozakov, I. K., Yarmolyuk, V. V., Kovach, V. P., Bibikova, E. V., Kirnozova, T. I., Kozlovskii, A. M., Plotkina, Y. V., Fugzan, M. M., Lebedev, V. I., & Erdenezhargal, C. (2012b). The Early Baikalian crystalline complex in the basement of the Dzabkhan microcontinent of the Early Caledonian orogenic area, Central Asia. *Stratigraphy and Geological Correlation*, 20(3), 231–239.
- Kröner, A., Demoux, A., Zack, T., Rojas-Agramonte, Y., Jian, P., Tomurhuu, D., & Barth, M. (2011). Zircon ages for a felsic volcanic rock and arc-related early Palaeozoic sediments on the margin of the Baydrag microcontinent, central Asian orogenic belt, Mongolia. *Journal of Asian Earth Sciences*, 42(5), 1008–1017.
- Kröner, A., Lehmann, J., Schulmann, K., Demoux, A., Lexa, O., Tomurhuu, D., Štípská, P., Liu, D., & Wingat, M. T. D. (2010). Lithostratigraphic and geochronological constraints on the evolution of the central Asian orogenic belt in SW Mongolia: Early paleozoic rifting followed by late paleozoic accretion. *American Journal of Science*, 310(September), 523–574.
- Kuzmichev, A. B., Bibikova, E. V., & Zhuravlev, D. Z. (2001). Neoproterozoic (800 Ma) orogeny in the Tuva-Mongolia Massif (Siberia): Island arc-continent collision at the northeast Rodinia margin. *Precambrian Research*, 110(1-4), 109–126.
- Kuzmichev, A. B., Kröner, A., Hegner, E., Dunyi, L., & Yusheng, W. (2005). The Shishkhid ophiolite, northern Mongolia: A key to the reconstruction of a Neoproterozoic island-arc system in central Asia. *Precambrian Research*, 138(1-2), 125–150.
- Kuzmichev, A. B., Sklyarov, E., Postnikov, A., & Bibikova, E. (2007). The Oka Belt (Southern Siberia and Northern Mongolia): A Neoproterozoic analog of the Japanese Shimanto Belt? *Island Arc*, 16(2), 224–242.
- Laurent, O., Martin, H., Moyen, J.-F., & Doucelance, R. (2014). The diversity and evolution of late-Archean granitoids: Evidence for the onset of “modern-style” plate tectonics between 3.0 and 2.5 Ga. *Lithos*, 205, 208–235.
- Le Bas, M. (2000). IUGS reclassification of the high-Mg and picritic volcanic rocks. *Journal of Petrology*, 41(10), 1467–1470.
- Lehmann, J., Schulmann, K., Lexa, O., Corsini, M., Kröner, A., Štípská, P., Tomurhuu, D., & Otgonbaatar, D. (2010). Structural constraints on the evolution of the Central Asian Orogenic Belt in SW Mongolia. *American Journal of Science*, 310(7), 575–628.
- Lehmann, J., Schulmann, K., Lexa, O., Závada, P., Štípská, P., Hasalová, P., Belyanin, G., & Corsini, M. (2017). Detachment folding of partially molten crust in accretionary orogens: A new magma-enhanced vertical mass and heat transfer mechanism. *Lithosphere*, 9(6), 889–909.
- Levashova, N. M., Kalugin, V. M., Gibsher, A. S., Yff, J., Ryabinin, A. B., Meert, J. G., & Malone, S. J. (2010). The origin of the Baydaric microcontinent, Mongolia: Constraints from paleomagnetism and geochronology. *Tectonophysics*, 485(1-4), 306–320.

- Long, X., Sun, M., Yuan, C., Xiao, W., & Cai, K. (2008). Early Paleozoic sedimentary record of the Chinese Altai: implications for its tectonic evolution. *Sedimentary Geology*, 208(3-4), 88–100.
- Markova, N. G. (1975). Stratigraphy of the Lower and Middle Paleozoic of Western Mongolia. *Transactions of Joint Soviet–Mongolian Scientific Research Geological Expedition*, 12, 1–119.
- Markova, N. G. & Sharkova, T. T. (1977). Silurian and Devonian of South Mongolia (in Russian). In N. S. Zaitsev & A. L. Yanshin (Eds.), *Osnovnye problemy geologii mongolii* (Vol. 22, pp. 52–61).
- Meschede, M. (1986). A method of discriminating between different types of mid-ocean ridge basalts and continental tholeiites with the Nb–Zr–Y diagram. *Chemical Geology*, 56(3), 207–218. doi:[https://doi.org/10.1016/0009-2541\(86\)90004-5](https://doi.org/10.1016/0009-2541(86)90004-5)
- Miall, A. D. (1978). Tectonic setting and syndepositional deformation of molasse and other nonmarine-paralic sedimentary basins. *Canadian Journal of Earth Sciences*, 15(10), 1613–1632.
- Middlemost, E. A. (1994). Naming materials in the magma/igneous rock system. *Earth-Science Reviews*, 37(3-4), 215–224.
- Miyashiro, A. (1974). Volcanic rock series in island arcs and active continental margins. *American Journal of Science*, 274(4), 321–355.
- Mongush, A. A., Lebedev, V. I., Kovach, V. P., Sal'nikova, E. B., Druzhkova, E. K., Yakovleva, S. Z., Plotkina, Y. V., Zagornaya, N. Y., Travin, A. V., & Serov, P. A. (2011). The tectono-magmatic evolution of structure-lithologic complexes in the Tannu-Ola zone, Tuva, in the Late Vendian-Early Cambrian (from geochemical, Nd isotope, and geochronological data). *Russian Geology and Geophysics*, 52(5), 503–516.
- Mossakovsky, A. A., Ruzhentsev, S. V., G, S. S., & Kheraskova, T. N. (1993). The Central Asian fold belt: geodynamic evolution and formation. *Geotectonics*, 6, 3–32.
- Nozhkin, A. D., Borisenko, A. S., & Nevolko, P. A. (2011). Stages of Late Proterozoic magmatism and periods of Au mineralization in the Yenisei Ridge. *Russian Geology and Geophysics*, 52(1), 124–143.
- Nozhkin, A. D., Turkina, O. M., Bibikova, E. V., & Ponomarchuk, V. A. (2001). Structure, composition, and formation conditions of metasedimentary-volcanogenic complexes of the Kan greenstone belt (northwestern Sayan region). *Geologiya i Geofizika*, 42(7), 1058–1078.
- Parfenov, L., Popeko, L., & Tomurtogoo, O. (2001). Problems of tectonics of the Mongol-Okhotsk orogenic belt. *Russian Journal of Pacific Geology*, 16(5), 797–830.
- Pearce, J. A. (1982). Trace element characteristics of lavas from destructive plate boundaries. *Andesites*, 8, 525–548.
- Pearce, J. A. (1996a). A user's guide to basalt discrimination diagrams: Short course notes. In D. A. Wyman (Ed.), *Trace element geochemistry of volcanic rocks: Applications for massive sulphide exploration* (Vol. 12, pp. 79–113). Geological Association of Canada.
- Pearce, J. A. (1996b). Sources and settings of granitic rocks. *Episodes*, 19, 120–125.
- Pearce, J. A. (2008). Geochemical fingerprinting of oceanic basalts with applications to ophiolite classification and the search for Archean oceanic crust. *Lithos*, 100(1-4), 14–48.
- Pearce, J. A. (2014). Geochemical fingerprinting of the Earth's oldest rocks. *Geology*, 42(2), 175–176.

- Pearce, J. A., Harris, N. B., & Tindle, A. G. (1984). Trace element discrimination diagrams for the tectonic interpretation of granitic rocks. *Journal of Petrology*, 25(4), 956–983.
- Pearce, J. A. & Peate, D. W. (1995). Tectonic implications of the composition of volcanic arc magmas. *Annual Review of Earth and Planetary Sciences*, 23(1), 251–285.
- Peccerillo, A. & Taylor, S. R. (1976). Geochemistry of Eocene calc-alkaline volcanic rocks from the Kastamonu area, northern Turkey. *Contributions to Mineralogy and Petrology*, 58(1), 63–81.
- Perfiliev, A. & Kheraskov, N. (1980). The diabase complexes and the problem of the tectonic layering of the oceanic crust. In *Tectonic layering of the lithosphere* [Proceedings of the geological institute of the ussr academy] (343, pp. 64–104). Moscow: Nauka.
- Rauzer, A. A., Zhanchiv, D. I., Golyakov, V. I., Ykhina, I. F., Ivanov, I. G., Tsukernik, A. B., Afonin, V. V., Smirnov, I. G., Bykhover, V. I., Kravtsev, A. V., Baatarkhuyag, A., Skoryukin, M. I., Khodikov, I. V., Mantsev, N. V., Okaemov, S. V., Mischin, V. A., & T, E. (1987). *Report on results of geological survey at a scale of 1: 200,000, performed in southeast part of the Mongolian Altay, Mongolian National Republic in 1983–1986*. Moscow.
- Rojas-Agramonte, Y., Kröner, A., Demoux, A., Xia, X., Wang, W., Donskaya, T., Liu, D., & Sun, M. (2011). Detrital and xenocrystic zircon ages from Neoproterozoic to Palaeozoic arc terranes of Mongolia: significance for the origin of crustal fragments in the Central Asian Orogenic Belt. *Gondwana Research*, 19(3), 751–763.
- Rudnev, S. N., Izokh, A. E., Kovach, V. P., Shelepaev, R. A., & Terent'eva, L. B. (2009). Age, composition, sources, and geodynamic environments of the origin of granitoids in the northern part of the Ozernaya Zone, Western Mongolia: growth mechanisms of the Paleozoic continental crust. *Petrology*, 17(5), 439–475.
- Rudnev, S. N., Kovach, V. P., & Ponomarchuk, V. a. (2013). Vendian-Early Cambrian island-arc plagiogranitoid magmatism in the Altai-Sayan folded area and in the Lake Zone of western Mongolia (geochronological, geochemical, and isotope data). *Russian Geology and Geophysics*, 54(10), 1272–1287.
- Ruzhentsev, S. V. & Nekrasov, G. E. (2009). Tectonics of the Aga zone, Mongolia-Okhotsk belt. *Geotectonics*, 43(1), 34–50.
- Safonova, I. Y., Utsunomiya, A., Kojima, S., Nakae, S., Tomurtogoo, O., Filippov, A. N., & Koizumi, K. (2009). Pacific superplume-related oceanic basalts hosted by accretionary complexes of Central Asia, Russian Far East and Japan. *Gondwana Research*, 16(3-4), 587–608.
- Salnikova, E. B., Kozakov, I. K., Kotov, A. B., Kröner, A., Todt, W., Bibikova, E. V., Nutman, A., Yakovleva, S. Z., & Kovach, V. P. (2001). Age of Palaeozoic granites and metamorphism in the Tuvino-Mongolian Massif of the Central Asian Mobile Belt: Loss of a Precambrian microcontinent. *Precambrian Research*, 110(1-4), 143–164.
- Schandl, E. S. & Gorton, M. P. (2002). Application of high field strength elements to discriminate tectonic settings in VMS environments. *Economic Geology*, 97(3), 629–642.
- Scotese, C. (2004). Cenozoic and Mesozoic paleogeography: changing terrestrial biogeographic pathways. *Frontiers of biogeography: new directions in the geography of nature*, 9–26.
- Sengör, A. M. C., Natal'in, B. A., & Burtman, V. S. (1993). Evolution of the Altaid tectonic collage and Paleozoic crustal growth in Eurasia. *Nature*, 364(6435), 299–307.

- Shand, S. J. (1943). *Eruptive rocks: Their genesis, composition, and classification, with a chapter on meteorites*. J. Wiley & sons, Incorporated.
- Skuzovatov, S. Y., Shatsky, V., Dril, S., & Perepelov, A. (2018). Elemental and isotopic (Nd-Sr-O) geochemistry of eclogites from the Zamtyn-Nuruu area (SW Mongolia): Crustal contribution and relation to Neoproterozoic subduction-accretion events. *Journal of Asian Earth Sciences*, 167, 33–51.
- Soejono, I., Buriánek, D., Janoušek, V., Svojtka, M., Čáp, P., Erban, V., & Ganpurev, N. (2017). A reworked Lake Zone margin: Chronological and geochemical constraints from the Ordovician arc-related basement of the Hovd Zone (western Mongolia). *Lithos*, 295, 112–132.
- Soejono, I., Buriánek, D., Svojtka, M., Žáček, V., & Čáp, P. (2016). Mid-Ordovician and Late Devonian magmatism in the Togtokhinshil Complex : new insight into the formation and accretionary evolution of the Lake Zone (western Mongolia). *Journal of Geosciences*, 61, 5–23.
- Soejono, I., Čáp, P., Míková, J., Janoušek, V., Buriánek, D., & Schulmann, K. (2018). Early Palaeozoic sedimentary record and provenance of flysch sequences in the Hovd Zone (western Mongolia): Implications for the geodynamic evolution of the Altai accretionary wedge system. *Gondwana Research*, 64, 163–183.
- Spear, F. S. (1993). *Metamorphic phase equilibria and pressure-temperature-time paths*. Mineralogical Society of America.
- Štípská, P., Schulmann, K., Lehmann, J., Corsini, M., Lexa, O., & Tomurhuu, D. (2010). Early Cambrian eclogites in SW Mongolia: Evidence that the Palaeo-Asian Ocean suture extends further east than expected. *Journal of Metamorphic Geology*, 28(9), 915–933.
- Sun, M., Long, X. P., Cai, K., Jiang, Y., Wang, B. Y., Yuan, C., Zhao, G. C., Xiao, W., & Wu, F. Y. (2009). Early Paleozoic ridge subduction in the Chinese Altai: Insight from the abrupt change in zircon Hf isotopic compositions. *Science in China, Series D: Earth Sciences*, 52(9), 1345–1358.
- Sun, S. S. & McDonough, W. F. (1989). Chemical and isotopic systematics of oceanic basalts: implications for mantle composition and processes. In A. D. Saunders & N. M. J. (Eds.), *Magmatism in the ocean basins* (Vol. 42, 1, pp. 313–345). Geological Society of London, Special Publications.
- Tatsumi, Y. & Eggins, S. (1995). *Subduction zone magmatism*. Wiley.
- Taylor, S. R. & McLennan, S. M. (1995). The geochemical evolution of the continental crust. *Reviews of Geophysics*, 33(2), 241–265.
- Tomurtogoo, O. (1980). *Geology of Ophiolitic Complex of Mongolia* (Scientific Report in Geological Funds of Mongolia No. 3135). MRAM, Ulaanbaatar.
- Tomurtogoo, O., Windley, B. F., Kröner, A., Badarch, G., & Liu, D. Y. (2005). Zircon age and occurrence of the Adaatsag ophiolite and Muron shear zone, central Mongolia: constraints on the evolution of the Mongol–Okhotsk ocean, suture and orogen. *Journal of the Geological Society*, 162(1), 125–134.
- Villaseca, C., Barbero, L., & Herreros, V. (1998). A re-examination of the typology of per-aluminous granite types in intracontinental orogenic belts. *Earth and Environmental Science Transactions of The Royal Society of Edinburgh*, 89(2), 113–119.
- Volkova, N., Stupakov, S., Tretyakov, G., Simonov, V., Travin, A., & Yudin, D. (2005). Blueschists from the Uimon Zone as evidence for Ordovician accretionary-collisional events in Gorny Altai. *Russian Geology and Geophysics*, 46, 361–378.

- Wang, T., Zheng, Y., Gehrels, G. E., & Mu, Z. (2001). Geochronological evidence for existence of South Mongolian microcontinent—A zircon U-Pb age of grantoid gneisses from the Yagan-Onch Hayrhan metamorphic core complex. *Chinese Science Bulletin*, *46*(23), 2005.
- Wei, C., Clarke, G., Tian, W., & Qiu, L. (2007). Transition of metamorphic series from the Kyanite-to andalusite-types in the Altai orogen, Xinjiang, China: evidence from petrography and calculated KMnFMASH and KFMASH phase relations. *Lithos*, *96*(3-4), 353–374.
- Wilde, S. A., Cawood, P. A., Wang, K., & Nemchin, A. A. (2005). Granitoid evolution in the Late Archean Wutai Complex, North China Craton. *Journal of Asian Earth Sciences*, *24*(5), 597–613.
- Wilhem, C., Windley, B. F., & Stampfli, G. M. (2012). The Altaids of Central Asia: a tectonic and evolutionary innovative review. *Earth-Science Reviews*, *113*(3-4), 303–341.
- Winchester, J. A. & Floyd, P. A. (1977). Geochemical discrimination of different magma series and their differentiation products using immobile elements. *Chemical Geology*, *20*, 325–343.
- Windley, B. F., Alexeiev, D., Xiao, W., Kröner, A., & Badarch, G. (2007). Tectonic models for accretion of the Central Asian Orogenic Belt. *Journal of the Geological Society*, *164*(2004), 31–47.
- Wood, D. A. (1980). The application of a Th-Hf-Ta diagram to problems of tectonomagmatic classification and to establishing the nature of crustal contamination of basaltic lavas of the British Tertiary Volcanic Province. *Earth and Planetary Science Letters*, *50*(1), 11–30.
- Xiao, W., Windley, B. F., Huang, B. C., Han, C. M., Yuan, C., Chen, H. L., Sun, M., Sun, S., & Li, J. L. (2009a). End-Permian to mid-Triassic termination of the accretionary processes of the southern Altaids: Implications for the geodynamic evolution, Phanerozoic continental growth, and metallogeny of Central Asia. *International Journal of Earth Sciences*, *98*, 1189–1217.
- Xiao, W., Windley, B. F., Yuan, C., Sun, M., Han, C. M., Lin, S. F., Lchen, H. L., Yan, Q. R., Liu, D. Y., Qin, K. Z., Li, J. L., & Sun, S. (2009b). Paleozoic multiple subduction-accretion processes of the southern Altaids. *American Journal of Science*, *309*, 221–270.
- Xiao, W., Windley, B. F., Badarch, G., Sun, S., Li, J., Qin, K., & Wang, Z. (2004). Palaeozoic accretionary and convergent tectonics of the southern Altaids: implications for the growth of Central Asia. *Journal of the Geological Society, London*, *161*, 339–342.
- Xiao, W., Windley, B. F., Sun, S., Li, J., Huang, B., Han, C., Yuan, C., Sun, M., & Chen, H. (2015). A tale of amalgamation of three Permo-Triassic collage systems in Central Asia: oroclines, sutures, and terminal accretion. *Annual Review of Earth and Planetary Sciences*, *43*, 477–507.
- Yakubchuk, A. (2008). Re-deciphering the tectonic jigsaw puzzle of northern Eurasia. *Journal of Asian Earth Sciences*, *32*(2-4), 82–101.
- Yarmolyuk, V. V., Kovach, V., & Kotov, A. (2000). Magma sources and the isotopic (Sr and Nd) evolution of alkaline granitoids in the Suktui Massif, Eastern Transbaikalian Region: Age and Magma Sources. *Doklady Earth Sciences*, *372*(4), 762–768.
- Yarmolyuk, V. V., Kovach, V., Kovalenko, V., Salnikova, E., Kozlovskii, A., Kotov, A., Yakovleva, S., & Fedoseenko, A. (2011). Composition, sources, and mechanism of continental

- crust growth in the Lake Zone of the Central Asian Caledonides: I. Geological and geochronological data. *Petrology*, 19(1), 55–78.
- Yarmolyuk, V. V., Kovalenko, V., Saĭnikova, E., Kozakov, I., Kotov, A., Kovach, V., Vladykin, N., & Yakovleva, S. (2005). U-Pb-Age of syn- and postmetamorphic granitoids from Southern Mongolia-evidence for the presence of grenvilides in the Central Asian Fold Belt. *Doklady Akademii Nauk-Rossijskaya Akademiya Nauk*, 404(1), 84–89.
- Yarmolyuk, V. V., Kuzmin, M. I., & Ernst, R. E. (2014). Intraplate geodynamics and magmatism in the evolution of the Central Asian Orogenic Belt. *Journal of Asian Earth Sciences*, 93, 158–179.
- Yuan, C., Sun, M., Xiao, W., Li, X., Chen, H., Lin, S., Xia, X., & Long, X. (2007). Accretionary orogenesis of the Chinese Altai: insights from Paleozoic granitoids. *Chemical Geology*, 242(1-2), 22–39.
- Zhang, Y.-H., Xu, W.-L., Tang, J., Wang, F., Xu, M.-J., & Wang, W. (2014). Age and provenance of the Ergunahe Group and the Wubinaobao Formation, northeastern Inner Mongolia, NE China: implications for tectonic setting of the Erguna Massif. *International Geology Review*, 56(6), 653–671.
- Zonenshain, L. P. (1970). *Summarizing report about results of group geological survey at a scale 1:1,000,000 done by expedition in years 1964-1966 (in Russian)*. Unpublished manuscript.
- Zonenshain, L. P. (1973). The evolution of Central Asiatic geosynclines through sea-floor spreading. *Tectonophysics*, 19(3), 213–232.
- Zonenshain, L. P. & Kuzmin, M. I. (1978). The Khan-Taishir ophiolitic complex of western Mongolia, its petrology, origin and comparison with other ophiolitic complexes. *Contributions to Mineralogy and Petrology*, 67(1), 95–109.
- Zonenshain, L. P., Kuzmin, M. I., & Kononov, M. V. (1985). Absolute reconstructions of the Paleozoic oceans. *Earth and Planetary Science Letters*, 74(1), 103–116.